

Copyright  
by  
Liang-Hai Lee  
2007

**The Dissertation Committee for Liang-Hai Lee Certifies that this is the  
approved version of the following dissertation:**

**ON THE DESIGN OF SLIP-ON BUCKLE ARRESTORS FOR  
OFFSHORE PIPELINES**

**Committee:**

---

Stelios Kyriakides, Supervisor

---

Eric B. Becker

---

Kenneth M. Liechti

---

Krishnaswa Ravi-Chandar

---

Karl H. Frank

**ON THE DESIGN OF SLIP-ON BUCKLE ARRESTORS FOR  
OFFSHORE PIPELINES**

**by**

**Liang-Hai Lee, B.S.; M.S.**

**Dissertation**

Presented to the Faculty of the Graduate School of

The University of Texas at Austin

in Partial Fulfillment

of the Requirements

for the Degree of

**Doctor of Philosophy**

**The University of Texas at Austin**

**December 2007**

## **Dedication**

To My Parents and Sisters



## **Acknowledgements**

I would like to express my deep appreciation to my advisor, Professor Stelios Kyriakides, who gave me the opportunity to be a member of his research group. Over the past few years his continuous guidance and support helped me throughout this remarkable journey. His enthusiasm and dedication to researches have been fundamental to my development as a researcher. I would also like to express my gratitude to the members of my supervisory committee for their comments on my work as well as the faculty of the Department of Aerospace Engineering and Engineering mechanics for all they have taught me.

Many thanks owe to staff members Travis Crooks, Joe Edgar, David Gray, Frank Wise, and Jim Williams for their help during my research. The friendship of my fellow graduate students and their help will be remembered forever. The precious advises from seniors, Edmundo Corona, Theodoro Antoun Netto, and Ali Limam, are appreciated.

I am truly grateful for the support of my family. The love and guidance of my parents are essential to every aspect of my life. I could not have made this accomplishment without the faith and unconditional love of my parents and sisters. Special thanks go to Stephanie L. Diaz for her love and encouragement over the years.

The work reported in this dissertation was conducted with the financial support of a group of industrial sponsors through the Joint Industry Project *Structural Integrity of Offshore Pipelines*. This support is acknowledged with thanks.

# **ON THE DESIGN OF SLIP-ON BUCKLE ARRESTORS FOR OFFSHORE PIPELINES**

Publication No. \_\_\_\_\_

Liang-Hai Lee, Ph.D.

The University of Texas at Austin, 2007

Supervisor: Stelios Kyriakides

Offshore pipelines are susceptible to the damage that leads to local collapse. If the ambient pressure is sufficiently high, local collapse can initiate a buckle that propagates at high velocity catastrophically destroying the pipeline. Buckle arrestors are circumferential local stiffeners that are placed periodically along the length of the pipeline. When properly designed, they arrest an incoming buckle thus limiting the damage to the structure to the distance between two adjacent arrestors. Slip-on type buckle arrestors are tight-fitting rings placed over the pipe. They are relatively easy to install and do not require welding. As a result they have been widely used in shallow waters. It has been known that such devices often cannot reach higher levels of arresting efficiency. The somewhat deficient performance is due to the fact that a buckle can penetrate such devices via a folded-up U-mode at pressures that are lower than the collapse pressure of the intact pipe. Because of this they have not seen extensive use in deeper waters. The aim of this study is to quantify the limits in arresting performance of slip-on

buckle arrestors in order to enable expanded use in pipelines installed in moderately deep and deep waters.

The performance of slip-on buckle arrestors is studied through a combination of experiments and analysis. The study concentrates on pipes with lower  $D/t$  values (18-35) suitable for moderately deep and deep waters. The arresting efficiency is studied parametrically through experiments and full scale numerical simulations. The results are used to generate an empirical design formula for the efficiency as a function of the pipe and arrestor geometric and mechanical properties.

The performance of slip-on arrestors is shown to be bounded by the so-called the confined propagation pressure. That is the lowest pressure that U-mode pipe collapse propagates inside a rigid circular cavity. Therefore, a quantitative study of this critical pressure is undertaken using experiments and numerical simulations. A new expression relating this critical pressure to the material and geometric parameters of the liner pipe is developed. This in turn is used to develop quantitative limits for the efficiency of slip-on buckle arrestors.

## Table of Contents

|  |    |
|--|----|
| Chapter 1 Introduction .....   | 1  |
| 1.1 Review of the Arresting Efficiency of Slip-On Buckle Arrestors .....                                 | 4  |
| 1.2 Limits on Slip-On Buckle Arrestor Efficiency .....   | 5  |
| 1.3 Outline of the Present Study .....   | 6  |
| Chapter 2 Experimental Set-Up and Procedure .....  | 8  |
| 2.1 Material Tests.....  | 8  |
| a. Uniaxial Tests.....   | 8  |
| b. Anisotropy Tests.....   | 9  |
| 2.2 Collapse Experiments.....  | 11 |
| 2.3 Experimental Determination of the Tube Propagation Pressure and<br>Arrestor Crossover Pressure ..... | 12 |
| 2.4 Experimental Determination of the Confined Propagation Pressure ....                                 | 14 |
| Chapter 3 Experimental Results .....   | 17 |
| 3.1 Parametric Study of the Crossover Pressure of Slip-On Buckle<br>Arrestors .....                      | 17 |
| a. Effect on the Variation of Arrestor Thickness .....   | 17 |
| b. Effect on the Variation of Arrestor Length.....   | 19 |
| c. Effect on the Variation of Arrestor Material Property.....  | 20 |
| 3.2 Effect of Material Hardening on $P_P$ and $P_{PC}$ .....   | 21 |
| Chapter 4 Efficiency of Slip-On Buckle Arrestors.....  | 23 |
| 4.1 Procedure for Fitting Experimental Data.....   | 24 |
| 4.2 Efficiency Bounds for Slip-On Buckle Arrestors .....   | 26 |
| Chapter 5 Numerical Analysis .....   | 28 |
| 5.1 Numerical Simulation of Arrestor Crossover .....   | 28 |
| a. Finite Element Model .....  | 28 |

|  |     |
|--|-----|
| b. Numerical Results .....                                       | 30  |
| 5.2 Numerical Simulation of Confined Buckle Propagation.....     | 33  |
| a. Finite Element Model .....                                    | 33  |
| b. Numerical Results of 3- <i>D</i> Simulations.....             | 35  |
| c. 2-D Models and Maxwell Construction.....                      | 37  |
| d. Additional Numerical Results .....                            | 38  |
| Chapter 6 Summary and Conclusions.....                           | 41  |
| 6.1 Arresting Efficiency of Slip-On Buckle Arrestors.....        | 41  |
| 6.2 Buckle Propagation in Confined Steel Tubes.....              | 42  |
| 6.3 Recommended Design Procedure .....                           | 44  |
| Tables.....  | 46  |
| Figures.....   | 65  |
| Appendix A: Design of Slip-On Buckle Arrestors: An Example... .. | 111 |
| Appendix B: Error Analysis.....                                  | 113 |
| References .....   | 115 |
| Vita .....   | 117 |

# **Chapter 1**

## **Introduction**

During the last three decades, oil and gas exploration and production offshore has seen a meteoric expansion. Simultaneously significant reserves have been and continue to be discovered in increasingly deeper waters, reaching water depths of 10,000 ft and beyond. Pipelines installed in deep waters are collapse prone due to the ambient external pressure (see Murphey & Langner, 1985; Yeh and Kyriakides, 1986; Kyriakides & Corona, 2007). Collapse is designed against by selecting the wall thickness and the steel grade appropriate for a given diameter. An additional concern is the potential occurrence of a propagating buckle. Propagating buckles are usually initiated from local damage to the pipe and can spread at high velocities if the ambient pressure is higher than the propagation pressure of the pipe. Because the propagation pressure is typically on the order of 15% of the collapse pressure, most pipelines are designed to resist collapse and are protected against catastrophic failure from a propagating buckle by periodic installation of buckle arrestors along the line. Buckle arrestors are usually stiff rings that locally increase the circumferential bending rigidity of the pipe to a level that can stop the spreading of collapse.

Figure 1.1 shows a schematic of a pipeline being installed by S-lay and a possible scenario for initiating and spreading of a propagating buckle. Pipe sections are welded on the lay barge and are paid into the sea over a long boom like support structure, the stinger. On the way to the sea floor, the line acquires the characteristic S-shape shown in the figure. The length and shape of the suspended section are governed by tension applied at the barge. Thus, near the surface of the sea the pipe experiences bending combined with tension. Further down, the tension decreases, while the pressure increases. In the sag bend, the

pipe is mainly under combined bending and external pressure and smaller tension. The curvature of the sagbend is typically kept in the elastic range by the tension applied at the top. Sudden movement of the vessel or loss of tension for whatever reason can result in excessive bending that can lead to local buckling and collapse. Local collapse can, in turn, initiate a propagating buckle as shown in the figure. Such an event flattens the pipe and renders it useless. The extent of damage is illustrated in Fig. 1.2, where the spreading of collapse propagating at the propagation pressure was interrupted, capturing the transition region joining the collapsed and intact sections.

The pipeline shown in Fig. 1.1 is equipped with buckle arrestors installed at regular intervals of a few hundred feet. Properly designed buckle arrestors engage the two propagating fronts of the collapsing pipe and arrest it. The collapse is thus limited to the length of pipe between two arrestors. Part of the pipeline is then retrieved, the collapsed section is repaired and the installation resumes.

Several types of buckle arrestors used in practice are shown in Fig. 1.3. Slip-on type arrestors consist of a tight fitting ring slipped over the pipe (Kyriakides & Babcock, 1980). It is often more practical to leave a gap between the ring and the pipe which is filled with grout (Langner, 1999). The clamped arrestor is a similar concept, in which the ring is split into two parts. The addition of flanges enables installation of the device on a continuous line. Such devices are commonly used in the case of pipeline installed by reel-lay, where several miles of line are prewound on a reel mounted on a seagoing vessel. The line is unwound on site and installed to the sea floor. Arrestors are thus clamped periodically onto the pipeline during the unspooling process (Bell et al., 20001).

The spiral arrestor (Kyriakides & Babcock, 1981) is another concept that was proposed for use in continuous pipelaying. A rod is wound onto the pipe,

forming a spiral as shown in Fig. 1.3. The ends are welded, keeping the spiral tightly wound. This arrestor behaves very much like a slip-on arrestor.

The welded arrestor is similar to the slip-on arrestor, but the ends are welded to the pipe as shown in the figure.

The integral arrestor is a heavier wall section of pipe that is welded periodically into the line between two pipe strings. The inner diameter of the thicker section matches that of the pipe, and the ends are machined to reduce stress concentrations as shown in the figure. Such devices are machined out of thicker wall pipe, but often are forgings finished by machining. This, plus the two extra girth welds, makes it perhaps the most expensive of the arrestor concepts.

The fact that slip-on buckle arrestors do not require welding is a significant advantage both from the point of view of ease of installation and of cost. However, it has been known that such devices often do not reach the highest levels of arresting efficiency (Kyriakides, 2002). The deficient performance is due to the fact that an incoming propagating buckle can penetrate such devices in a characteristic U-mode, shown in Fig. 1.4, at pressures that are lower than the collapse pressure of the pipe. Inadequate understanding of the extent of this deficiency has limited the use of slip-on arrestors to relatively shallow waters, while the integral arrestor has been preferred for deeper waters.

This dissertation addresses two main issues of concern in the design of slip-on buckle arrestors. The original work on slip-on buckle arrestors was experimental and dated back to 1980 (Kyriakides & Babcock, 1980). That study dealt with relatively thin-walled pipes used in shallow waters. A new experimental study is performed, followed by numerical simulation of the quasi-static crossover of such arrestors by propagating buckles. The combined experimental and numerical results are used to generate new design guidelines for such devices. The second issue deals with the limitations of slip-on buckle



arrestors. These are addressed by generating bounds for their performance. The bounds are based on the confined propagation pressure of a pipe inside a stiff contacting circular cavity in the spirit of Kyriakides's recommendations on the subject in 2002.

### 1.1 Review of the Arresting Efficiency of Slip-On Buckle Arrestors

The slip-on buckle arrestor was studied experimentally by Johns et al. (1978) and by Kyriakides & Babcock (1979, 1980) using mainly small diameter tubes and pipes of relatively high  $D/t$  ratios. The arresting performance of buckle arrestors was established as follows: a buckle was initiated in a long tube and propagated quasi-statically under volume-controlled conditions. A ring arrestor placed along the tube eventually engaged the buckle and arrested it, in the process forcing the pressure in the vessel to increase as the volume is increased. At a certain pressure, the buckle crossed the ring; this pressure is defined as the *crossover pressure* ( $P_X$ ) of the arrestor. The main thrust of the experiments was to establish the parametric dependence of the arrestor crossover pressure.

The following definition of arresting efficiency ( $\eta$ ) provides a more general measure of the effectiveness of buckle arrestors:

$$\eta = \frac{P_X - P_P}{P_{CO} - P_P} \quad (1.2)$$

where  $P_{CO}$  and  $P_P$  are the collapse and propagation pressure, respectively (Kyriakides & Babcock, 1979). Thus, an efficiency of 1.0 guarantees that the arrestor maintains the integrity of the downstream pipe until it collapses without influence from the collapsed pipe upstream of the arrestor. By contrast, in the

absence of a buckle arrestor, collapse propagates at the propagation pressure of the pipe and thus the system has an arresting efficiency of zero.

Kyriakides and Babcock [1980] developed an empirical expression for  $\eta$  as a function of the geometric and material parameters of pipes and arrestors. The formula was based on experiments performed mainly on Al-6061-T6 seamless tubes of D/t values in the range of 28.6 to 50. The relatively high D/t values and the use of aluminum limit the applicability of this expression to pipelines installed in shallow waters (as was the custom in the early 1980s). The present study aims to develop new design formulae that are applicable to deepwater pipelines.

## **1.2 Limits on Slip-On Buckle Arrestor Efficiency**

For slip-on type buckle arrestors, arresting efficiency of 1.0 is not always achievable. This is because for standard steel grades, there exists a pipe D/t range for which a buckle penetrates the arrestor at a pressure that is lower than the collapse pressure, irrespective of how long or stiff the arrestor is (Kyriakides, 2002). For example, Fig. 1.4 shows a buckle that penetrated a relatively massive clamp arrestor by folding up in a characteristic “U-mode.” By definition, if the clamp is penetrated, then  $P_X < P_{CO}$ . This point was not emphasized in the early studies. Furthermore, because the majority of the experiments of Kyriakides & Babcock [1980] were conducted on aluminum alloy tubes of relatively high D/ts, this deficiency did not show up in many of the cases considered. Aluminum has a lower elastic modulus, and as a result, the buckling pressure of the tubes used was of the order of 3 times lower than that of steel tubes with the same D/t. Because of the lower collapse pressure, the crossover pressure, which demands on arrestors for aluminum tubes, is significantly lower. Indeed, most arrestors were found to have an efficiency of 1.0 which, as demonstrated in Kyriakides [2002], is often

not the case for steel pipes with the range of  $D/ts$  of interest in deep water applications.

The apparent deficiency in performance of slip-on arrestors is related to an alternate propagating instability affecting shell liners of stiff circular cavities. A third characteristic pressure of long liner tubes exists, known as the *confined propagation pressure* ( $P_{PC}$ ) (Kyriakides, 1986). This is the pressure at which the liner folds up in the U-mode shown in Fig. 1.5 and propagates quasi-statically inside the cavity (Kyriakides, 1986, 1993, 2002). Kyriakides (2002) argued that when  $P_{PC} < P_{CO}$ , a lower bound for the arresting efficiency of such an arrestor is given by

$$\eta_{PC} = \frac{P_{PC} - P_P}{P_{CO} - P_P}. \quad (1.4)$$

One of the goals of the present study is to test the veracity of this idea experimentally. In addition, for this bound to become more widely acceptable, a more accurate expression for  $P_{PC}$  will have to be developed.

### 1.3 Outline of the Present Study

Several sets of experiments are carried out to establish the parametric dependence of the crossover pressure of slip-on arrestors. The experimental set-ups that are developed and associated their procedures are described in Chapter 2. These include the determination of the collapse pressure, propagation pressure, confined propagation pressures of tubes and pipes, and the arrestor crossover pressure. The characterization of mechanical properties of tubes and arrestors used is outlined in the same chapter.

Chapter 3 presents the experimentally measured collapse, propagation and

confined propagation pressures, and the results of the parametric study of slip-on arrestor crossover pressure.

The methodology of developing the new empirical design formula of slip-on buckle arrestors is described in Chapter 4. This is followed by the presentation of an improved empirical expression relating the confined propagation pressure to the material properties, which accounts for the post-yield characteristics of the material, and geometric parameters of the liner tube.

The quasi-static propagation of a buckle in a tube, its arrest by a slip-on buckle arrestor, the subsequent crossing of the arrestor, and the quasi-static propagation of confined collapse have been simulated using finite element models developed in this study. A detailed description of models, and results of simulations of the problems of interest appear in Chapter 5.

Chapter 6 contains a summary of the work along with major conclusions. In addition, a procedure to be used in the design of slip-on buckle arrestors is presented.

## **Chapter 2**

### **Experimental Set-Up and Procedures**

Several sets of experiments were performed in order to establish the crossover pressure of slip-on buckle arrestors and its parametric dependence. This Chapter describes the experimental set-ups and procedures used. The mechanical properties of the tubes and arrestors used had to be determined. The material tests performed are also outlined in this chapter.

#### **2.1 Material Tests**

The tests were performed on small scale, seamless stainless steel (SS-304). Such tubes typically come in 20 ft lengths. The stress-strain response in the axial direction of the tube was measured for each tube used in the structural tests. Seamless tubes can exhibit yield anisotropy introduced by the manufacturing process. Thus, additional tests were performed to characterize such anisotropies when necessary.

##### **a. Uniaxial Tests**

The stress-strain behavior of the tube material was measured using a strip cut along the axis of the tube. The strips were approximately 5.5 inches long and 0.375 inches wide. Two strain gages were mounted on each strip for the purpose of measuring the strain up to a level of about 5%. In addition, an extensometer was used to measure strains up to 15%.

Each specimen was pulled in tension in an electromechanical testing machine at a constant strain rate of about  $10^{-4}$ . During the test, the signals from the strain gages, suitably amplified, the extensometer and the load cell were monitored, and recorded by a computer-operated data acquisition system

(LabVIEW). Post-processing the data involved averaging the signals from the two gages. A typical engineering stress-strain response is shown in Fig. 2.1. In this case, strain gage data shown in Fig. 2.1(a) was recorded up to a strain of 7.5%. By contrast the extensometer data extended to a strain of 16%. The elastic modulus and yield stress of the material were obtained from the strain gage response. The large strain response was obtained from the extensometer data.

The arrestors were machined from a solid round stock. In this case a strip 3 in long, 0.35 in wide, and 0.05 in thick was extracted from the axial direction, and used to measure the mechanical properties of the stock.

## b. Anisotropy Tests

Yield anisotropy in tubes and pipes is adequately represented through Hill's quadratic yield function (Hill, 1948, Kyriakides and Yeh, 1988). The plane stress version of this yield function can be written as

$$f = \sigma_e = \left[ \sigma_x^2 - \left( 1 + \frac{1}{S_\theta^2} - \frac{1}{S_r^2} \right) \sigma_x \sigma_\theta + \frac{1}{S_\theta^2} \sigma_\theta^2 + \frac{1}{S_{x\theta}^2} \sigma_{x\theta}^2 \right]^{1/2} = \sigma_{e \max} \quad (2.1)$$

where  $S_\theta = \frac{\sigma_{o\theta}}{\sigma_{ox}}$ ,  $S_r = \frac{\sigma_{or}}{\sigma_{ox}}$ ,  $S_{x\theta} = \frac{\sigma_{ox\theta}}{\sigma_{ox}}$  and  $\{\sigma_{ox}, \sigma_{or}, \sigma_{o\theta}\}$  are the yield stresses in the respective directions and  $\sigma_{ox\theta}$  is the yield stress under pure shear. These are determined through four independent experiments as described in Appendix B of Kyriakides and Corona, 2007.

In the present study, anisotropy characterization was limited to measuring  $S_\theta$ . This was determined by conducting a *lateral* pressure test on a section of tube as follows: The test was performed in a biaxial servo hydraulic testing machine that was coupled with a closed loop control pressurizing system as shown in Fig.

2.2. A section of tube was mounted in the testing machine using custom circumferential grips shown in the figure. The specimen was filled with a pressurizing fluid such as hydraulic oil. The pressuring unit consists of a 10,000 psi pressure intensifier that operates on standard 3,000 psi hydraulic power. It has its own independent closed-loop control system, and is operated under volume control. A pressure transducer whose output was amplified so that it had an output of 10V at 10,000 psi was used to monitor the pressure. The testing machine was operated in load control. The pressure, axial force, axial strain, and circumferential strain were recorded on a data acquisition system for later processing.

Pure lateral pressure loading was accomplished by providing an axial compressive load to compensate the load due to the internal pressure at the end of the tube ( $PA_i$  where  $A_i$  is the internal cross sectional area of the tube). The output of the pressure transducer, suitably amplified through an inverting amplifier, was used as the command signal for the axial servo-controller. As the pressure in the tube was gradually increased, the actuator moved to maintain the axial force at  $-PA_i$ . In this fashion, the axial force due to internal pressure was reacted by the testing machine, and as a result, the tube experienced stresses  $\sigma_x = 0$ , and  $\sigma_\theta = PR/t$ .

Typically, when anisotropy was present the stress-strain response in the circumferential direction had a somewhat lower yield stress than the one in the axial direction. Figure 2.3 shows a comparison of two such responses from one of the SS-304 tubes used in the structural experiments. The yield stress in the circumferential direction is seen to be lower resulting in  $S_\theta = 0.880$ .  $S_r$  was assumed to be the same as  $S_\theta$  while the material was assumed to exhibit no anisotropies in shear.

## 2.2 Collapse Experiments

The collapse pressure of tubes used in the buckle arrest experiments is required for establishing the arrestor efficiency. For this reason at least one collapse test was conducted for each set of tubes used. A section of tube typically  $20D$  long was used in such tests. Several diameter measurements were made at intervals of about  $4D$  in length. The mean value of the measurements was designated as the diameter of the tube ( $D$ ). At each location the ovality was established as follows:

$$\Delta_o = \frac{D_{\max} - D_{\min}}{D_{\max} + D_{\min}}. \quad (2.2)$$

The biggest value in the set was designated as the ovality of the tube ( $\Delta_o$ ).

Wall thickness measurements were performed at each end of the tube. The average value of the measurements was designated as the thickness of the tube ( $t$ ). Wall eccentricity parameters were also established from the measurements as follows:

$$\Xi_o = \frac{t_{\max} - t_{\min}}{t_{\max} + t_{\min}}. \quad (2.3)$$

The eccentricity of the tube ( $\Xi_o$ ) is the biggest value of the two measured values.

The tube was sealed at both ends with plugs, and placed inside the pressure vessel. The experimental set-up used is shown schematically in Fig. 2.4. The vessel is vertically arranged, and has inner diameter and length of 3 in and 68.5 in respectively. It has a pressure capacity of 10,000 psi. Once the specimen was installed, the vessel was sealed and the cavity was completely filled with



water. The system was pressurized using a positive displacement pump which discharges water into the system at a nearly constant rate. This loading can be considered to approximate volume-controlled loading. The pressure of the system was monitored by pressure gages and a pressure transducer. It was recorded via a computer operated data acquisition system as well as a strip-chart recorder (see Fig. 2.4).

In such a test the pressure typically rises nearly linearly as shown in the pressure-time history in Fig. 2.5. Collapse is sudden and catastrophic and results in the formation of a locally flattened section as shown in Fig. 2.6. The maximum pressure recorded is defined as the collapse pressure ( $P_{CO}$ ).

### **2.3 Experimental Determination of the Tube Propagation Pressure and Arrestor Crossover Pressure**

An effective buckle arrestor should arrest a propagating buckle propagating at a pressure corresponding to the maximum water depth of a given pipeline. This pressure usually lies between the propagation pressure ( $P_P$ ) of the pipe and its collapse pressure ( $P_{CO}$ ). The main objective of this set of experiments was to establish parametrically the effectiveness of slip-on rings as buckle arrestors. The test facilities and experimental procedure used are described in the following.

The experiments were carried out in the same facility as the collapse tests. The tubes used in the experiments were measured in the same manner to obtain the geometric parameters. The arrestor rings were machined from either a solid SS-304 stock (A4) or from a thick tube of the same material (A3). The rings were machined individually to slip-fit over the tube on which they were mounted, and great care was taken to ensure not hardening the arrestor material during

machining. The dimensional tolerance allowed for the arrestor was  $10^{-3}$  in for arrestor length, and  $0.5 \times 10^{-3}$  in for arrestor thickness.

Arrestors were usually tested in pairs using the experimental set-up shown in Fig. 2.7. The test specimen usually had an overall length of 48 tube diameters. The two arrestors were placed far enough apart on the tube so as not to influence each crossover event. After mounting the rings on the tube, it was sealed at both ends with solid plugs. A dent was induced at one end (about  $5D$  from the plug) in order to initiate local collapse. In order to keep the length of tube that collapses initially to a minimum, the dent should be large enough. After placing the specimen in the vessel it was filled with water and pressurized using a pump that discharges a nearly constant volume of water per unit time.

A typical pressure history from Exp. No. 2 on a tube with nominal  $D/t = 25.5$  is shown in Fig. 2.8(a). A sequence of deformed configurations corresponding to the points identified on the response with numbered flags is shown schematically in Fig. 2.8(b). The exact parameters of the tube and arrestors involved are given in Table 3.5. The pressure initially rises sharply with time until the dented section collapses at a pressure of approximately 770 psi. Collapse is accompanied by a sharp drop in pressure. The resulting unloading of the closed system makes fluid available for spreading the collapse. The high stiffness of the vessel and the relatively small volume of pressurizing fluid limited the extent of this initial spreading of collapse. Subsequently, the collapse propagates essentially quasi-statically at a rate dictated by the rate at which water is pumped into the closed system. The first pressure plateau represents the *propagation pressure* ( $P_P$ ) of the tube, which in this case was 507 psi. The propagating collapse eventually engages the first arrestor and stops, causing a rise in pressure. The rise is not instantaneous, because as the pressure increases the collapsed section flattens further. At a pressure indicated in the figure by  $P_{X1}$  the buckle crosses the

arrestor. This pressure is defined as the *crossover pressure* ( $P_X$ ) of the arrestor. The pressure drops, but in quasi-static manner for this particular arrestor. Continued pumping of water into the system spreads the collapse to the second arrestor where it is once more halted. The pressure rises to a level of  $P_{X2}$ , when the second arrestor is crossed. This crossover event is accompanied by dynamic drop in pressure. The experiment is terminated at this stage, and the test specimen is removed from the vessel.

Buckles crossed slip-on buckle arrestors in two modes. Relatively thin and short arrestors, like the first one in Exp. No. 2, were deformed by flattening by the incoming buckle as shown in the photograph in Fig. 2.9a. In the process, the tube just downstream of the arrestor ovalized, and at some stage allowed the buckle to cross. This particular arrestor crossed the arrestor at a pressure of  $P_{X1} = 1.507P_P$ . Relatively thick and long arrestors were not deformed significantly by the incoming buckle. Instead, the collapsed pipe folded up, and crossed the ring in the characteristic U-mode shown in Fig. 2.9b. This mode of crossing was observed in the second arrestor of Exp. No. 2 in which the crossover pressure was  $P_{X2} = 2.639P_P$ . A third mode in which the arrestor is crossed by flipping of the mode of collapse by  $90^\circ$ , as reported in Kyriakides and Babcock (1980), was not obtained in this study. This mode was observed to take place in the past for relatively short and stiff arrestors. In the present study, all arrestors tested were  $0.5D$  long or longer.

## 2.4 Experimental Determination of the Confined Propagation Pressure

As mentioned in Chapter 1 slip-on buckle arrestors often are incapable of achieving efficiency of 100% irrespective of how long, thick or stiff they are made. Collapse penetrates them in the U-mode at a pressure that is lower than the collapse pressure of the downstream tube. Kyriakides (2002) showed that the so-

called the *confined propagation pressure* ( $P_{PC}$ ) can serve as a dependable lower bound of arresting efficiency. Because of the importance of  $P_{PC}$  in arrestor design, in this study the subject was revisited in order to develop a more dependable relationship for  $P_{PC}$ . A number of quasi-static confined propagation tests were conducted to enrich the previously developed database. The procedure followed is described next.

The confined buckle propagation experiments were conducted in the manner first set up in Kyriakides (1986). The test specimen was  $50D$  to  $60D$  long depending on the  $D/t$  of the tube. It was placed concentrically inside a thick steel shell as shown in Fig. 2.10(a). The specimen surface was first lubricated. Subsequently, the annulus between the tube and the steel shell was filled with plaster of Paris for higher  $D/t$  tubes, or with Portland cement for lower  $D/t$  specimens. Close fitting aluminum centralizing rings were used at the two ends of the mold. This arrangement leaves a section approximately 20 tube diameters long outside the mold. The free end of the tube was dented as shown in the figure in order to help initiate local collapse. Once the grout was cured, the whole assembly was placed in a pressure vessel as shown in Fig. 2.10(b).

The pressure vessel has a 7 in internal diameter, a length of 13 ft and a pressure capacity of 9,000 psi. It is pressurized with water using a constant discharge pump. The pressure was monitored in the same manner used in the collapse experiments.

A typical pressure-time history from such an experiment is shown in Fig. 2.11. At pressure  $P_I$  the dented section collapses initiating a propagating buckle in the unconfined section of tube. The buckle propagates quasi-statically in the typical “dogbone” collapse mode. In the process, it traces a pressure plateau, which represents the propagation pressure ( $P_P$ ) of the tube. The buckle stops propagating once it reaches the edge of the confined section ( $t_3$ ). Continued

pumping of water into the vessel leads to a relatively sharp rise in pressure. The pressure does not increase instantaneously, because a finite volume of water is required to further flatten the already collapsed section of tube and to expand the vessel. The confined part of the tube remains virtually undisturbed until the collapsed section at the entrance of the confinement snaps into a U-shape, enabling the buckle to start penetrating the confinement ( $t_4$ ). The pressure at which this occurs ( $P_{IC}$ ) is usually the highest pressure experienced during such an experiment.  $P_{IC}$  represents the initiation pressure of the confined propagating buckle under the particular experimental conditions described here. In some experiments  $P_{IC}$  was not well-defined as it was affected by the tightness of the ring at the entrance of the confinement.

The profile of steady-state confined propagation is fully developed within about five tube diameters from the edge of the confinement. The profile of the buckle connecting the U-shaped collapsed section behind it and the circular tube ahead of it is relatively short (2.5 tube diameters long for the case in Fig. 2.12). This implies that, in addition to bending deformations, parts of the profile undergo significant stretching. Note also that for the case shown in the figure the walls of the collapsed cross section are in contact for a significant part of the perimeter. This again is a sign of very significant deformation. The corresponding experimental responses are shown in Fig. 2.13. As the buckle reaches steady-state propagation, the pressure stabilizes at a new plateau. The rate at which water was discharged into the vessel was maintained constant until most of the tube had collapsed. The value of the second pressure plateau is defined as the *confined propagation pressure* ( $P_{PC}$ ) of the tube. It is emphasized that the steady-state confined propagation process is independent of the initiation process. By contrast, the confined initiation pressure ( $P_{IC}$ ) depends on the condition of the entrance of the confinement. In Fig.2.13 the confined initiation pressure is not defined.

## Chapter 3

### Experimental Results

#### 3.1 Parametric Study of the Crossover Pressure of Slip-On Buckle Arrestors

The crossover pressure ( $P_X$ ) of arrestors was studied parametrically through experiments by varying the major non-dimensional parameters of the problem. If the arrestor is too short, the buckle crosses over via the flipping mode at pressures lower than  $P_{CO}$  (see Fig. 4c in Kyriakides, 2002). The shortest arrestor required to avoid this depends on the tube  $D/t$  and its material properties. In this study the length was selected to be  $\geq 0.5D$ . Stainless steel tubes (SS-304) of three different  $D/t$  ratios in the range of 18 to 35 were used in these experiments. The material properties of tubes used were measured as described in §2.1, and are summarized in Table 3.1. The yield stresses of the tubes ranged between 38 and 56 ksi. The majority of the experiments were conducted using an arrestor material with a yield stress of 41.6 ksi. A select number of tests were conducted using a second arrestor material with a yield stress of 86.2 ksi. The stress-strain responses of two arrestor materials are compared in Fig. 3.1. Their major parameters are listed in Table 3.2.

Two major sets of tests were performed for each of three tubes  $D/t$  ratios. In the first set, the arrestor length was kept constant, and the thickness was varied; in the second series, the thickness was held fixed, and the length was varied.

##### a. Effect on the Variation of Arrestor Thickness

Figure 3.2(a) shows a set of experimental results for tubes with a nominal  $D/t$  of 25.5. Here the length of the arrestor was  $0.5D$ , while the arrestor thickness ( $h$ ) was varied from about  $0.65t$  to  $3.0t$ . The crossover pressure is seen to increase in a powerlaw manner with  $h$ . The monotonic increase with  $h$  stops at around

$2.53t$ . Further increase in  $h$  is seen to produce the same crossover pressure of about  $P_X \approx 3.3P_P$ . The U-mode crossover occurs irrespective of the arrestor thickness. Included in the figure is the calculated collapse pressure based on the average geometric and material properties of the tubes used in this series of tests ( $\bar{P}_{CO} = P_{CO}/P_P = 5.184$ ). Clearly, for this combination of pipe geometric and material parameters the slip-on arrestor does not develop an efficiency of more than about 0.53.

It is interesting to test the validity of the two bounds in arrestor performance based on  $P_{IC}$  and  $P_{PC}$  as suggested in Kyriakides (2002) (see Chapter 4 for details). The two tube characteristic pressures were estimated from the empirical relationships from the following empirical relationships using the mean values of  $D$ ,  $t$  and  $\sigma_o$  for the tubes involved in these tests (Kyriakides 1986, 2002):

$$\frac{P_{EE}}{\sigma_o} = A \left( \frac{t}{D} \right)^\beta. \quad (3.1)$$

where  $\sigma_o$  is the yield stress of the material. The parameter  $A$  and  $\beta$  obtained from least squares fits of data listed in Table 3.3 along with the corresponding (multiple) correlation coefficients ( $R^2$ ).  $P_P$  was based on the average value measured in the tests involved. The two bounds represented by  $\bar{P}_{IC}$  ( $=P_{IC}/P_P$ ) and  $\bar{P}_{PC}$  ( $=P_{PC}/P_P$ ) are included in the plot, and are listed in Table 3.4. They are seen to bound the maximum arrestor performance quite well.  $\bar{P}_{PC}$  is a bit conservative while  $\bar{P}_{IC}$  is closer to the actual performance.

Figures 3.3(a) and 3.4(a) show similar plots for tubes with respective nominal  $D/t$  values of 19.2 and 34.7. The arrestor thickness was varied from  $0.65t$

to  $3.31t$  for the first and from  $0.84t$  to  $4.25t$  for the second. Once again the powerlaw increase of  $P_X$  with  $h$  can be seen in the figures, and is bounded by these two the confined initiation and propagation pressures,  $P_{IC}$  and  $P_{PC}$ . For tubes with the nominal  $D/t = 19.2$  the maximum arresting efficiency was about 0.76, and the corresponding crossover pressure was around  $P_X = 3.3P_P$ . For tubes with the nominal  $D/t = 34.7$  the crossover pressure ceases to increase at a pressure level about  $P_X = 3.4P_P$ , corresponding to an arresting efficiency of approximately 0.61. The data once more are seen to agree well with these two bounding pressures. The experimental results of this series are listed in full detail in Tables 3.5-3.7.

#### **b. Effect on the Variation of Arrestor Length**

In the second series of experiments the arrestor thickness was kept constant while the arrestor length was varied. The constant arrestor thickness of each set was chosen based on the results from the experiments of the first series. In the case of tubes with nominal  $D/t = 25.5$ , the arrestor thickness was set at  $1.73t$  inches while the arrestor length was varied from  $0.04D$  to  $1.199D$ . Results showing how the crossover pressure depends on the arrestor length for this tube  $D/t$  are shown in Fig. 3.2(b).  $P_X$  increases nearly linearly with  $L$ . (A similar trend was observed in Kyriakides and Babcock [1980] in experiments on aluminum tubes and arrestors.) The crossover pressure stops increasing after a length of about one tube diameter; it peaks at around the same pressure level as the results in Fig. 3.2(a). Further increase in  $L$  has no effect on the arrestor performance. The bounds on the maximum performance based on  $P_{IC}$  and  $P_{PC}$  were estimated in the manner discussed above, and are included in the plot. Again, they are seen to bound nicely the three experimental points at maximum arrestor performance.



Similar plots for tubes with respective nominal  $D/t$  values of 19.2 and 34.7 are shown in Fig 3.3(b), and Fig. 3.4(b). Both plots show the same linear dependence of crossover pressure on the arrestor length. In Fig. 3.4(b) the two bounds of arrestor performance are once more seen to agree with the trend of the experimental results. By contrast, in Fig. 3.3(b) the experimental points corresponding to the maximum crossover pressure fall somewhat lower than both the  $P_{IC}$  and  $P_{PC}$  bounds. This particular set of tubes had wall thickness eccentricities, which were consistently larger than those of other tubes in this  $D/t$  category. We established that this could influence all three of the characteristic pressures involved in establishing the bounds. We thus suspect that this effect may be responsible for the discrepancy between the bounds and the measured maximum values of  $P_X/P_P$ . The experimental results of this series are listed in detail in Tables 3.8-3.10.

### c. Effect on the Variation of Arrestor Material Property

In the study of the arresting efficiency of slip-on type buckle arrestors the arrestor rings were mainly machined from a thick SS-304 tube of the same material (A3) with a yield stress of 41.6 ksi. In order to assess the effect of the yield stress of the arrestor material on the crossover pressure, an additional set of tests were performed using a SS-304 arrestor material (A4) with a yield stress of 86.2 ksi. These tests were performed on tubes with nominal  $D/t = 25.5$ . The arrestor length was kept constant at  $L = 0.5D$ , and the arrestor thickness was varied from about  $0.815t$  to  $2.080t$ .

The measured crossover pressures are listed in Table 3.11 and are plotted against  $h/t$  in Fig. 3.5. Included in the figure are corresponding data obtained from the same tube  $D/t$  for arrestor material A3 (with the lower yield stress). The usual powerlaw dependence of the crossover pressure ( $P_X$ ) on the arrestor thickness ( $h$ )

is observed for both sets of results. However, for the higher yield stress arrestors, a lower thickness is required to achieve a chosen crossover pressure. The tubes used had approximately the same mechanical properties. Since the bounding pressure ( $\bar{P}_{IC}$ ) depends strictly on the tube geometry and material properties, the two sets of tubes have similar values. Material A4 reaches the bounding pressure at  $h = 1.76t$  whereas material A3 achieves this crossover pressure at  $h = 2.53t$ . Once again we observe that increasing the arrestor wall thickness beyond these values does not produce a higher crossover pressure.

### 3.2 Effect of Material Hardening on $P_P$ and $P_{PC}$

The maximum performance of slip-on type buckle arrestors measured experimentally has confirmed that the confined initiation and propagation pressures can be used to generate bounding limits for the efficiency of slip-on type buckle arrestors. In view of the importance of these characteristic pressures, a new set of experiments was conducted in order to enrich previously developed data, and thus enable the development of more accurate empirical expressions for them. In particular, the new experiments were conducted using stainless steel materials that exhibited a lower hardening than the previous set as described below.

Table 3.12 (Set II) lists eleven sets of confined and unconfined propagation pressures first reported in (Kyriakides, 2002). Included are the yield stress and post yield modulus ( $E'$ ) of the SS-304 material used.  $P_P/\sigma_o$  and  $P_{PC}/\sigma_o$  were then fitted to powerlaw fits of  $D/t$  as mentioned in Eq. (3.1). It has been long known that the post-yield hardening of the material can affect these characteristic pressures (Dyau and Kyriakides, 1993). The simplest extension of these fits is to include a term that approximately represents the post-yield modulus of the material. This was pursued by fitting the post-yield part of the stress-strain

data linearly from the yield strain to a strain of about 10%. The slope of this line, depicted as  $E'$ , is included in Table 3.12. The range of  $D/t$  ratio in experimental Set II was approximately from 14.5 to 45.9. The yield stress of this set of tubes ranged between 38 and 58 ksi, and the post-yield slopes varied between 195 and 280 ksi.

The new set of experiments (Set III) was conducted on SS-304 1/8 Hard tubes. This alloy has a higher yield stress and significantly lower hardening as illustrated in the comparison of two typical stress-strain responses of the two materials in Fig. 3.6. Five tests were conducted on tubes with nominal  $D/ts$  that ranged between 19.25 and 37.46. The yield stresses of this set ranged from about 81 to 99 ksi while the post yield moduli ranged from 70 to 99 ksi.

The measured values of  $P_P/\sigma_o$  and  $P_{PC}/\sigma_o$  from Set II and Set III are plotted against  $D/t$  in log-log scales in Fig. 3.7. Powerlaw fits of the type given in Eq. (3.1) are also included in the figure. The parameter  $A$  and  $\beta$  obtained from least squares fits of each set of data listed in Table 3.13 along with the corresponding (multiple) correlation coefficients ( $R^2$ ). As observed in (Kyriakides, 1986, 1994, 2002),  $P_{PC}$  is significantly higher than  $P_P$ . For both characteristic pressures, the main effect of the lower hardening slope of data Set III is a shift of the data downwards. This suggests that a more accurate representation of the two characteristic pressures must include a measure of the post-yield hardening. Such a fit will be presented in Chapter 4.

## Chapter 4

### Efficiency of Slip-On Buckle Arrestors

The arresting performance of slip-on buckle arrestors will now be established using the arresting efficiency ( $\eta$ ) introduced in Kyriakides and Babcock [1980] defined as follows:

$$\eta = \frac{P_X - P_P}{P_{CO} - P_P}. \quad (4.1)$$

where  $P_X$  is the crossover pressure of the arrestor, and  $P_{CO}$  and  $P_P$  are the collapse and propagation pressures of the pipe respectively. Thus, an arresting efficiency of 1 means that an incoming buckle is held, and arrested until the collapse pressure is reached, at which level the intact downstream section of pipe collapses without any influence from the collapsed section upstream. On the other hand, the arresting efficiency is zero in the absence of the arrestor.

We will now use the experimental results to develop an empirical relation of arresting efficiency as a function of all problem parameters. Following the procedure of Kyriakides and Babcock [1980], dimensional analysis considerations result in the following parametric dependence of  $P_X$  (parameters defined in Fig. 4.1):

$$\frac{P_X}{P_P} = F\left(\frac{E}{\sigma_o}, \frac{\sigma_{oa}}{\sigma_o}, \frac{D}{t}, \frac{L}{t}, \frac{h}{t}\right). \quad (4.2)$$

Alternatively, it can be expressed in terms of the following series:

$$\frac{P_X}{P_P} = \sum_{n=0}^N A_n \left[ \left( \frac{E}{\sigma_o} \right)^{\alpha_1} \left( \frac{\sigma_{oa}}{\sigma_o} \right)^{\alpha_2} \left( \frac{D}{t} \right)^{\alpha_3} \left( \frac{L}{t} \right)^{\alpha_4} \left( \frac{h}{t} \right)^{\alpha_5} \right]^n. \quad (4.3)$$

For physical consideration  $\frac{P_X}{P_P} \geq 1$ , thus  $A_0 = 1$ . As in the Kyriakides and Babcock [1980], just the first term of the series is considered leading to

$$\frac{P_X}{P_P} \approx 1 + A_1 \left( \frac{E}{\sigma_o} \right)^{\alpha_1} \left( \frac{\sigma_{oa}}{\sigma_o} \right)^{\alpha_2} \left( \frac{D}{t} \right)^{\alpha_3} \left( \frac{L}{t} \right)^{\alpha_4} \left( \frac{h}{t} \right)^{\alpha_5}. \quad (4.4)$$

Using (4.1), the arresting efficiency can be then be written as follows:

$$\eta \approx \frac{A_1 \left( \frac{E}{\sigma_o} \right)^{\alpha_1} \left( \frac{\sigma_{oa}}{\sigma_o} \right)^{\alpha_2} \left( \frac{D}{t} \right)^{\alpha_3} \left( \frac{L}{t} \right)^{\alpha_4} \left( \frac{h}{t} \right)^{\alpha_5}}{\left( \frac{P_{CO}}{P_P} - 1 \right)}. \quad (4.5)$$

The constants  $A_1$ , and  $\alpha_i$ ,  $i=1,5$ , are evaluated from the experimental data.

#### 4.1 Procedure for Fitting Experimental Data

The exponent  $\alpha_5$  is evaluated first using the experimental results in which the arrestor thickness was varied. Figure 4.2(a) shows plots of  $P_X/P_P$  vs.  $(h/t)^{\alpha_5}$  for three tubes of different  $D/t$  using arrestor material A3. For  $\alpha_5 = 2.1$  the three sets of results fall on linear trajectories. For  $D/t$  of 19 and 34, the results merged quite well, whereas the slope of the  $D/t = 25$  data is different. This

discrepancy is caused by differences in the mechanical properties of the three sets of tubes.

Figure 4.2(b) shows the same plot but with results from arrestor material A4 included. A4 had a yield stress of 86.8 ksi whereas A3 yielded at 41.6 ksi. This difference is accounted for with the parameter  $(\sigma_{oa}/\sigma_o)^{\alpha_2}$ . In Fig. 4.3 the crossover pressure is plotted against  $(\sigma_{oa}/\sigma_o)^{0.8}(h/t)^{2.1}$  and the four sets of data have bundled together.

We next consider the experiments in which the arrestor length was varied while keeping all other parameters constant. Figure 4.4 shows a plot of  $P_X/P_P$  vs.  $(L/t)^{\alpha_4}$ .  $\alpha_4 = 0.98$  results in the three sets of results falling together in nearly linear trajectories. All the data from two sets of experiments mentioned so far are plotted together against  $(\sigma_{oa}/\sigma_o)^{0.8}(h/t)^{2.1}(L/t)^{0.98}$ . Each set of data is nearly linear, but the different sets exhibit some scatter. This scatter can be reduced by including parameter  $(D/t)^{\alpha_3}$ . Figure 4.5(b) shows that all the data come together in a nearly linear trajectory when  $\alpha_3 = -0.75$ .

The final parameter  $(E/\sigma_o)$  was dropped because  $E$  did not vary significantly in the experiments.

Using these parameters determined from experimental data, the arresting efficiency of a slip-on type buckle arrestor can be expressed as

$$\eta = \frac{A_1 \left( \frac{\sigma_{oa}}{\sigma_o} \right)^{0.8} \left( \frac{t}{D} \right)^{0.75} \left( \frac{L}{t} \right)^{0.98} \left( \frac{h}{t} \right)^{2.1}}{\left( \frac{P_{CO}}{P_P} - 1 \right)}. \quad (4.6)$$

The collapse pressures used for determining the arresting efficiency were obtained from experiments, for all cases that it was available. Otherwise, the collapse pressure was calculated from BEPTICO [1994] using the individual tube mechanical and geometric properties. The propagation pressures used were the ones recorded in the experiments.

The efficiency is plotted against the RHS of Eq. (4.6) in Fig. 4.6. The data are seen to have coalesced reasonably well to form a linear band. The least squares linear fit of the data, which has a correlation coefficient ( $R^2$ ) of 0.9349, is shown in the figure. It has a slope of  $A_1 = 0.3211$ . Unlike the similar plot for the integral arrestor (Park and Kyriakides, 1997), in this case the efficiency stops well below 1.0. Consequently, in design, this empirical fit must be used in conjunction with one or both of the efficiency bounds as described in Chapter 6. The uncertainty in the arresting efficiency calculated through Eq. (4.6) is estimated for three representative examples in Appendix B. The same procedure is applicable to any use of the formula.

## 4.2 Efficiency Bounds for Slip-On Buckle Arrestors

The maximum efficiency of slip-on type buckle arrestors depends only on the mechanical properties and geometries of the tubes, and it is independent of the material properties and the dimension of the arrestor as long as the arrestor is long and stiff enough (Kyriakides, 2002). It has been shown in experiments that the confined propagation ( $P_{PC}$ ) can serve as the lower bound of the performance of slip-on type buckle arrestors while the confined initiation pressure is a good upper bound. Empirical formulae of these characteristic pressures were first established in Kyriakides [1986, 1994], and extended in [2002].

The results in Chapter 3 further extended the databases to include the parameter ( $E'/\sigma_o$ ) as follows:

$$\frac{P_{\Xi\Xi}}{\sigma_o} = \left[ B + C \frac{E'}{\sigma_o} \right] \left( \frac{t}{D} \right)^\beta. \quad (4.7)$$

Table 4.1 gives fit parameters of Eq. (4.7) for the two characteristic pressures. The fit parameters were established from the experimental data, which was enriched with numerical results generated in Chapter 5.



## Chapter 5

### Numerical Analysis

#### 5.1 Numerical Simulation of Arrestor Crossover

##### a. Finite Element Model

The quasi-static propagation of a buckle in a tube, its arrest by a slip-on buckle arrestor, and the subsequent crossing of arrestor have been simulated using a finite element model developed within nonlinear the FE code ABAQUS/6.1. The general geometric characteristics of the model are shown in Fig. 5.1. The model consists of a tube of diameter  $D$  and wall thickness  $t$ . It has an upstream section of length  $L_1$ , a downstream section of length  $L_2$ , and the section around the arrestor of length  $L$ , chosen to correspond to the length of the arrestor. The boundary conditions used are guided by the pipe deformation seen in the experiments. The buckle crosses the arrestor in the two modes discussed in Chapter 2: the flattening mode and the U-mode. For both modes, plane 1-2 is assumed to be a plane of symmetry. Furthermore, as in past buckle arrestor models (Park & Kyriakides, 1997; Olso & Kyriakides, 2003), a local imperfection is added in the neighborhood of  $x_1 = 0$ , and the plane 2-3 is also assumed to be a plane of symmetry. The end of the tube at  $x_1 = (L_1 + L + L_2)$  has radially fixed boundary conditions, but is free to expand axially. The local imperfection has the following form:

$$w_o(\theta) = -\Delta_o \left( \frac{D}{2} \right) \exp \left[ -\beta \left( \frac{x_1}{D} \right)^2 \right] \cos(2\theta). \quad (5.1)$$

where  $w_o$  is the radial displacement, and  $\theta$  is the polar angular coordinate (measured from  $x_2$ ). Typical imperfection parameters used are  $\Delta_o = 0.02$  and  $\beta = 4.6$  (this allows the imperfection decay to zero in a length of one tube diameter).

In the typical case that will be discussed below,  $L_1$  was  $9.5D$ , and  $L_2$  was  $6.6D$ . The tubes and the arrestors were discretized by three-dimensional, 27-node quadratic brick elements with reduced integration (*C3D27R*). Two elements were used through the thickness of the tube and two through the thickness of the arrestor. In the case of the tube, the elements have the following angular spans in the top quadrant: starting from the  $x_2$ -axis  $5^\circ$ - $7.5^\circ$ - $7.5^\circ$ - $7.5^\circ$ - $6.7^\circ$ - $6.7^\circ$ - $6.7^\circ$ - $10^\circ$ - $10^\circ$ - $10^\circ$ - $5^\circ$ - $5^\circ$ - $5^\circ$ - $5^\circ$ . The mesh of the bottom quadrant is symmetrical to that of the top. In the axial direction, the upstream section of the tube has twenty  $0.4D$  long elements, followed by six  $0.2D$  elements and two  $0.15D$  elements adjacent to the arrestor. Below the arrestor five  $0.2L$  elements were used. In the downstream section, four  $0.15D$  elements were used next to the arrestor, the next eight were  $0.5D$  long, and two were one diameter long. The arrestor was discretized axially with four equal length elements. In the circumferential direction, the elements in the top quadrant were at:  $5^\circ$ - $7.5^\circ$ - $7.5^\circ$ - $12.5^\circ$ - $12.5^\circ$ - $12.5^\circ$ - $12.5^\circ$ - $7.5^\circ$ - $7.5^\circ$ - $5^\circ$ . In the lower quadrant the distribution was symmetric. This distribution of elements was determined from the usual convergence studies.

The contact between the tube and the arrestor is a challenging issue for slip-on buckle arrestors. The interaction between the tube and the arrestor depends on the stiffness of each component, and the friction between them. Proper modeling of the friction was necessary in order to avoid rigid-body motion or over-constraining of the arrestor.

Contact between the walls of the collapsing tube and between the tube and the arrestor was modeled by using surface-based contact; the strict master-slave algorithm was adopted. In this scheme, the specified master surface is defined

internally by the code as a surface, whereas the slave surface is defined by the surface nodes. The contact direction is always normal to the master surface, and the slave nodes are constrained not to penetrate into the master surface. Both small sliding and finite sliding options were used. Small sliding was used between the arrestor (master: coarse mesh) and the tube (slave: fine mesh) while this contact was frictional (the friction coefficient was chosen to be 0.4). Finite sliding was prescribed between the collapsing walls of the tube.

The materials of the tubes and arrestors were modeled as  $J_2$ -type, elastoplastic, finitely deforming solids that harden isotropically. The anisotropic yielding observed in the experiments was treated through Hill's anisotropic yield function (ABAQUS Manual). It was assumed that the through thickness and transverse yield stresses were the same, but generally lower than the yield stress in the axial direction by the factor  $S$  established in the experiments. The models were calibrated to multilinear approximations of the true-logarithmic strain versions of the measured stress-strain response of the tube and the arrestor materials.

A “volume-controlled” loading procedure was adopted using the hydrostatic fluid elements of ABAQUS (a combination of  $F3D3$  and  $F3D4$ ). These elements allow prescription of the change in volume inside a control region defined around the structure. The pressure becomes an additional unknown, while the volume change is enforced as a constraint via the Lagrange multiplier method.

## **b. Numerical Results**

Results from a typical simulation on a tube with a  $D/t = 25.43$  are shown in Fig. 5.2. The simulation corresponds to Exp. No. 5b and the properties of tube PIP45 (see Table 3.1). The arrestor length was  $L = 0.5D$ , and its thickness was  $h = 2.87t$ . Figure 5.2(a) shows the calculated pressure ( $P$ ) vs. the change in volume

response ( $\delta v/v_o$  where  $v_o$  is the initial volume of the artificial cavity formed around the specimen). Figure 5.2(b) shows the initial and a sequence of deformed configurations corresponding to the numbered points on the response. The main characteristics of the calculated response are similar to those that were seen in the experiments. The structure is initially relatively stiff, and the pressure rises sharply. This terminates into a limit load, which corresponds to the onset of local collapse in the region that has the geometric imperfection as illustrated in configuration ①. The value of the pressure maximum is governed by the amplitude and extent of the local imperfection, and does not affect subsequent events. With the pressure dropping, the local collapse grows, until in configuration ②, the walls of the tube come into contact. Local collapse is arrested, and the buckle starts to spread down the tube as seen in configurations ③ and ④. The spreading of collapse reaches the steady state, represented by the relatively flat pressure plateau that is traced in the neighborhood of configuration ③.

The pressure plateau at a level of 467 psi is the propagation pressure of the tube. This compares with the measured value of 472 psi. As the collapse approaches the ring arrestor, its stiffening effect is felt, the buckle is arrested, and the pressure starts to rise sharply as in the experiments. Configuration ④ shows that the buckle essentially stopped. As the pressure rises further, the buckle front starts folding up, going from the doubly symmetric shape of steady-state propagation to the singly symmetric U-shape seen in configuration ⑤. At a pressure of 1521 psi, the U-shaped collapse penetrates the arrestor with relatively little visible deformation of the arrestor. The crossover is followed by a precipitous drop in pressure back down to the propagation pressure level. This calculated value of crossover pressure ( $\hat{P}_X$ ) is 35 psi or 2.3% lower than the measured value (Table 5.1). The simulation is carried past the crossover pressure

to better capture the crossover mode, which is illustrated in configuration ⑥. It is comparable to the experimental one in Fig. 2.9(b), though in that case the collapse propagated further downstream of the arrestor.

The model was used to carry out direct simulations of several of the experiments conducted. For numerical expediency in these simulations, the length of the upstream section  $L_1$  was usually reduced to  $5D$ . This limited and often masked steady-state propagation of the collapse, but did not otherwise affect the crossover event. Predicted crossover pressures for many of the cases ( $D/t = 25.5$ ) are included in the Table 5.1. They are also plotted together with the corresponding experimental results in Fig. 5.3. Overall, the comparison between experimental and predicted crossover pressures is very favorable. For this set of results the absolute difference ranged from 1%-7.8%.

Additional simulations were conducted for experiments on the other two tube  $D/t$  values used in the study. The predicted crossover pressures are compared to the experimental results in Table 5.2. The predictions are uniformly of good quality, which raises confidence in the numerical model developed. The numerical results are also compared to the experimental ones in Fig. 5.4.

An alternate model was also developed in which the tube is discretized with 8-noded linear elements with full integration ( $C3D8$ ). In this case, four elements were used through the thickness, and the mesh was much more refined than the one shown in Fig. 5.1 (27192 linear elements vs. 1612 quadratic elements for the tube). The predictions for the cases presented here were of comparable accuracy. However, in parametric studies of the problem the model with linear elements was found to be more robust. Crossover pressure results from this model for tubes with nominal  $D/t = 25.5$  are included in Table 5.3.

## 5.2 Numerical Simulation of Confined Buckle Propagation

### a. Finite Element Model

During the last 20 years, three levels of modeling of increasing accuracy have been used to estimate the propagation pressure of unconfined tubes (Kyriakides, 1993). The first involves kinematically admissible collapse mechanisms where the deformation is concentrated in plastic hinges. Here, the work done by the pressure is assumed to be balanced by the energy expended in the hinges. The first example of this class of models is the four-hinge model (Palmer & Martin, 1975). The second class of models is again two-dimensional (2-*D*) where the collapsing section is modeled in a more numerically accurate manner (uniform collapse). Once again, an energy balance is used to estimate the propagation pressure, leading to the well-known Maxwell construction (Kyriakides *et al.*, 1984; Chater & Hutchinson, 1984; Dyau & Kyriakides, 1993; Kyriakides, 1993). The third level model is a full 3-*D* numerical simulation of the localized collapse and its quasi-static propagation. The first level models are useful for order of magnitude parametric studies. The second class of models can provide engineering type estimates of  $P_p$  for higher  $D/t$  tubes, but become increasingly less accurate as the  $D/t$  decreases. By contrast, the 3-*D* models can predict the propagation pressure to a very significant degree of accuracy.

For the confined buckle propagation problem, previous work has shown that 2-*D* models based on energy balance arguments underpredict  $P_{PC}$  by unacceptably large amounts (Kyriakides, 1993). Thus, the only useful alternative is the more complex 3-*D* simulation. In the following, a FE model developed within the framework of the nonlinear finite element code ABAQUS6.3 is used to simulate several of the experiments conducted. The result will then be used to explain the inadequacies of 2-*D* uniform collapse models for this problem.

The general geometric characteristics of the model are shown in Fig. 5.5. A section of tube  $9D$  long ( $L_2$ ) is surrounded by a rigid circular confining cavity, which is in perfect contact with the tube. In the experiments the tubes were well lubricated, and consequently a frictionless condition between the tube and the rigid cavity was assumed in the model. A section  $2.5D$  long ( $L_1$ ) is outside the confinement in order to initiate the collapse. Guided by the deformation of the collapsing tubes observed in the experiments, plane 1-2 is assumed to be a plane of symmetry. A local imperfection of the type defined in (5.1) is added in the neighborhood of  $x_1 = 0$ , and plane 2-3 is also assumed to be a plane of symmetry.

The main challenges of modeling confined buckle propagation are the large deformations of the deforming pipe and the contact with the cavity wall. It is important to select the appropriate element for this particular application. It is well known that the first-order elements have better performance for problems involving contact and large strains. Therefore, the tube is discretized by 3- $D$ , 8-node linear brick elements with full integration ( $C3D8$ ). The following distribution of elements was found to be adequate from convergence studies. Four elements are used through the thickness of the tube, 66 rectangular shaped elements around the half circumference, and 110 elements along the length. The contact algorithm mentioned in the previous section is adopted. The finite sliding and hard contact option are applied for contact between the walls of the collapsing tube, and between the tube and the rigid cavity.

The tube material was idealized as a  $J_2$ -type, elastoplastic, finitely deforming solid with isotropic hardening. For simulations of individual experiments, the true stress-logarithmic strain responses from uniaxial tensile tests were approximated as multilinear, and used in the analysis.

A fluid cavity was formed around the structure using the hydrostatic fluid elements of ABAQUS. The cavity was pressurized by prescribing the volume of fluid inside the cavity, resulting in volume-controlled pressurization.

### **b. Numerical Results of 3-D Simulations**

Results from a representative simulation (Exp. 0425) on a tube with a  $D/t = 25.6$  are shown in Fig. 5.6. Figure 5.6(a) shows the calculated pressure ( $P$ ) - change in volume response ( $\delta v/v_o$  where  $v_o$  is the initial volume of the artificial cavity formed around the specimen). Figure 5.6(b) shows the initial and a sequence of deformed configurations corresponding to the numbered points on the response. The structure is initially relatively stiff, and the pressure rises sharply. This terminates into a limit load that corresponds to the onset of local collapse in the region that has the geometric imperfection. The value of the pressure maximum is governed by the amplitude and extent of the local imperfection, and does not affect subsequent events. With the pressure dropping, the local collapse grows until in configuration ① the walls of the tube come into contact. Local collapse is arrested, and the buckle starts to spread down the tube in the characteristic dogbone cross section seen in configuration ②. The length of the unconfined section is relatively short, and as a result steady-state propagation is not achieved. When the collapse reaches the entrance of the cavity, it is arrested. The pressure then increases and the collapsed section flattens further. A new pressure maximum develops, corresponding to the switch from the dogbone to the U-mode of collapse (configuration③) which allows the buckle to start penetrating the rigid cavity. The initial penetration can be viewed as a transient event, which affects a section about  $3D$  long from the entrance to the cavity. Shortly after configuration ④, the U-mode collapse reaches steady state represented by the relatively flat pressure plateau that is traced in the neighborhood of configuration



⑤ and beyond. The pressure plateau at a level of 2,815 psi is the confined propagation pressure of the tube ( $\hat{P}_{PC}$ ). This prediction compares very well with the measured value of 2,755 psi. The simulation was terminated before the end of the tube was reached.

The extent of the deformation induced by the propagating front of the confined tube is illustrated in Fig. 5.7. Figure 5.7(a) shows an axial cross sectional view of the model. Figure 5.7(b) shows eight cross sectional views taken through the profile of the collapsed profile. This profile length, depicted as  $a$  in Fig. 5.7(a), is about  $2.6D$  long, and connects the circular cross section of the undisturbed tube to the U-shaped collapsed section (distance between the crest of the collapse and the point of first contact of the opposite walls). The corresponding profile length measured in the tube tested was of similar value. The deformation affects mainly the upper half of the cross section, which is seen to progressively become more detached from the cavity wall and to collapse inwards. Eventually, the collapsing half comes into contact with the other side. The length of the section in contact increases, and simultaneously the two wings of the cross section detach from the cavity and come closer together, as seen in the last configuration. The resemblance of the experimental and calculated profiles is very good indeed.

As mentioned above, the length of the profile is of the order of two-to-three diameters. Considering generators in the top half of the tube, they start straight, undergo bending, reverse bending and end up straight once more. Furthermore, because of the relatively short profile, they undergo significant stretching. Thus, the loading seen by points along and across these zones is complex and non-proportional. This is the main reason why energy balance type analyses based on uniform collapse models yield poor predictions for  $P_{PC}$  (Kyriakides, 1993). This last point will be illustrated by results from a uniform, plane strain collapse model of a section of the same tube.

### c. 2-D Models and Maxwell Construction

In this case, we consider the plane strain collapse of a tube confined by a rigid contacting and frictionless cavity. The tube has a small initial imperfection involving a span of about  $20^\circ$  detached from the wall. The imperfection is introduced by a point force, which pulls the crown point a distance  $0.5t$  away from the rigid wall. The deformed configuration is frozen, the stresses are removed, and pressure is applied in a cavity that surrounds the whole system.

The  $P - \delta v$  response calculated for a tube with a  $D/t = 25.6$  is shown in Fig. 5.8(a). A set of deformed configurations corresponding to the points marked on the response with numbered flags is shown in Fig. 5.8(b) (the configuration count goes from ① at the top to ⑦ at the bottom). It is quite clear that the ring configurations are quite different from those in the buckle profile shown in Fig. 5.7(b). This is because the stress paths experienced by different points on the cross sections in the two models are very different. Despite this, we will use this  $P - \delta v$  response to develop the Maxwell construction as follows: Referring to the auxiliary schematic  $P - \delta v$  response in Fig. 5.9, consider a confined buckle propagating in a steady-state, quasi-static fashion at a pressure of  $\hat{P}_{PC}$ . The external work done when the buckle propagates along a unit length of the tube is given by

$$\hat{P}_{PC}(\delta v_C - \delta v_A). \quad (5.1)$$

where A is a relatively undeformed equilibrium state on the initial stable branch of the response, and C is a collapsed configuration on the stable post-buckling response on the right. We assume that the material behavior is path independent. As a result, the change in internal work is strictly a function of the initial and final configurations of the cross section, i.e. states A and C. The change in internal work will be equal to the external work done, thus

$$\hat{P}_{PC}(\delta v_C - \delta v_A) = \int_{\delta v_A}^{\delta v_C} P(\delta v) d\delta v. \quad (5.2)$$

Equation (5.2) is satisfied when  $\hat{P}_{PC}$  is drawn at a level that makes the area under the  $P - \delta v$  response above the line ( $A_1$ ) equal to the area below the line and the response ( $A_2$ ). In essence, the argument states that equilibrium state C can be achieved either by following the response or by propagating the collapse at  $\hat{P}_{PC}$  in which case a stationary point goes through a similar sequence of configurations. An essential aspect of this argument is material path independence. Thus, for an elastic confined shell this argument is exact and yields the estimate of  $\hat{P}_{PC}$  given in (Kyriakides, 1986, 1993). Plastic deformations are invariably path dependent. As a result the argument only holds exactly for points, which experience proportional loading paths. In the present problem we have seen that this is hardly the case. As a consequence,  $\hat{P}_{PC}$  yielded by (5.2) is 1140 psi, which is only 41% of the measured value. Furthermore, the final deformed configuration corresponding to this pressure in the 2-D analysis is quite different from the final configuration in Fig. 5.7(b).

#### **d. Additional Numerical Results**

Similar simulations were performed for a total of ten of the physical experiments conducted. The predicted confined propagation pressures are listed in Table 5.4. Overall, the 3-D model does very well in reproducing the experimental values. The average absolute difference between predicted and measured  $P_{PC}$  values is 3.8%. In one case the difference is 7.9%, while in the rest it is less than 5%. As in similar calculations of the propagation pressure, small differences between measured and predicted values are due to variations in both geometric and material properties along the tube not accounted for, or due to yield anisotropy, which was not established for most tubes. Comparisons of measured

and predicted confined propagation pressure plotted in log-log scales are shown in Fig. 5.10.

The length of the profile of a confined buckle propagating at steady state ( $a$ ) has been defined as the distance between the crest of the collapse and the point of first contact of the opposite walls. Figure 5.11 shows a plot of the profile length vs.  $D/t$  for all experiments in which it was available. The profile is seen to increase nearly linearly with  $D/t$ . Also, the results from the 1/8H material (lower hardening) are lower than those from the higher hardening material. Measuring the profile length is somewhat inexact and this contributes to the observed scatter in the results. Included in the figure are the corresponding results from the ten simulations, measured in the same manner. The predicted values exhibit less scatter, and follow well the trends of the experimental results. As pointed out earlier, the profiles vary in length from about  $2.5D$  for the lower  $D/t$  values considered ( $\sim 15$ ) to about  $3.75D$  for the higher  $D/t$  values ( $\sim 40$ ).

The experimental part of this study pointed out that  $P_{PC}$  is affected first by the yield stress but also by the post-yield hardening of the material. Because small-scale steel tubes are only available in limited ranges of post-yield hardening, it was not possible to further explore this issue experimentally. Instead, a series of calculations were performed in which  $\hat{P}_{PC}$  was established for tubes of three different  $D/t$  values and three different post-yield slopes. The engineering stress-strain response was assumed to be bilinear, with elastic modulus of  $E = 30$  Msi and yield stress of 52 ksi. The post yield modulus ( $E'$ ) was assigned values of 80, 180 and 280 ksi. The three tube  $D/t$  values considered are 19.0, 27.0 and 40.0. The propagation and confined propagation pressures were evaluated in separate calculations for each tube and each material. The results are tabulated in Table 5.5, while the values of  $\hat{P}_{PC}$  are plotted against  $D/t$  in log-log scales in Fig. 5.12. For completeness, a similar plot of  $\hat{P}_P$  vs.  $D/t$  is shown in Fig. 5.13.

The post-yield hardening affects both propagation pressures, with the effect being more pronounced in the case of  $\hat{P}_{PC}$ . For example, for tubes with  $D/t = 19.0$  increasing the hardening from 80 to 280 ksi results in a nearly 24% increase in  $\hat{P}_{PC}$ . By contrast, for  $D/t = 40.0$  the corresponding increase is just over 12%. In the log-log plot in Fig. 5.12, the data shows once more the powerlaw dependence of  $\hat{P}_{PC}/\sigma_o$  on  $D/t$ . Increase in the post-yield hardening results in a nearly upward shift of the linear plot. This trend is similar to that seen in the experiments. In the case of  $\hat{P}_P$ , the effect of increasing the post-yield hardening from 80 to 280 ksi has the same upward shift trend, but only 12% increase in  $\hat{P}_P$  for tubes with  $D/t = 19.0$ . For  $D/t = 40.0$ , the corresponding increase in  $\hat{P}_P$  is about 9%.

The data obtained from this parametric study are used to enrich experimental results, and to find an improved empirical formula in the case of  $\hat{P}_{PC}$  (see Table 4.1).

## **Chapter 6**

### **Summary and Conclusions**

This dissertation presented a combined experimental/analytical study of slip-on buckle arrestors for pipes with lower  $D/t$  values (18-35) suitable for application in moderately deep and deepwater pipelines. The main thrust of the work involved a parametric study of the efficiency of slip-on buckle arrestors. The second part of the work involved quantifying the *confined propagation pressure* that serves as a lower bound of efficiency limits of slip-on type buckle arrestors. Both problems were first examined experimentally using small-scale tubes, followed by numerical models that can simulate the associated nonlinear phenomena.

#### **6.1 Arresting Efficiency of Slip-On Buckle Arrestors**

The effectiveness of slip-on buckle arrestors has been evaluated through combined experimental and numerical efforts. The parametric dependence of the crossover pressure and the efficiency of this arrestor were established through a broad set of experiments. The experiments involved small-scale SS-304 tubes with  $D/t$  values in the range of 18-35. Arrestors of various lengths, wall thicknesses and of two different yield stresses were mounted on the tubes. The experiments involved quasi-static propagation of buckles, engagement of an arrestor, and the eventual crossing of it at a specific crossover pressure. In each family of tests, the arrestor parameters were varied until the highest crossover pressure was achieved. Results from 84 such experiments are reported. The results were used to develop a new empirical design formula for arresting efficiency.

The quasi-static buckle propagation, arrest and crossover events observed experimentally were simulated numerically using a custom FE model. The model was used to simulate a number of the experiments conducted for the three tube D/t ratios analyzed spanning all pressure levels. The simulations were shown to capture successfully all important aspects of the experiments including accurate prediction of the crossover pressure. Although such calculations remain somewhat lengthy, they provide a way of proving a design based that is based on empirical design procedure developed.

The results of the study confirmed that slip-on type buckles arrestors do not always reach efficiency of 1. This is because often a buckle penetrates such arrestors by folding up into a characteristic U-mode at a pressure that is lower than the collapse pressure of the pipe. This takes place irrespective of how long, thick or stiff the ring arrestor is made. The results clearly demonstrated that a lower bound for the maximum efficiency of such arrestors is the confined propagation pressure of the pipe.

## **6.2 Buckle Propagation in Confined Steel Tubes**

The problem of propagation of collapse in a long circular tube surrounded by a relatively stiff confinement has been revisited. The lowest pressure at which confined collapse will propagate is defined as the confined propagation pressure ( $P_{PC}$ ). This is a characteristic pressure of confined tubes and is an important parameter in the design of liner tubes. In addition,  $P_{PC}$  has been shown provide a lower bound for the maximum crossover pressure of slip-on buckle arrestors. The present work used experiments and analysis to develop a more accurate empirical relationship between  $P_{PC}$  and the material and geometric parameters of the liner.

A previously developed set of experimental data of confined propagation pressures has been extended by the addition of results from new experiments from

SS-304 tubes with lower hardening slopes. It was known that  $P_{PC}$  is proportional to the yield stress of the tube material and has a powerlaw dependence on  $D/t$ . The new results have demonstrated that  $P_{PC}$  also depends on the hardening characteristics of the material. Lower hardening leads to lower values for  $P_{PC}$ .

The quasi-static initiation and propagation of confined collapse was modeled using 3-D finite elements. The model accounts for the finite deformations associated with this type of collapse, and it also addresses the contact nonlinearities, which govern the phenomenon. The material is modeled as a finitely deforming elastic-plastic solid. The model was first validated by simulating successfully several of the experiments performed. One-to-one comparisons between experimentally and predicated values of  $P_{PC}$  showed that this critical pressure can be predicated to a very significant degree of accuracy (differences generally were less than 5%). 2-D uniform collapse models of steady-state propagation and associated energy balance arguments leading to Maxwell pressure estimates of  $P_{PC}$ , were shown to lead to unacceptably low values. Measurements and predictions of the length of confined propagation profile were shown to be in the range of  $2.5D$  to  $3.5D$ . The shortness of the profiles and the severity and nature of the associated deformations indicate that material points undergo very complex loading histories, including reverse and generally nonproportional loading. This complexity in the induced stress histories is a significant contributor to the failure of the Maxwell pressure to be representative of  $P_{PC}$ . An important condition for the Maxwell construction to be applicable is path-independent material behavior. The 3-D model was used to conduct a parametric study of  $P_{PC}$ . The experimental data enriched with the numerical values generated were used to develop an improved empirical relationship for  $P_{PC}$ , which also accounts for the post-yield modulus of the material. The new formula can provide engineering level estimates  $P_{PC}$ . More accurate predictions



can be obtained by a full numerical simulation of the collapse and propagation process along the lines of the FE model presented here.

### 6.3 Recommended Design Procedure

Based on the results of this study, we recommend the following procedure to be followed in the design of an effective slip-on buckle arrestor (see Example in Appendix A):

1. Calculate the collapse and propagation pressure of the pipeline.
2. Calculate  $P_{IC}$  and  $P_{PC}$  using the empirical formula.
3. Calculate the desired crossover pressure  $P_X$  based on the maximum pipeline depth, and ensure that  $P_X < P_{PC}$ . If this test fails, then the pipeline thickness or steel grade must be increased, and return to step 1.
4. Use  $P_X$  to calculate the required arrestor efficiency  $\eta$ .
5. Use the problem variables in the empirical expression for efficiency to evaluate either the arrestor thickness or its length.
6. Test your design by a dependable numerical model like the one discussed in Chapter 5, or preferably, by a full-scale test conducted as outlined in Chapter 2.
7. If  $\eta > \eta_{PC}$ , then a slip-on arrestor is not appropriate for this pipeline. If increase of the pipeline wall thickness or steel grade is acceptable, implement such a change and return to step 1. If such changes are not possible, an integral buckle arrestor should be considered for this project.

It should be noted that like all empirical expressions of results of complex phenomena can be a dependable design tool provided that the parameters of the arrestor and pipe being designed do not deviates significantly from the range of variables of the data used to generate it. If the problem parameters deviate

significantly from those of the present database, new dependable data must be added to it, and if necessary, a new fit should be attempted before such an empirical formula is used directly in design.

Table 3.1 Mechanical properties of tubes used in the slip-on buckle arrestor experiments

| Tube  | $\frac{D}{t}$ | $E$<br>ksi | $\sigma_o$<br>ksi | $\sigma'_o$<br>ksi | $E'$<br>ksi | $S = \frac{\sigma_\theta}{\sigma_x}$ |
|-------|---------------|------------|-------------------|--------------------|-------------|--------------------------------------|
| PSO2  | 35.71         | 28.47      | 48.42             | 50.50              | 268.6       | -                                    |
| PSO4  | 35.71         | 29.25      | 47.07             | 49.35              | 242.0       | -                                    |
| PSO8  | 35.71         | 26.99      | 45.30             | 47.10              | 219.4       | -                                    |
| PSO5  | 25.51         | 28.45      | 49.60             | 51.24              | 222.3       | -                                    |
| PSO12 | 25.51         | 29.84      | 41.60             | 44.10              | 331.6       | -                                    |
| PIP44 | 25.51         | 28.59      | 42.64             | 44.67              | 242.3       | -                                    |
| PIP45 | 25.51         | 26.79      | 37.75             | 39.24              | 229.0       | -                                    |
| PIP46 | 25.51         | 27.10      | 40.00             | 41.41              | 219.6       | -                                    |
| PSO1  | 19.23         | 29.90      | 55.92             | 57.97              | 221.5       | 0.86                                 |
| PSO3  | 19.23         | 30.81      | 49.73             | 51.38              | 235.2       | -                                    |
| PSO6  | 19.23         | 30.13      | 52.65             | 54.57              | 221.5       | -                                    |
| PSO7  | 19.23         | 30.45      | 52.75             | 54.83              | 207.1       | 0.88                                 |
| PSO16 | 19.23         | 26.56      | 46.42             | 47.75              | 201.2       | -                                    |
| PSO17 | 19.23         | 27.08      | 50.99             | 52.24              | 200.6       | -                                    |
| PSO21 | 19.23         | 27.29      | 47.86             | 50.28              | 209.9       | -                                    |
| PSO22 | 19.23         | 29.04      | 46.14             | 48.77              | 223.4       | -                                    |

Table 3.2 Mechanical properties of arrestor materials

| Mat. | $E$<br>ksi | $\sigma_o$<br>ksi | $\sigma'_o$<br>ksi | $E'$<br>ksi |
|------|------------|-------------------|--------------------|-------------|
| A3   | 26.26      | 41.59             | 44.35              | 230.4       |
| A4   | 26.14      | 86.82             | 84.69              | 79.21       |

Table 3.3 Powerlaw fit parameters of three critical pressures (Kyriakides, 2002)

|                           | $A$   | $\beta$ | $R^2$  |
|---------------------------|-------|---------|--------|
| $\frac{P_P}{\sigma_o}$    | 39.25 | 2.500   | 0.9679 |
| $\frac{P_{IC}}{\sigma_o}$ | 34.85 | 2.095   | 0.9885 |
| $\frac{P_{PC}}{\sigma_o}$ | 61.61 | 2.301   | 0.9771 |

Table 3.4 Bounds of arrestor performance established from empirical formulas using the average measured geometries and material properties of tubes used

| $\frac{L}{D}$ | $\frac{h}{t}$ | $\bar{D}$<br>in | $\bar{t}$<br>in | $\bar{\sigma}_o$<br>ksi | $\hat{P}_{CO}$<br>psi | $\hat{P}_{IC}$<br>psi | $\hat{P}_{PC}$<br>psi | $\hat{P}_P$<br>psi | $\frac{\hat{P}_{CO}}{\bar{P}_P}$ | $\frac{\hat{P}_{IC}}{\bar{P}_P}$ | $\frac{\hat{P}_{PC}}{\bar{P}_P}$ |
|---------------|---------------|-----------------|-----------------|-------------------------|-----------------------|-----------------------|-----------------------|--------------------|----------------------------------|----------------------------------|----------------------------------|
| 0.5           | ---           | 1.2500          | 0.0366          | 47.75                   | 1434                  | 1022                  | 873                   | 276                | 281                              | 5.1032                           | 3.6370                           |
| 0.5           | ---           | 1.2515          | 0.0495          | 41.36                   | 2597                  | 1661                  | 1510                  | 503                | 501                              | 5.1836                           | 3.3154                           |
| 0.5           | ---           | 1.2511          | 0.0649          | 49.56                   | 4693                  | 3507                  | 3370                  | 1176               | 1075                             | 4.3656                           | 3.2623                           |
| 0.5           | A4            | 1.2475          | 0.0497          | 41.60                   | 2554                  | 1696                  | 1544                  | 515                | 503                              | 5.0775                           | 3.3718                           |
| ---           | 1.94          | 1.2514          | 0.0351          | 45.30                   | 1406                  | 882                   | 746                   | 235                | 227                              | 6.1938                           | 3.8855                           |
| ---           | 1.73          | 1.2510          | 0.0493          | 40.00                   | 2514                  | 1594                  | 1448                  | 482                | 475                              | 5.2926                           | 3.3558                           |
| ---           | 1.60          | 1.2510          | 0.0686          | 47.29                   | 5027                  | 3755                  | 3650                  | 1285               | 1331                             | 3.7769                           | 2.8212                           |
|               |               |                 |                 |                         |                       |                       |                       |                    |                                  |                                  | 2.7423                           |

Table 3.5 Experimental results of arrester (A3) and tube parameters for  $D/t = 25.5$ : variation of arrester thickness

| Exp No. | Tube No. | $D$<br>In | $t$<br>in | $\Delta_o$<br>% | $\Xi_o$<br>% | $\frac{h}{t}$ | $\frac{L}{D}$ | $P_P$<br>psi | $P_X$<br>psi | $\hat{P}_{CO}$<br>psi | $\eta$ |
|---------|----------|-----------|-----------|-----------------|--------------|---------------|---------------|--------------|--------------|-----------------------|--------|
| 1a      | PIP44    | 1.2514    | 0.0504    | 0.10            | 3.48         | 1.399         | 0.5           | 500          | 935          | 2679                  | 0.1996 |
| 1b      |          |           |           |                 |              | 1.696         | 0.5           |              | 1160         |                       | 0.3029 |
| 2a      | PIP44    | 1.2516    | 0.0501    | 0.032           | 4.37         | 1.106         | 0.5           | 507          | 764          | 2797                  | 0.1122 |
| 2b      |          |           |           |                 |              | 2.002         | 0.5           |              | 1338         |                       | 0.3629 |
| 4a      | PIP45    | 1.2514    | 0.0494    | 0.044           | 1.42         | 2.338         | 0.5           | 475          | 1512         | 2537                  | 0.5029 |
| 4b      |          |           |           |                 |              | 2.532         | 0.5           |              | 1788         |                       | 0.6368 |
| 5a      | PIP45    | 1.2511    | 0.0492    | 0.052           | 1.52         | 2.707         | 0.5           | 472          | 1529         | 2499                  | 0.5215 |
| 5b      |          |           |           |                 |              | 2.868         | 0.5           |              | 1557         |                       | 0.5353 |
| 6a      | PIP45    | 1.2513    | 0.0494    | 0.056           | 1.21         | 2.761         | 0.5           | 465          | 1530         | 2508                  | 0.5213 |
| 6b      |          |           |           |                 |              | 3.002         | 0.5           |              | 1537         |                       | 0.5247 |
| 33a     | PSO5     | 1.2519    | 0.0487    | 0.036           | 4.72         | 0.653         | 0.5           | 585          | 663          | 2917                  | 0.0334 |
| 33b     |          |           |           |                 |              | 0.877         | 0.5           |              | 708          |                       | 0.0527 |

Table 3.6 Experimental results of arrestor (A3) and tube parameters for  $D/t = 19.2$ : variation of arrestor thickness

| Exp No. | Tube No. | $D$<br>in | $t$<br>in | $A_o$<br>% | $E_o$<br>% | $\frac{h}{t}$ | $\frac{L}{D}$ | $P_P$<br>psi | $P_X$<br>psi | $\hat{P}_{CO}$<br>psi | $\eta$ |
|---------|----------|-----------|-----------|------------|------------|---------------|---------------|--------------|--------------|-----------------------|--------|
| 7a      | PSO1     | 1.2514    | 0.0651    | 0.09       | 2.5        | 1.235         | 0.5           | 1123         | 1632         | 4383                  | 0.1561 |
| 7b      |          |           |           |            |            | 1.467         | 0.5           |              | 1831         |                       | 0.2172 |
| 8a      | PSO1     | 1.2523    | 0.0652    | 0.19       | 3.1        | 1.693         | 0.5           | 1145         | 2172         | 4205                  | 0.3356 |
| 8b      |          |           |           |            |            | 2.078         | 0.5           |              | 2727         |                       | 0.5170 |
| 9a      | PSO1     | 1.2512    | 0.0645    | 0.14       | 3.3        | 2.253         | 0.5           | 1116         | 2654         | 4213                  | 0.4966 |
| 9b      |          |           |           |            |            | 2.409         | 0.5           |              | 2988         |                       | 0.6045 |
| 26a     | PSO6     | 1.2508    | 0.0647    | 0.11       | 2.7        | 2.563         | 0.5           | 1014         | 2917         | 4871                  | 0.4934 |
| 26b     |          |           |           |            |            | 2.702         | 0.5           |              | 3138         |                       | 0.5507 |
| 27a     | PSO6     | 1.2504    | 0.0645    | 0.14       | 2.1        | 2.873         | 0.5           | 1012         | 3162         | 4789                  | 0.5692 |
| 27b     |          |           |           |            |            | 3.040         | 0.5           |              | 3005         |                       | 0.5277 |
| 28a     | PSO7     | 1.2507    | 0.0651    | 0.15       | 1.7        | 3.143         | 0.5           | 1065         | 3424         | 4177                  | 0.7580 |
| 28b     |          |           |           |            |            | 3.306         | 0.5           |              | 3435         |                       | 0.7616 |
| 32a     | PSO3     | 1.2512    | 0.0651    | 0.11       | 1.5        | 0.653         | 0.5           | 1053         | 1213         | 4784                  | 0.0429 |
| 32b     |          |           |           |            |            | 0.922         | 0.5           |              | 1363         |                       | 0.0831 |

Table 3.7 Experimental results of arrestor (A3) and tube parameters for  $D/t = 35.7$ : variation of arrestor thickness

| Exp No. | Tube No. | $D$<br>in | $t$<br>in | $A_o$<br>% | $E_o$<br>% | $\frac{h}{t}$ | $\frac{L}{D}$ | $P_P$<br>psi | $P_X$<br>psi | $\hat{P}_{CO}$<br>psi | $\eta$ |
|---------|----------|-----------|-----------|------------|------------|---------------|---------------|--------------|--------------|-----------------------|--------|
| 11a     | PSO2     | 1.2501    | 0.0367    | 0.036      | 5.85       | 1.649         | 0.5           | 282          | 497          | 1491                  | 0.1778 |
| 11b     |          |           |           |            |            | 2.052         | 0.5           |              | 635          |                       | 0.2920 |
| 13a     | PSO2     | 1.250     | 0.0365    | 0.073      | 5.72       | 2.611         | 0.5           | 281          | 815          | 1417                  | 0.4701 |
| 13b     |          |           |           |            |            | 2.882         | 0.5           |              | 901          |                       | 0.5458 |
| 15a     | PSO2     | 1.2501    | 0.0365    | 0.040      | 5.61       | 3.159         | 0.5           | 285          | 832          | 1464                  | 0.4640 |
| 15b     |          |           |           |            |            | 3.427         | 0.5           |              | 861          |                       | 0.4885 |
| 17a     | PSO4     | 1.2497    | 0.0368    | 0.175      | 3.95       | 3.685         | 0.5           | 281          | 905          | 1365                  | 0.5756 |
| 17b     |          |           |           |            |            | 3.951         | 0.5           |              | 941          |                       | 0.6089 |
| 18a     | PSO4     | 1.250     | 0.0366    | 0.056      | 4.10       | 1.383         | 0.5           | 279          | 442          | 1472                  | 0.1366 |
| 18b     |          |           |           |            |            | 4.246         | 0.5           |              | 948          |                       | 0.5608 |
| 36a     | PSO4     | 1.2501    | 0.0367    | 0.044      | 2.73       | 0.837         | 0.5           | 276          | 339          | 1502                  | 0.0514 |
| 36b     |          |           |           |            |            | 1.158         | 0.5           |              | 393          |                       | 0.0954 |



Table 3.8 Experimental results of arrester (A3) and tube parameters for  $D/t = 25.5$ : variation of arrester length

| Exp No. | Tube No. | $D$<br>in | $t$<br>in | $\Delta_o$<br>% | $\Xi_o$<br>% | $\frac{h}{t}$ | $\frac{L}{D}$ | $P_P$<br>psi | $P_X$<br>psi | $\hat{P}_{CO}$<br>psi | $\eta$ |
|---------|----------|-----------|-----------|-----------------|--------------|---------------|---------------|--------------|--------------|-----------------------|--------|
| 19a     | PIP46    | 1.2507    | 0.0492    | 0.148           | 2.34         | 1.740         | 0.251         | 472          | 759          | 2395                  | 0.1492 |
| 19b     |          |           |           |                 |              | 1.740         | 0.750         |              | 1356         |                       | 0.4597 |
| 21a     | PIP46    | 1.2509    | 0.0493    | 0.060           | 2.13         | 1.730         | 0.640         | 478          | 1287         | 2553                  | 0.3899 |
| 21b     |          |           |           |                 |              | 1.732         | 0.890         |              | 1400         |                       | 0.4443 |
| 22a     | PIP46    | 1.2512    | 0.0493    | 0.052           | 2.23         | 1.738         | 0.400         | 472          | 960          | 2570                  | 0.2326 |
| 22b     |          |           |           |                 |              | 1.732         | 1.000         |              | 1479         |                       | 0.4800 |
| 23a     | PIP46    | 1.2511    | 0.0495    | 0.056           | 2.02         | 1.733         | 1.099         | 478          | 1474         | 2581                  | 0.4736 |
| 23b     |          |           |           |                 |              | 1.729         | 1.199         |              | 1516         |                       | 0.4936 |

Table 3.9 Experimental results of arrestor (A3) and tube parameters for  $D/t = 19.2$ : variation of arrestor length

| Exp No. | Tube No. | $D$<br>in | $t$<br>in | $\Delta_o$<br>% | $\Xi_o$<br>% | $\frac{h}{t}$ | $\frac{L}{D}$ | $P_P$<br>psi | $P_X$<br>psi | $\hat{P}_{CO}$<br>psi | $\eta$ |
|---------|----------|-----------|-----------|-----------------|--------------|---------------|---------------|--------------|--------------|-----------------------|--------|
| 30a     | PSO7     | 1.2507    | 0.0649    | 0.12            | 1.5          | 1.710         | 0.253         | 1065         | 1549         | 4214                  | 0.1537 |
| 30b     |          |           |           |                 |              | 1.704         | 0.640         |              | 2457         |                       | 0.4420 |
| 31a     | PSO7     | 1.2509    | 0.0650    | 0.19            | 1.5          | 1.70          | 0.376         | 1072         | 1831         | 4101                  | 0.2506 |
| 31b     |          |           |           |                 |              | 1.70          | 0.748         |              | 2079         |                       | 0.5404 |
| 44a     | PSO16    | 1.2505    | 0.0694    | 0.04            | 1.66         | 1.59          | 0.701         | 1295         | 2884         | 5093                  | 0.4184 |
| 44b     |          |           |           |                 |              | 1.59          | 0.779         |              | 3148         |                       | 0.4879 |
| 47a     | PSO17    | 1.2505    | 0.0699    | 0.04            | 1.50         | 1.59          | 0.500         | 1326         | 2503         | 5639                  | 0.2729 |
| 47b     |          |           |           |                 |              | 1.59          | 0.600         |              | 2803         |                       | 0.3425 |
| 45      | PSO17    | 1.2503    | 0.0698    | 0.07            | 1.72         | 1.58          | 0.302         | 1333         | 1919         | 5537                  | 0.1394 |
| 48      | PSO17    | 1.2505    | 0.0698    | 0.06            | 1.22         | 1.58          | 0.400         | 1300         | 2168         | 5550                  | 0.2042 |

Table 3.9 Experimental results of arrestor (A3) and tube parameters for  $D/t = 18.1$ : variation of arrestor length (Cont.)

| Exp No. | Tube No. | $D$<br>in | $t$<br>in | $\Delta_o$<br>% | $\Xi_o$<br>% | $\frac{h}{t}$ | $\frac{L}{D}$ | $P_P$<br>psi | $P_X$<br>psi | $\hat{P}_{CO}$<br>psi | $\eta$ |
|---------|----------|-----------|-----------|-----------------|--------------|---------------|---------------|--------------|--------------|-----------------------|--------|
| 50a     | PSO21    | 1.2510    | 0.0689    | 0.06            | 3.9          | 1.60          | 0.880         | 1345         | 2999         | 4955                  | 0.4582 |
| 50b     |          |           |           |                 |              | 1.60          | 1.000         |              | 3278         |                       | 0.5355 |
| 51a     | PSO21    | 1.2510    | 0.0692    | 0.07            | 3.7          | 1.60          | 1.099         | 1358         | 3309         | 4970                  | 0.5401 |
| 51b     |          |           |           |                 |              | 1.60          | 1.198         |              | 3454         |                       | 0.5803 |
| 52a     | PSO21    | 1.2511    | 0.0689    | 0.07            | 5.7          | 1.60          | 0.803         | 1361         | 3014         | 4915                  | 0.4651 |
| 52b     |          |           |           |                 |              | 1.60          | 1.300         |              | 3358         |                       | 0.5619 |
| 53a     | PSO21    | 1.2507    | 0.0687    | 0.08            | 5.3          | 1.61          | 0.552         | 1332         | 2496         | 4879                  | 0.3282 |
| 53b     |          |           |           |                 |              | 1.61          | 0.680         |              | 2756         |                       | 0.4015 |
| 54a     | PSO22    | 1.2511    | 0.0678    | 0.06            | 4.2          | 1.63          | 0.349         | 1300         | 1945         | 4771                  | 0.1858 |
| 54b     |          |           |           |                 |              | 1.63          | 0.448         |              | 2281         |                       | 0.2826 |
| 55a     | PSO22    | 1.2509    | 0.0678    | 0.06            | 4.2          | 1.63          | 0.198         | 1290         | 1666         | 4765                  | 0.1082 |
| 55b     |          |           |           |                 |              | 1.63          | 0.400         |              | 2127         |                       | 0.2409 |

Table 3.10 Experimental results of arrestor (A3) and tube parameters for  $D/t = 35.7$ : variation of arrestor length

| Exp No. | Tube No. | $D$<br>in | $t$<br>in | $A_o$<br>% | $E_o$<br>% | $\frac{h}{t}$ | $\frac{L}{D}$ | $P_P$<br>psi | $P_X$<br>psi | $\hat{P}_{CO}$<br>psi | $\eta$ |
|---------|----------|-----------|-----------|------------|------------|---------------|---------------|--------------|--------------|-----------------------|--------|
| 37a     | PSO8     | 1.2521    | 0.0351    | 0.064      | 2.14       | 1.95          | 0.500         | 222          | 553          | 1260                  | 0.3189 |
| 37b     |          |           |           |            |            | 1.95          | 0.600         |              | 645          |                       | 0.4075 |
| 38a     | PSO8     | 1.2519    | 0.0350    | 0.052      | 2.72       | 1.94          | 0.799         | 230          | 699          | 1268                  | 0.4518 |
| 38b     |          |           |           |            |            | 1.94          | 0.959         |              | 785          |                       | 0.5347 |
| 39a     | PSO8     | 1.2513    | 0.0351    | 0.036      | 3.70       | 1.95          | 0.361         | 225          | 437          | 1306                  | 0.1961 |
| 39b     |          |           |           |            |            | 1.95          | 0.720         |              | 762          |                       | 0.4968 |
| 41a     | PSO8     | 1.2502    | 0.0350    | 0.044      | 3.29       | 1.95          | 0.260         | 229          | 359          | 1164                  | 0.1390 |
| 41b     |          |           |           |            |            | 1.95          | 0.881         |              | 798          |                       | 0.6086 |

Table 3.11 Experimental results of arrestor (A4) and tube parameters for  $D/t = 25.5$ : variation of arrestor thickness

| Exp No. | Tube No. | $D$<br>in | $t$<br>in | $\Delta_o$<br>% | $\Xi_o$<br>% | $\frac{h}{t}$ | $\frac{L}{D}$ | $P_P$<br>psi | $P_X$<br>psi | $\hat{P}_{CO}$<br>psi | $\eta$ |
|---------|----------|-----------|-----------|-----------------|--------------|---------------|---------------|--------------|--------------|-----------------------|--------|
| 59a     | PSO12    | 1.2476    | 0.0498    | 0.048           | 0.70         | 1.010         | 0.5           | 504          | 734          | 2563                  | 0.1117 |
| 59b     |          |           |           |                 |              | 1.422         | 0.5           |              | 1140         |                       | 0.3089 |
| 60a     | PSO12    | 1.2476    | 0.0497    | 0.060           | 0.51         | 1.225         | 0.5           | 503          | 875          | 2528                  | 0.1837 |
| 60b     |          |           |           |                 |              | 1.626         | 0.5           |              | 1428         |                       | 0.4568 |
| 61a     | PSO12    | 1.2474    | 0.0497    | 0.044           | 0.70         | 1.763         | 0.5           | 502          | 1683         | 2564                  | 0.5727 |
| 61b     |          |           |           |                 |              | 1.928         | 0.5           |              | 1750         |                       | 0.6052 |
| 62a     | PSO12    | 1.2474    | 0.0497    | 0.040           | 0.5          | 0.815         | 0.5           | 508          | 658          | 2573                  | 0.0726 |
| 62b     |          |           |           |                 |              | 2.080         | 0.5           |              | 1741         |                       | 0.5971 |

Table 3.12 Parameters and propagation and confined propagation pressures of two sets of SS-304 tubes tested

| Exp. Set   | Exp. No.                         | D<br>in | $\frac{D}{t}$ | $\sigma_o$<br>ksi | $E'$<br>ksi | $\frac{P_P}{\sigma_o} \times 10^3$ | $\frac{P_{PC}}{\sigma_o} \times 10^3$ | $\frac{\hat{P}_{PC}}{\sigma_o} \times 10^3$ |
|------------|----------------------------------|---------|---------------|-------------------|-------------|------------------------------------|---------------------------------------|---|
| <b>II</b>  | 009                              | 1.745   | 14.54         | 46.40             | 195         | 50.11                              | 106.7                                 | -   |
|            | 0011                             | 1.249   | 14.98         | 38.4              | 280         | 55.83                              | 133.1                                 | -   |
|            | 0010                             | 1.503   | 15.69         | 47.82             | 220         | 37.43                              | 97.45                                 | -   |
|            | 003                              | 2.001   | 16.45         | 43.05             | 230         | 35.61                              | 91.36                                 | -   |
|            | 994                              | 1.252   | 18.89         | 58.6              | 235         | 21.91                              | 69.51                                 | 68.46                                       |
|            | 001                              | 2.004   | 21.46         | 40.52             | 275         | 19.55                              | 55.82                                 | 58.89                                       |
|            | 002                              | 2.006   | 24.14         | 42.7              | 245         | 13.11                              | 36.72                                 | -   |
|            | 995                              | 1.251   | 25.69         | 48.33             | 235         | 10.08                              | 32.59                                 | 33.81                                       |
|            | 006                              | 1.753   | 26.35         | 38.63             | 175         | 11.34                              | 36.24                                 | -   |
|            | 993                              | 1.248   | 34.99         | 42.15             | 260         | 5.386                              | 19.98                                 | 20.78                                       |
| <b>III</b> | 992                              | 1.252   | 45.85         | 46.6              | 195         | 2.833                              | 10.73                                 | 11.12                                       |
|            | 0427                             | 1.2532  | 19.25         | 87.04             | 99          | 20.20                              | 55.84                                 | 58.20                                       |
|            | 0429                             | 1.5025  | 23.37         | 99.18             | 82          | 12.00                              | 36.00                                 | 36.27                                       |
|            | 0425                             | 1.2515  | 25.65         | 93.55             | 88          | 9.022                              | 29.45                                 | 30.09                                       |
|            | 0430                             | 1.5016  | 29.96         | 91.58             | 97          | 6.868                              | 23.58                                 | 22.25                                       |
|            | 0423                             | 1.2512  | 37.36         | 81.25             | 70          | 4.135                              | 14.87                                 | 15.37                                       |
|            | Set II: 2002 [11]. Set III: 2004 |         |               |                   |             |                                    |                                       |   |

Table 3.13 Powerlaw fit of two critical pressures with two parameters

| Exp.                      | Set II |         |        | Set III |         |        |
|---------------------------|--------|---------|--------|---------|---------|--------|
|                           | $A$    | $\beta$ | $R^2$  | $A$     | $\beta$ | $R^2$  |
| $\frac{P_P}{\sigma_o}$    | 36.68  | 2.482   | 0.9478 | 20.69   | 2.362   | 0.9930 |
| $\frac{P_{PC}}{\sigma_o}$ | 27.05  | 2.039   | 0.9290 | 17.54   | 1.956   | 0.9945 |

Table 4.1 Powerlaw fit of two critical pressures with three parameters

|                             | $B$   | $C$  | $\beta$ |
|-----------------------------|-------|------|---------|
| $\frac{P_P^a}{\sigma_o}$    | 25.37 | 0.62 | 2.429   |
| $\frac{P_{PC}^a}{\sigma_o}$ | 15.59 | 1.43 | 1.975   |
| $\frac{P_{PC}^b}{\sigma_o}$ | 17.27 | 1.43 | 2.000   |

<sup>a</sup>Experiments only

<sup>b</sup>Experiments with numerical results



Table 5.1 Arrestor (A3), tube parameters and measured and calculated crossover pressures  
for tubes with nominal  $D/t = 25.5$

| Exp<br>No. | Tube<br>No. | $D$<br>in | $t$<br>in | $\sigma_o$<br>ksi | $\Delta_o$<br>(%) | $\Xi_o$<br>(%) | $\frac{h}{t}$ | $\frac{L}{D}$ | $P_p$<br>psi | $P_X$<br>psi | $\hat{P}_X$<br>psi | $\left(\frac{\hat{P}_X - 1}{P_X}\right)$<br>% | $\eta$ |
|------------|-------------|-----------|-----------|-------------------|-------------------|----------------|---------------|---------------|--------------|--------------|--------------------|---|--------|
| 1a         | PIP44       | 1.2514    | 0.0504    | 42.64             | 0.10              | 3.5            | 1.399         | 0.5           | 500          | 935          | 869                | -7.1  | 0.1996 |
| 1b         |             |           |           |                   |                   |                | 1.696         | 0.5           |              | 1160         | 1070               | -7.8  | 0.3029 |
| 2a         | PIP44       | 1.2516    | 0.0501    | 42.64             | 0.032             | 4.4            | 1.106         | 0.5           | 507          | 764          | 747                | -2.2  | 0.1122 |
| 2b         |             |           |           |                   |                   |                | 2.002         | 0.5           |              | 1338         | 1356               | 1.3   | 0.3629 |
| 4a         | PIP45       | 1.2514    | 0.0494    | 37.75             | 0.044             | 1.4            | 2.338         | 0.5           | 475          | 1512         | 1490               | -1.5  | 0.5029 |
| 4b         |             |           |           |                   |                   |                | 2.532         | 0.5           |              | 1788         | -                  | -   | 0.6368 |
| 5a         | PIP45       | 1.2511    | 0.0492    | 37.75             | 0.052             | 1.5            | 2.707         | 0.5           | 472          | 1529         | 1475               | -3.5  | 0.5215 |
| 5b         |             |           |           |                   |                   |                | 2.868         | 0.5           |              | 1557         | 1521               | -2.3  | 0.5353 |
| 6a         | PIP45       | 1.2513    | 0.0494    | 37.75             | 0.056             | 1.2            | 2.761         | 0.5           | 465          | 1530         | -                  | -   | 0.5213 |
| 6b         |             |           |           |                   |                   |                | 3.002         | 0.5           |              | 1537         | -                  | -   | 0.5247 |
| 33a        | PSO5        | 1.2519    | 0.0487    | 49.60             | 0.036             | 4.7            | 0.653         | 0.5           | 585          | 663          | 643                | -3.0  | 0.0334 |
| 33b        |             |           |           |                   |                   |                | 0.877         | 0.5           |              | 708          | 681                | -3.8  | 0.0527 |

Table 5.2 Miscellaneous, arrestor and tube parameters and measured and calculated crossover pressures

| Ex<br>p<br>No. | Tube<br>No. | $D$<br>in | $t$<br>in | $\frac{D}{t}$ | $\sigma_o$<br>ksi | $\Delta_o$<br>(%) | $\Xi_o$<br>(%) | $\frac{h}{t}$ | $\frac{L}{D}$ | $P_P$<br>psi | $P_X$<br>psi | $\hat{P}_X$<br>psi | $\left(\frac{\hat{P}_X}{P_X} - 1\right)$<br>% | $\eta$ |
|----------------|-------------|-----------|-----------|---------------|-------------------|-------------------|----------------|---------------|---------------|--------------|--------------|--------------------|---|--------|
| 22b            | PIP46       | 1.2512    | 0.0493    | 25.38         | 40.00             | 0.052             | 2.2            | 1.732         | 0.5           | 472          | 1479         | 1501               | 1.49  | 0.4800 |
| 13a            | PSO2        | 1.250     | 0.0365    | 34.25         | 48.42             | 0.073             | 5.7            | 2.611         | 0.5           | 281          | 815          | 826                | 1.35  | 0.4701 |
| 11b            | PSO2        | 1.2501    | 0.0367    | 34.06         | 48.42             | 0.036             | 5.6            | 2.052         | 0.5           | 282          | 635          | 629                | -1.0  | 0.2920 |
| 18a            | PSO4        | 1.250     | 0.0366    | 34.15         | 47.07             | 0.056             | 4.1            | 1.383         | 0.5           | 279          | 442          | 339                | -9.7  | 0.1366 |
| 7a             | PSO1        | 1.2514    | 0.0651    | 19.22         | 55.92             | 0.090             | 2.5            | 1.235         | 0.5           | 1123         | 1632         | 1698               | 4.0   | 0.1561 |
| 8a             | PSO1        | 1.2523    | 0.0652    | 19.21         | 55.92             | 0.190             | 3.1            | 1.693         | 0.5           | 1145         | 3272         | 2191               | 0.9   | 0.3356 |
| 27a            | PSO6        | 1.2504    | 0.0645    | 19.39         | 52.65             | 0.140             | 2.1            | 2.873         | 0.5           | 1012         | 3162         | 3270               | 3.4   | 0.5692 |

Table 5.3 Calculations of crossover pressures for tubes with nominal  $D/t = 25.5$   
using quadratic and linear elements

| Exp No. | Tube No. | $D$<br>in | $t$<br>in | $\sigma_o$<br>ksi | $\frac{h}{t}$ | $\frac{L}{D}$ | $P_X$<br>psi | $\hat{P}_X$ psi<br>Quad. | $\left(\frac{\hat{P}_X - 1}{P_X}\right)$<br>% | $\hat{P}_X$ psi<br>Linear | $\left(\frac{\hat{P}_X - 1}{P_X}\right)$<br>% | $\eta$ |
|---------|----------|-----------|-----------|-------------------|---------------|---------------|--------------|--------------------------|---|---------------------------|---|--------|
| 1a      | PIP44    | 1.2514    | 0.0504    | 42.64             | 1.399         | 0.5           | 935          | 869                      | -7.1  | 907                       | -3.0  | 0.1996 |
| 1b      |          |           |           |                   | 1.696         | 0.5           | 1160         | 1070                     | -7.8  | 1092                      | -5.9  | 0.3029 |
| 2a      | PIP44    | 1.2516    | 0.0501    | 42.64             | 1.106         | 0.5           | 764          | 747                      | -2.2  | 786                       | 2.9   | 0.1122 |
| 2b      |          |           |           |                   | 2.002         | 0.5           | 1338         | 1356                     | 1.3   | 1364                      | 1.9   | 0.3629 |
| 4a      | PIP45    | 1.2514    | 0.0494    | 37.75             | 2.338         | 0.5           | 1512         | 1490                     | -1.5  | 1591                      | 5.2   | 0.5029 |
| 4b      |          |           |           |                   | 2.532         | 0.5           | 1788         | -                        | -   | -                         | -   | 0.6368 |
| 5a      | PIP45    | 1.2511    | 0.0492    | 37.75             | 2.707         | 0.5           | 1529         | 1475                     | -3.5  | 1556                      | 1.8   | 0.5215 |
| 5b      |          |           |           |                   | 2.868         | 0.5           | 1557         | 1521                     | -2.3  | 1587                      | 1.9   | 0.5353 |
| 6a      | PIP45    | 1.2513    | 0.0494    | 37.75             | 2.761         | 0.5           | 1530         | -                        | -   | -                         | -   | 0.5213 |
| 6b      |          |           |           |                   | 3.002         | 0.5           | 1537         | -                        | -   | -                         | -   | 0.5247 |
| 33a     | PSO5     | 1.2519    | 0.0487    | 49.60             | 0.653         | 0.5           | 663          | 643                      | -3.0  | 674                       | 1.7   | 0.0334 |
| 33b     |          |           |           |                   | 0.877         | 0.5           | 708          | 681                      | -3.8  | 722                       | 2.0   | 0.0527 |

Table 5.4 Parameters and propagation and confined propagation pressures of two sets of SS-304 tubes tested

| Exp. Set   | Exp. No. | D<br>in | $\frac{D}{t}$ | $\sigma_o$<br>ksi | $E'$<br>ksi | $\frac{P_P}{\sigma_o} \times 10^3$ | $\frac{P_{PC}}{\sigma_o} \times 10^3$ | $\frac{\hat{P}_{PC}}{\sigma_o} \times 10^3$ |
|------------|----------|---------|---------------|-------------------|-------------|------------------------------------|---------------------------------------|---|
| <b>II</b>  | 009      | 1.745   | 14.54         | 46.40             | 195         | 50.11                              | 106.7                                 | -   |
|            | 0011     | 1.249   | 14.98         | 38.40             | 280         | 55.83                              | 133.1                                 | -   |
|            | 0010     | 1.503   | 15.69         | 47.82             | 220         | 37.43                              | 97.45                                 | -   |
|            | 003      | 2.001   | 16.45         | 43.05             | 230         | 35.61                              | 91.36                                 | -   |
|            | 994      | 1.252   | 18.89         | 58.60             | 235         | 21.91                              | 69.51                                 | 68.46                                       |
|            | 001      | 2.004   | 21.46         | 40.52             | 275         | 19.55                              | 55.82                                 | 60.24                                       |
|            | 002      | 2.006   | 24.14         | 42.70             | 245         | 13.11                              | 36.72                                 | -   |
|            | 995      | 1.251   | 25.69         | 48.33             | 235         | 10.08                              | 32.59                                 | 33.81                                       |
|            | 006      | 1.753   | 26.35         | 38.63             | 175         | 11.34                              | 36.24                                 | -   |
|            | 993      | 1.248   | 34.95         | 42.15             | 260         | 5.386                              | 19.98                                 | 20.78                                       |
| <b>III</b> | 992      | 1.252   | 45.85         | 46.60             | 195         | 2.833                              | 10.73                                 | 11.12                                       |
|            | 0427     | 1.2532  | 19.25         | 87.04             | 99          | 20.20                              | 55.84                                 | 58.20                                       |
|            | 0429     | 1.5025  | 23.37         | 99.18             | 82          | 12.00                              | 36.00                                 | 36.27                                       |
|            | 0425     | 1.2515  | 25.65         | 93.55             | 88          | 9.022                              | 29.45                                 | 30.09                                       |
|            | 0430     | 1.5016  | 29.68         | 91.58             | 97          | 6.868                              | 23.48                                 | 22.25                                       |
|            | 0423     | 1.2512  | 37.46         | 81.25             | 70          | 4.135                              | 14.87                                 | 15.37                                       |

Set II: 2002 (Kyniakides, 2002). Set III: 2004.  $\hat{P}_{PC}$  = Predicted

Table 5.5 Calculated propagation and confined propagation pressures for tubes with different hardening characteristics

| $\frac{D}{t}$ | $\frac{E'}{\sigma_o}$ | $\frac{\hat{P}_P}{\sigma_o} \times 10^3$ | $\frac{\hat{P}_{PC}}{\sigma_o} \times 10^3$ |
|---------------|-----------------------|--|---|
| 19.0          | 1.538                 | 20.71                                    | 56.94                                       |
| 19.0          | 3.462                 | 21.88                                    | 63.94                                       |
| 19.0          | 5.385                 | 23.29                                    | 70.40                                       |
| 27.0          | 1.538                 | 8.942                                    | 27.40                                       |
| 27.0          | 3.462                 | 9.231                                    | 29.50                                       |
| 27.0          | 5.385                 | 9.538                                    | 31.90                                       |
| 40.0          | 1.538                 | 3.327                                    | 12.39                                       |
| 40.0          | 3.462                 | 3.481                                    | 13.00                                       |
| 40.0          | 5.385                 | 3.615                                    | 13.92                                       |

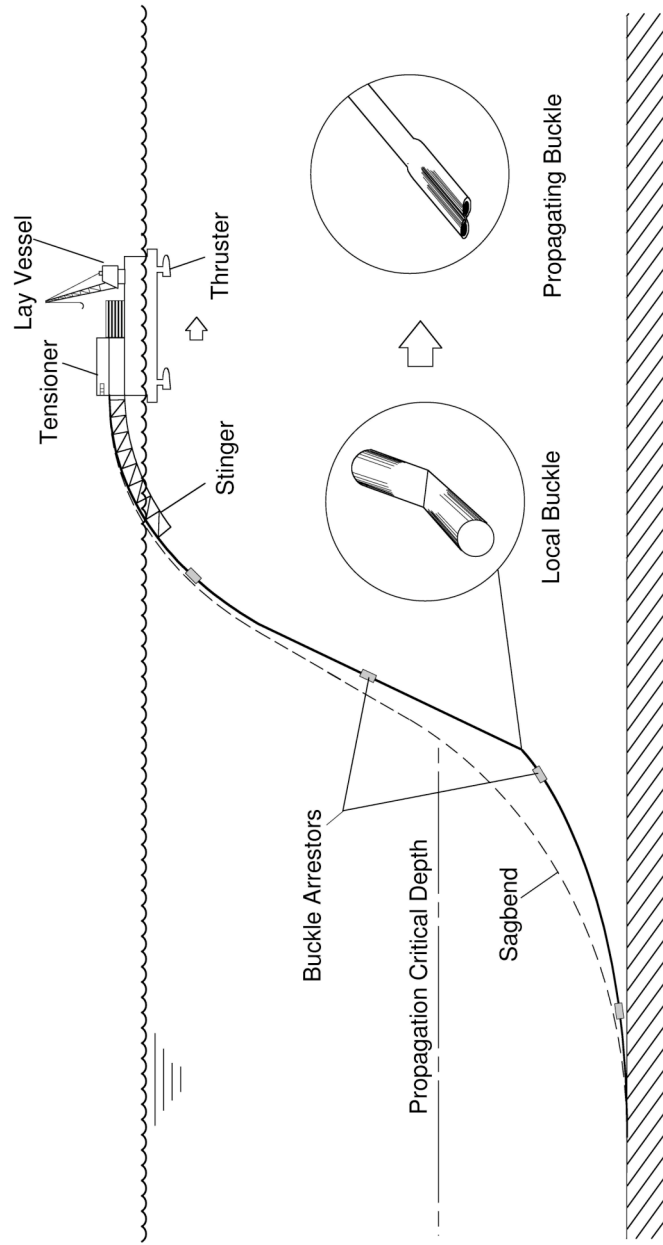


Fig. 1.1 Schematic showing the initiation of a propagating buckle in a pipeline by a local bending collapse mode. Collapse propagates flattening the pipeline. The extent of damage is limited by periodic installation of buckle arrestors (after Fig. 2.17 Corona & Kyriakides [2007])

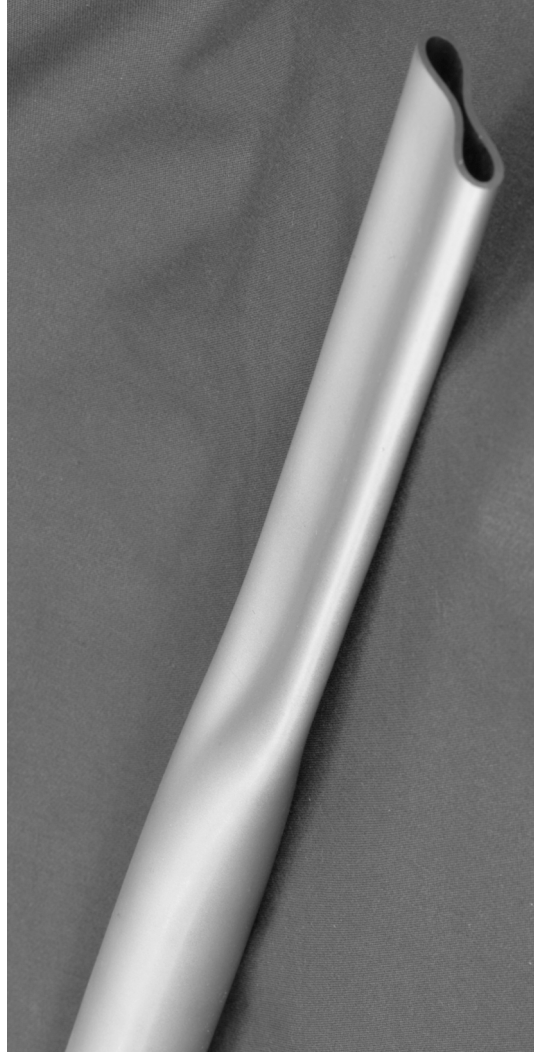


Fig. 1.2 Transition between collapsed and intact sections of pipe that developed a propagating buckle  
(from Kyriakides & Corona, 2007)

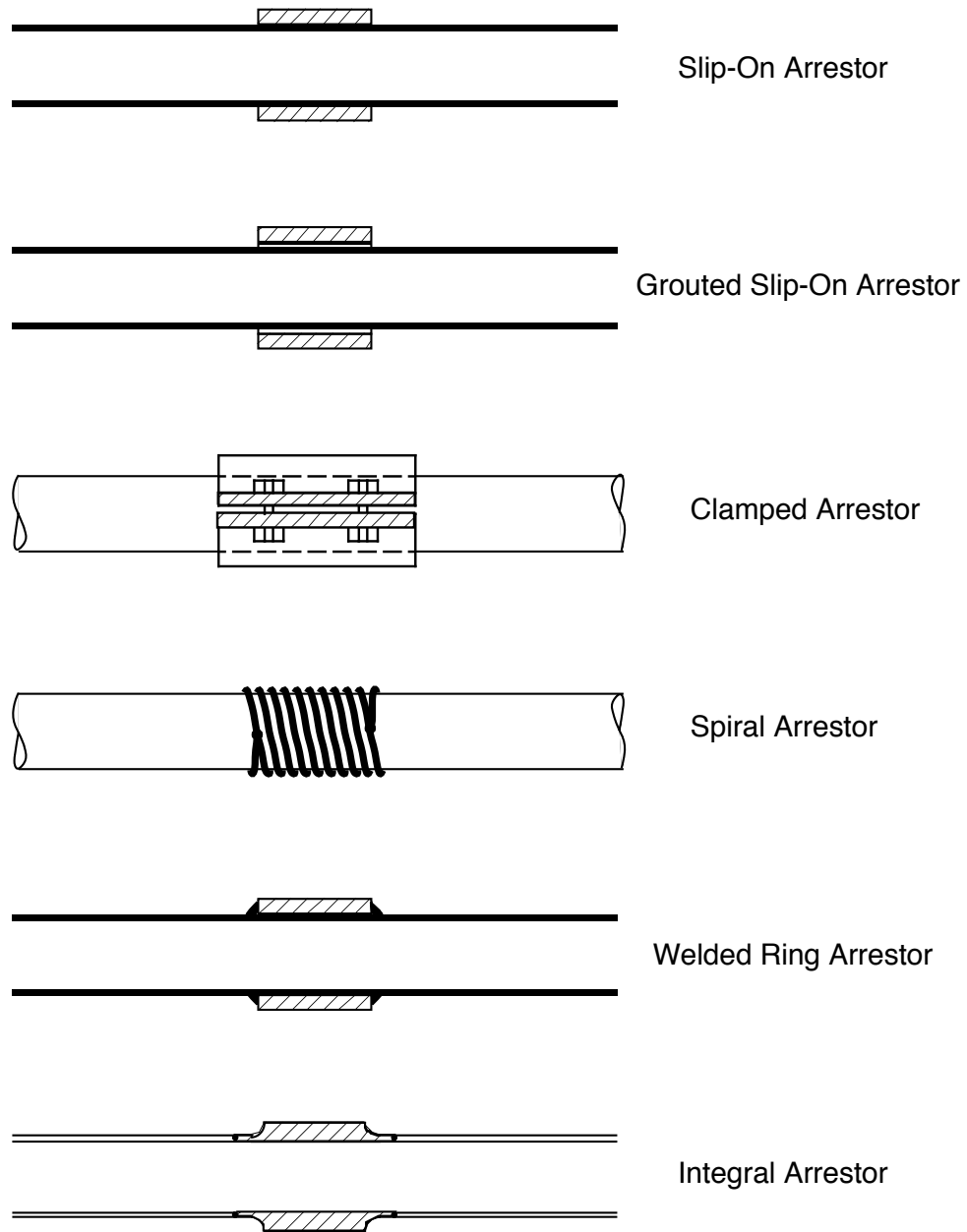


Fig. 1.3 Buckle arrestor concepts for offshore pipelines



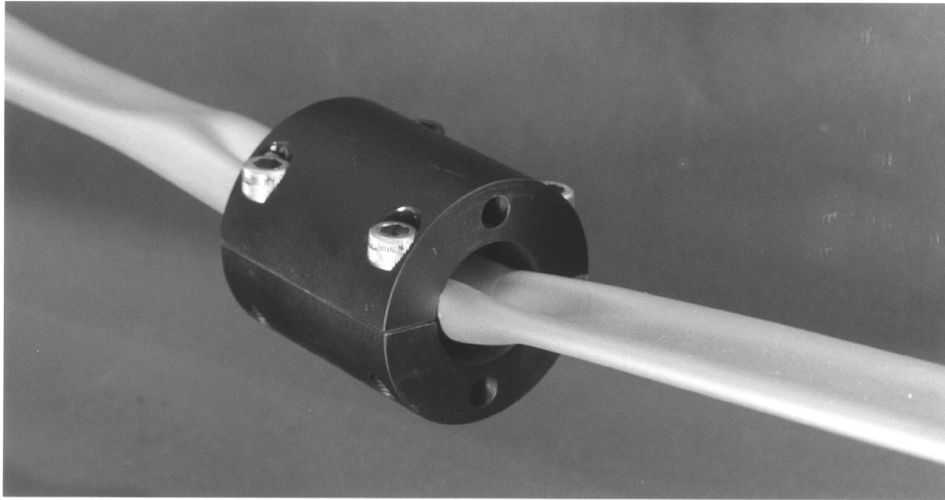


Fig. 1.4 U-mode crossover of a long and thick two-part slip-on buckle arrestor

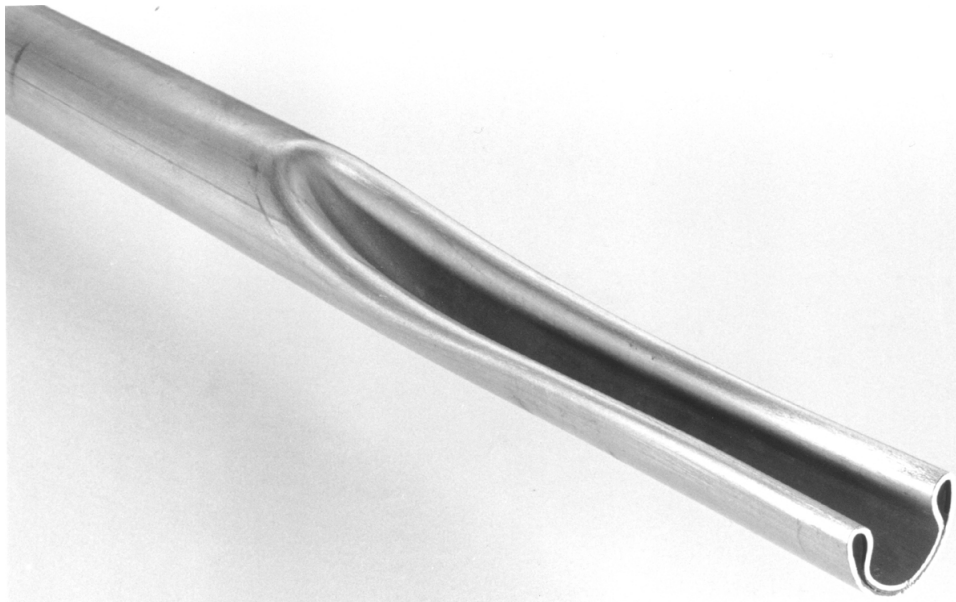


Fig. 1.5 Profile of confined propagating buckle with its characteristic U-mode

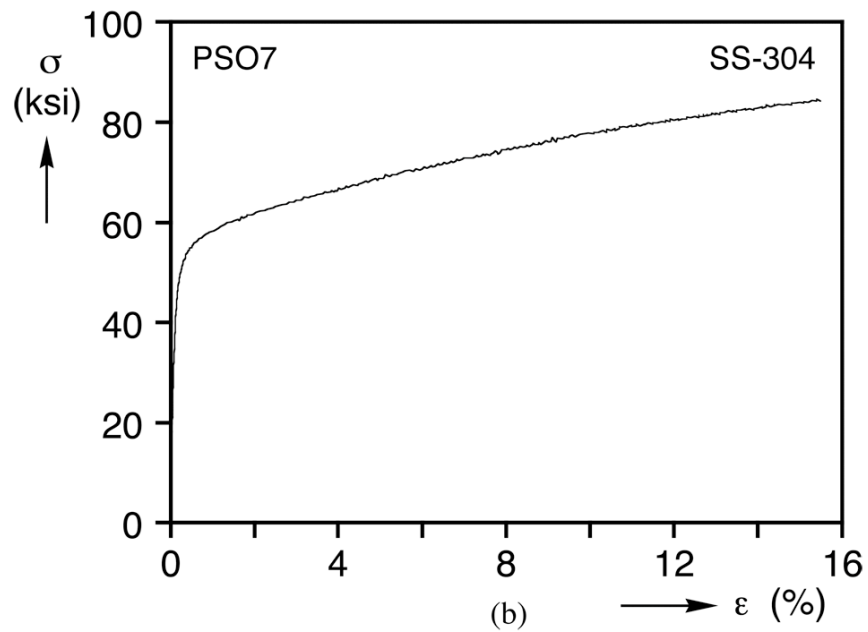
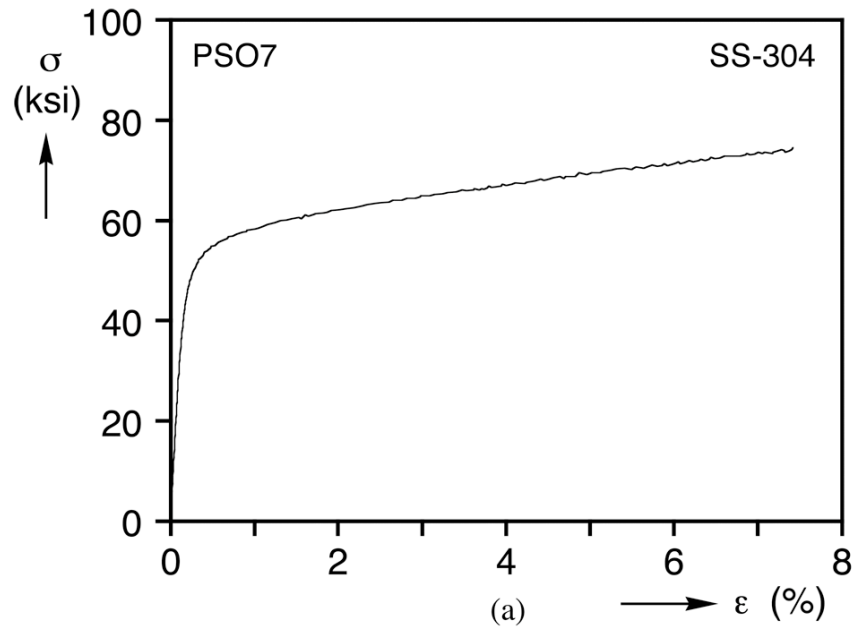


Fig. 2.1 Stress-strain response of uniaxial tests from: (a) Strain gage (b) Extensometer

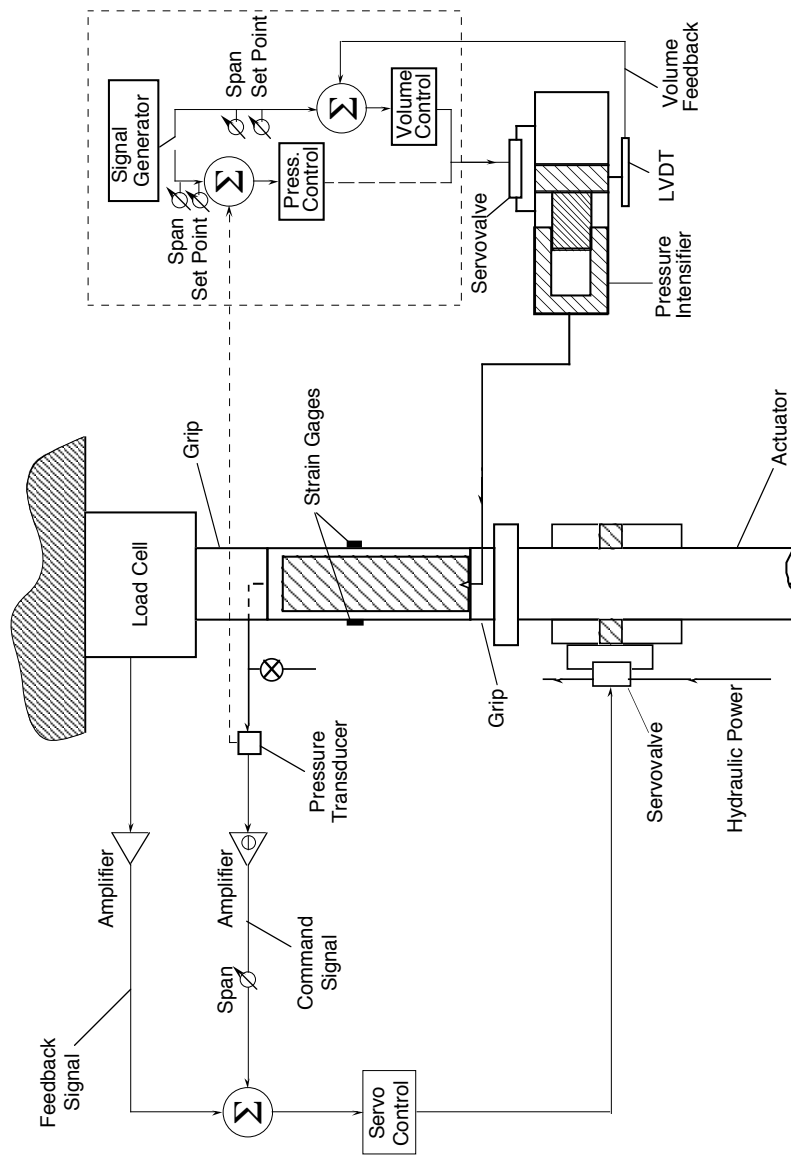


Fig. 2.2 Experimental set-up used to establish anisotropy constants

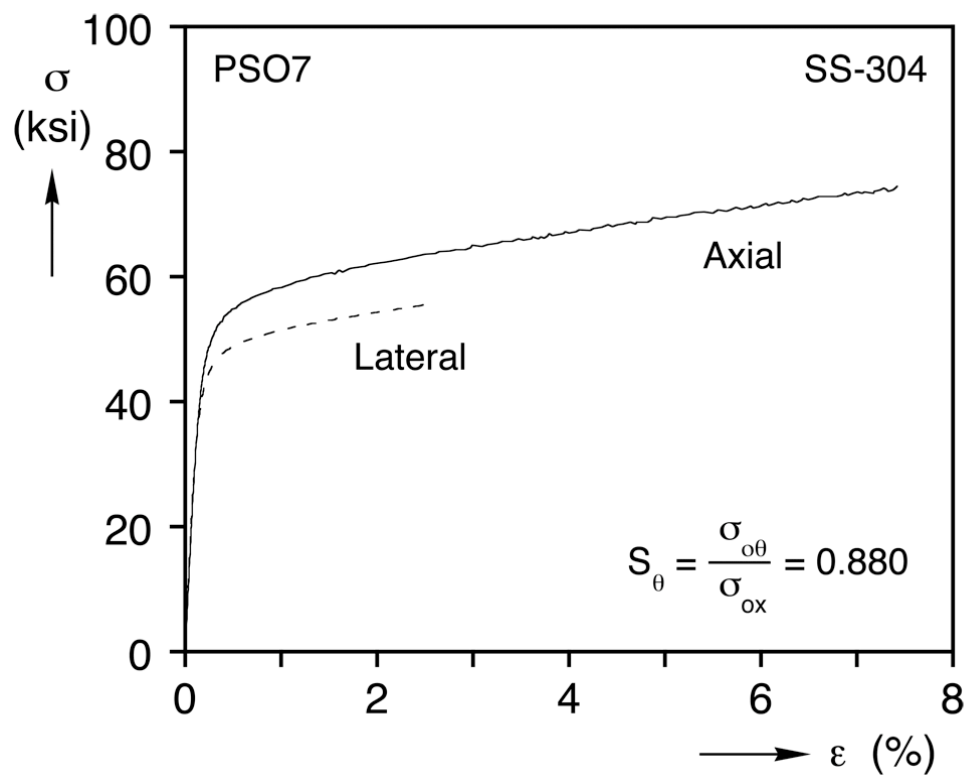


Fig. 2.3 Comparison of stress-strain responses in axial and circumferential direction

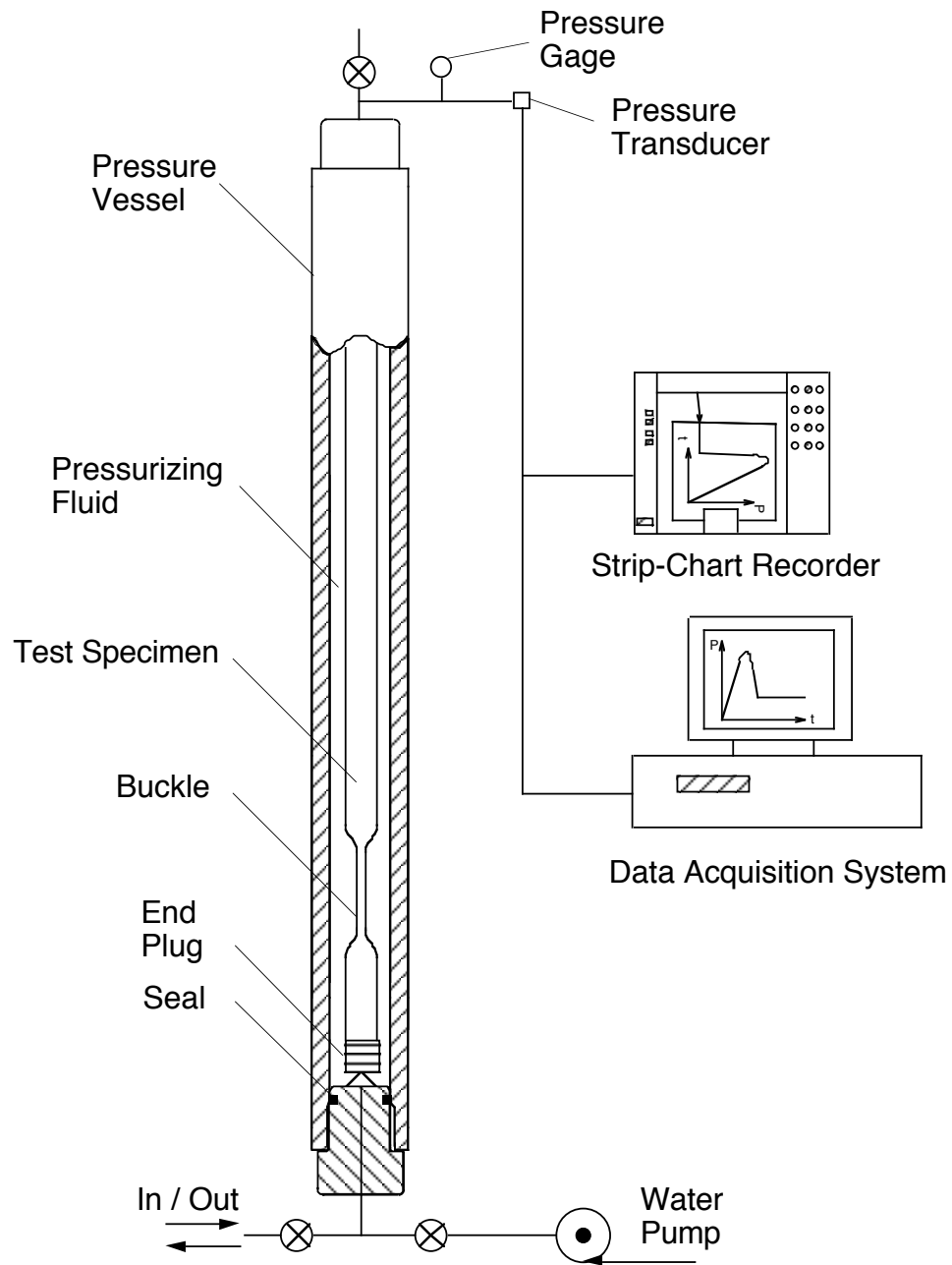


Fig. 2.4 Experimental set-up used to establish the collapse pressure

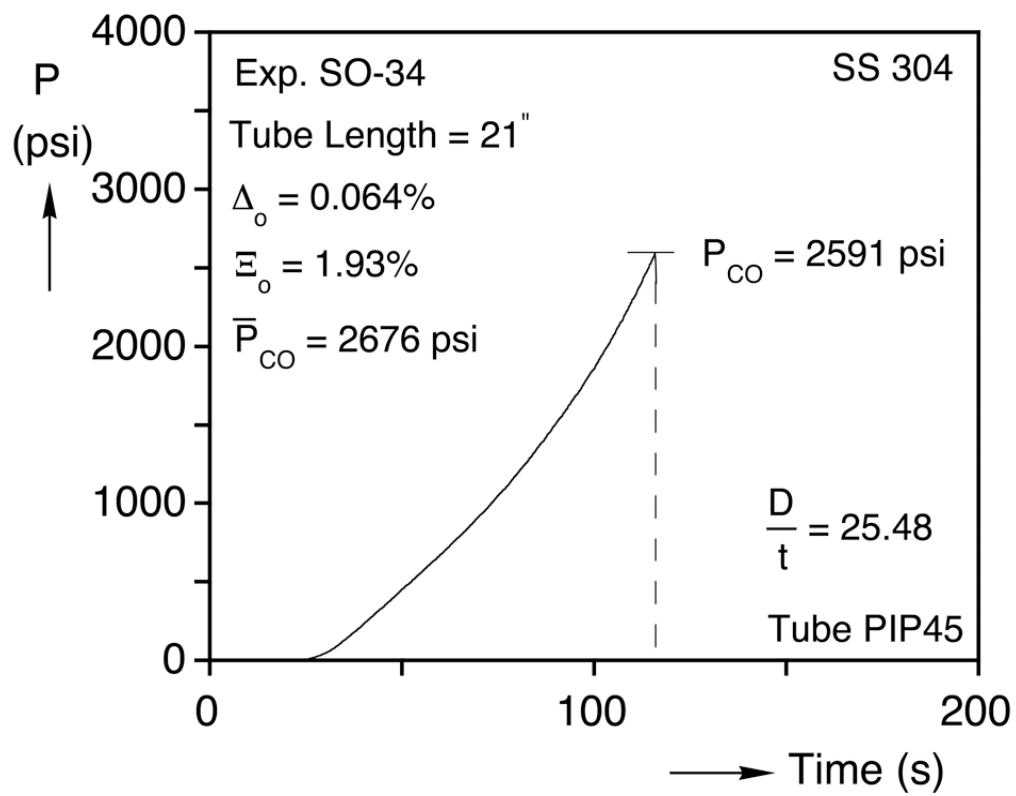


Fig. 2.5 Pressure-time history of a typical collapse experiment

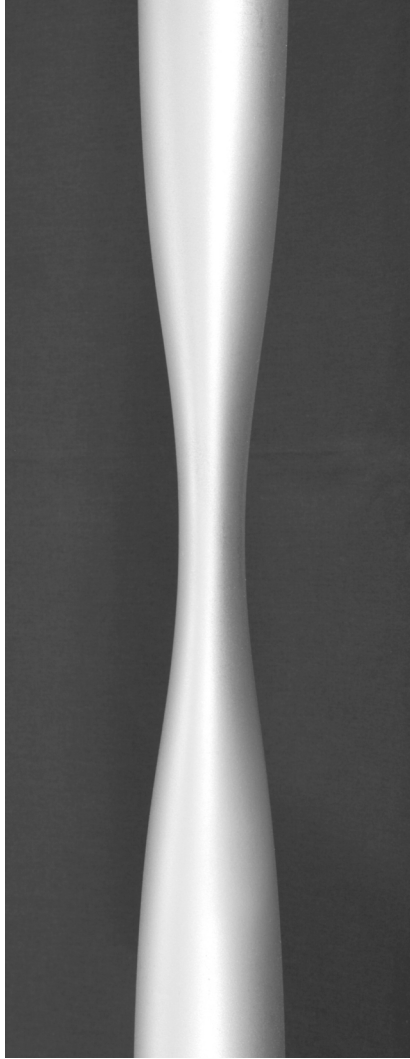


Fig. 2.6 The formation of a local flattened section of a collapse tube

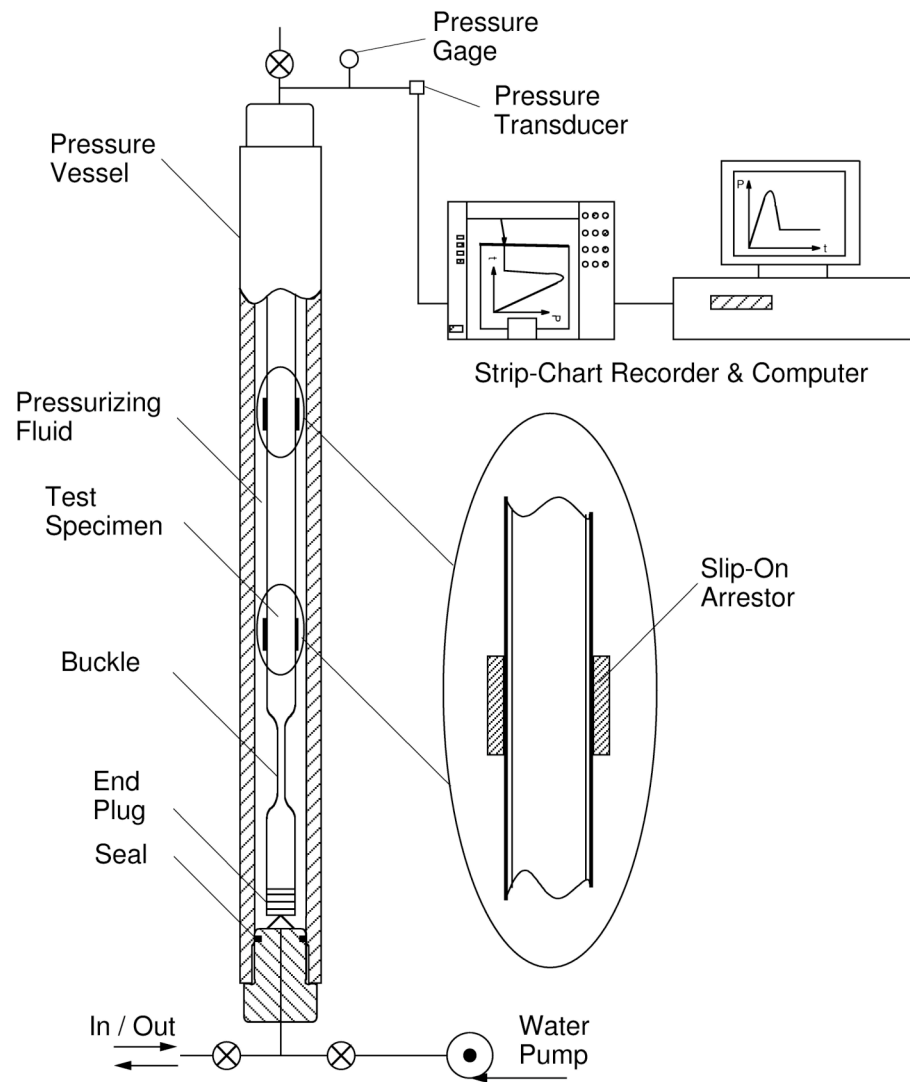
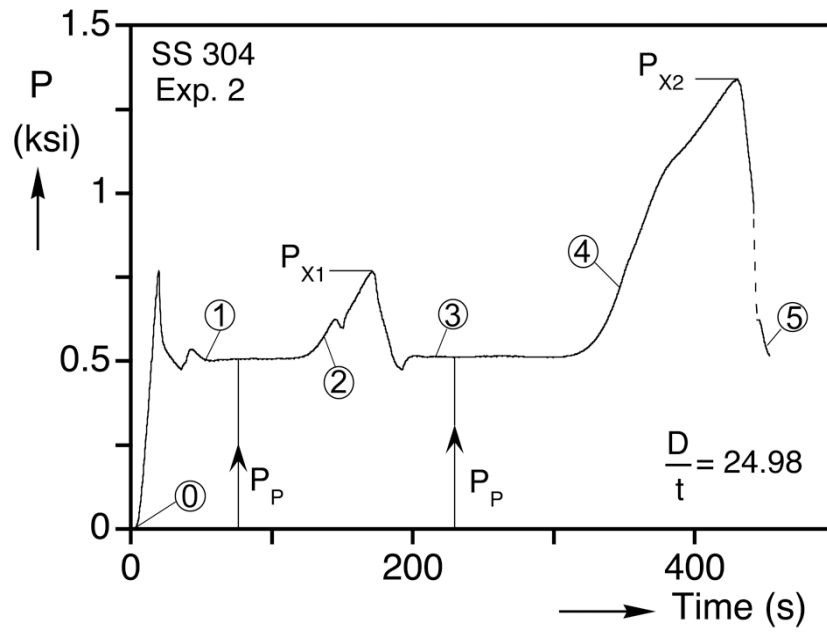
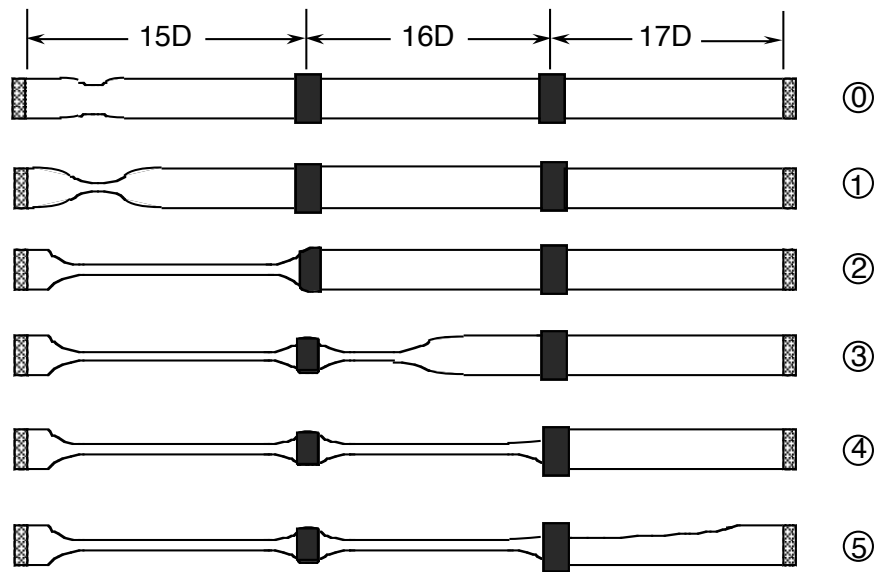


Fig. 2.7 Experimental set-up and assembling used to establish arrestor crossover pressure



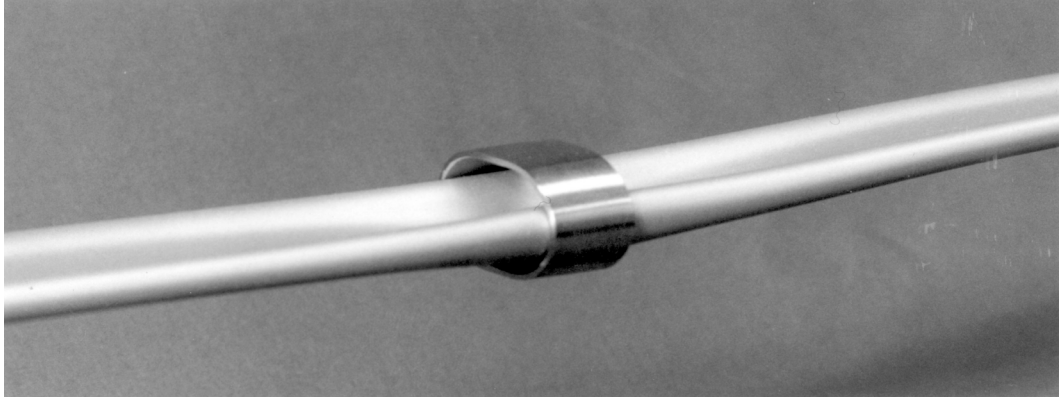


(a)



(b)

Fig. 2.8 (a) Pressure-time history of a typical experiment and (b) corresponding specimen deformed configurations illustrating buckle initiation, quasi-static propagation, arrest and crossover



(a)



(b)

Fig. 2.9 Two slip-on arrestor crossover modes: (a) the flattening and (b) the U-mode

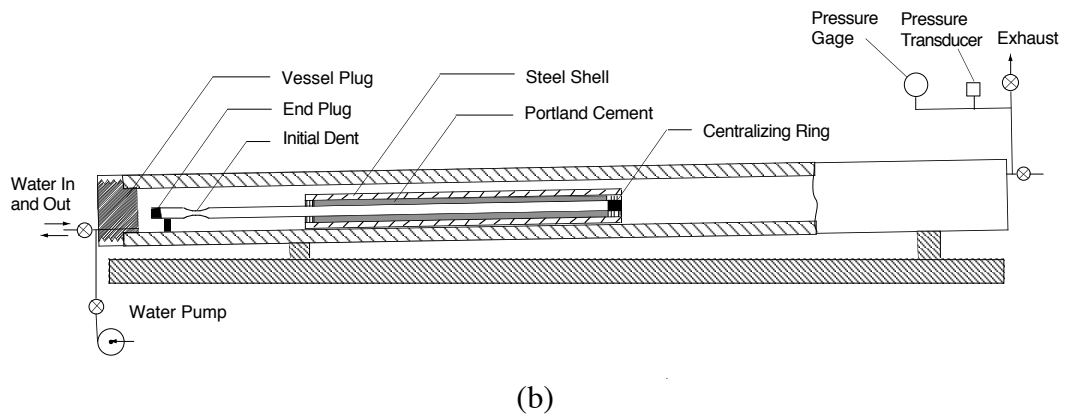
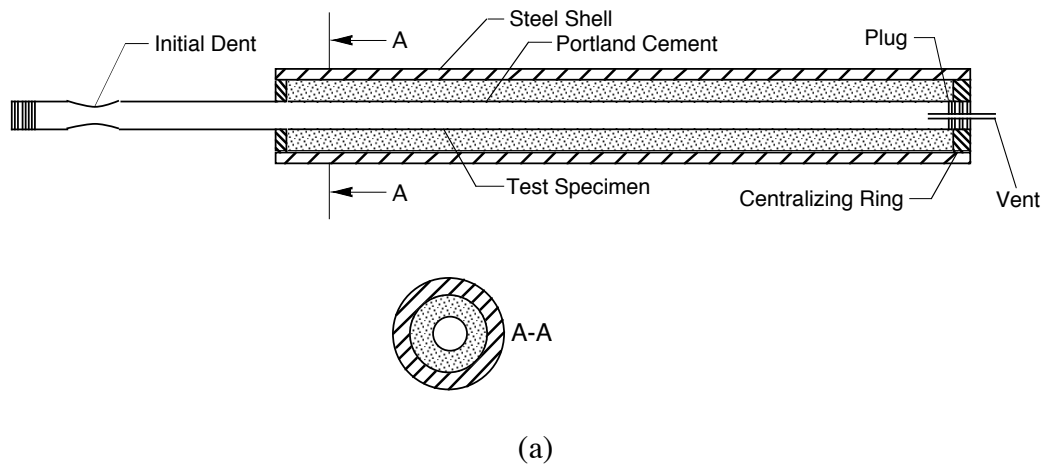


Fig. 2.10 (a) Schematic of a tube partially confined by cement, and  
(b) Experimental set-up to establish the confined propagation pressure

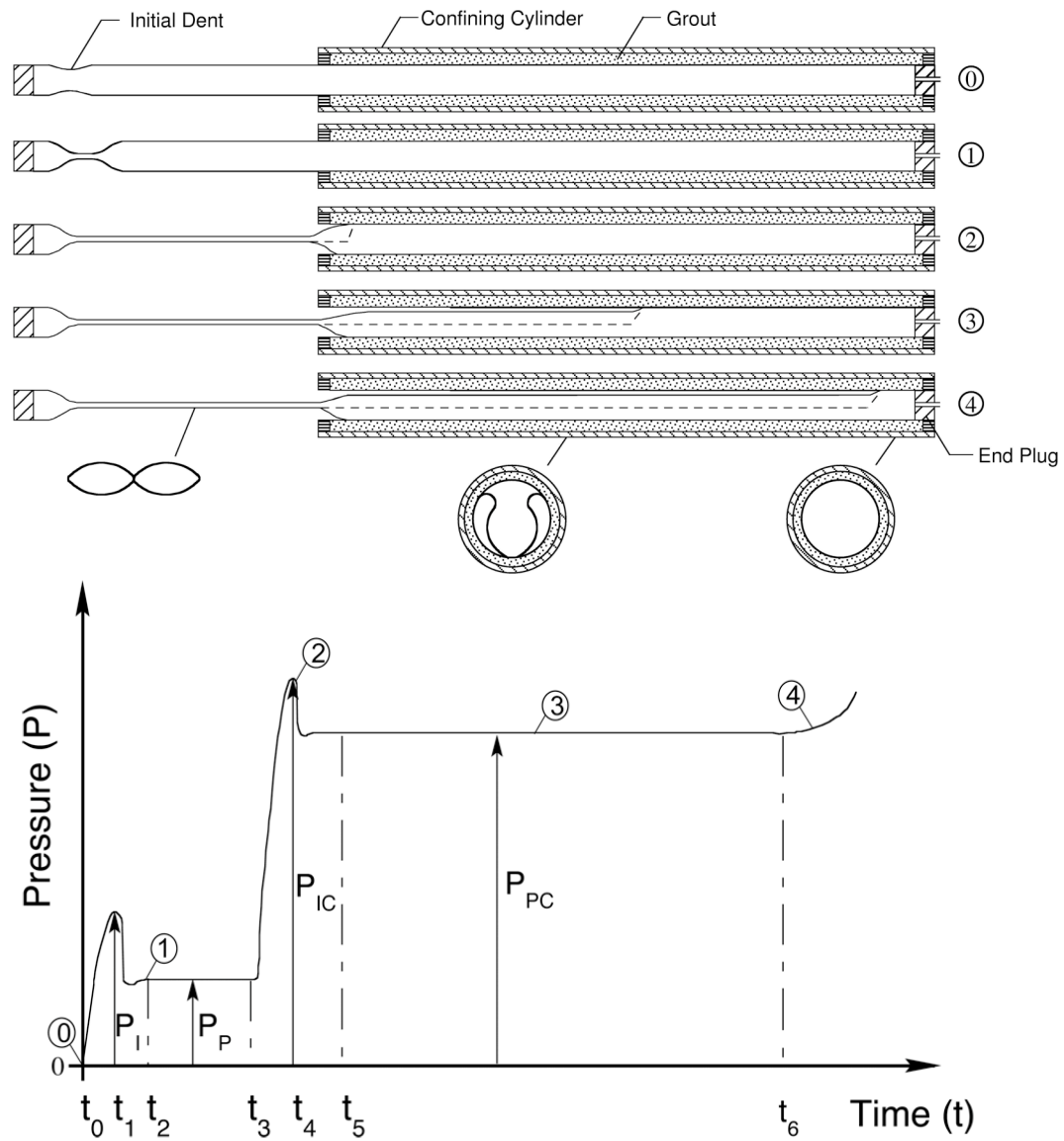


Fig. 2.11 Pressure-time history of a typical quasi-static test on a partially confined tube

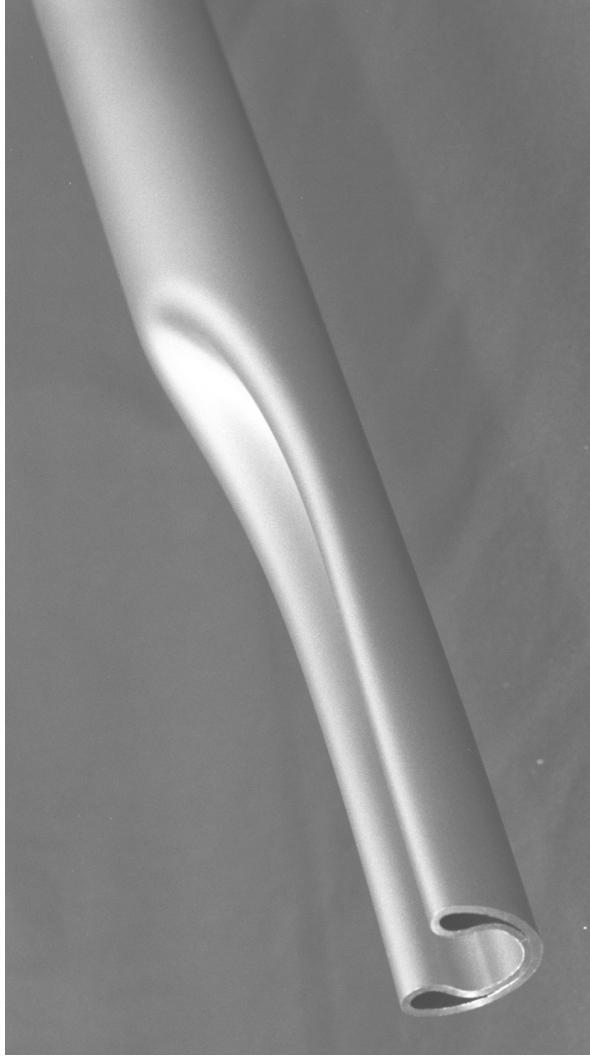


Fig. 2.12 Profile of a confined propagating buckle (SS-304 1/8H,  $D/t = 23.4$ )

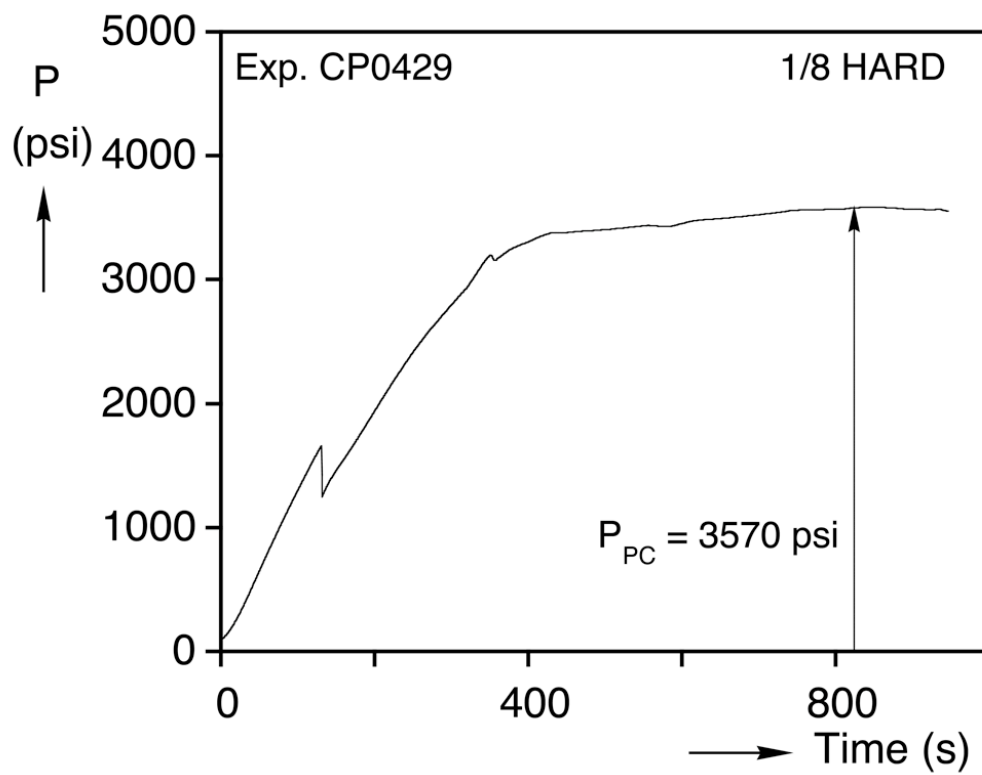


Fig. 2.13 Pressure-time histories from the confined propagation pressure experiment on tubes  $D/t = 23.4$

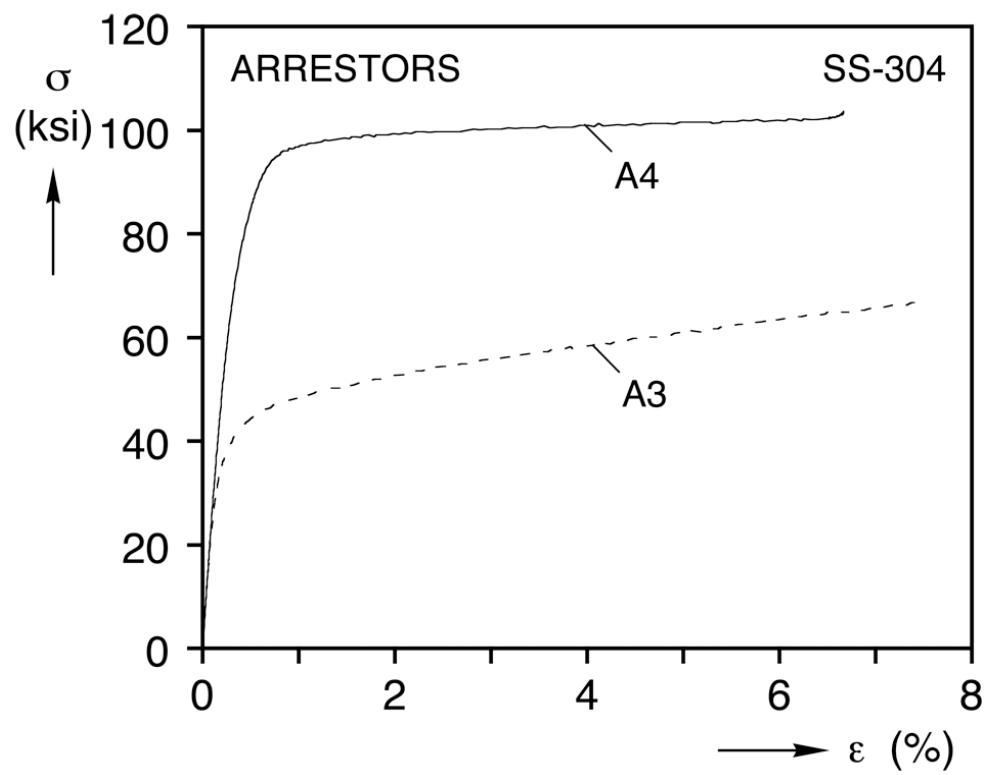


Fig. 3.1 Comparison of stress-strain responses of two arrestor materials

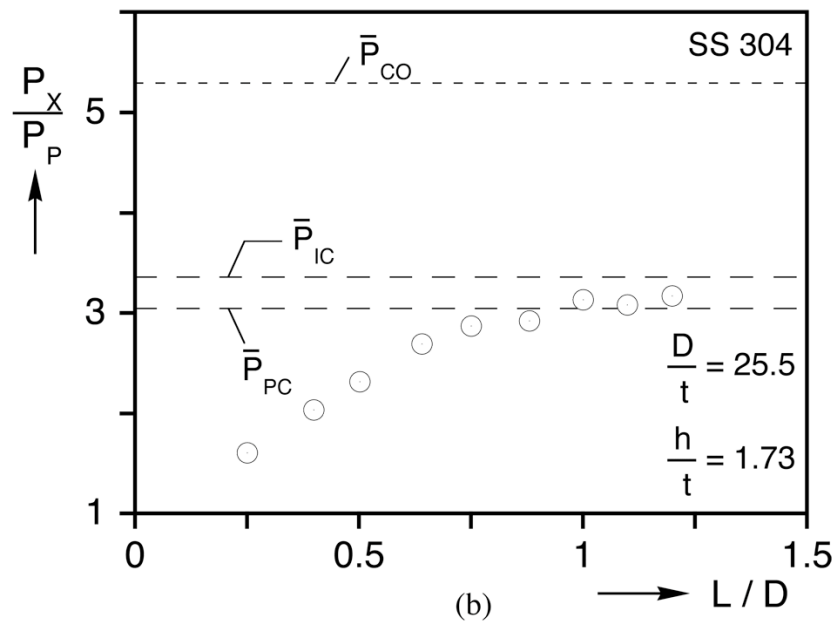
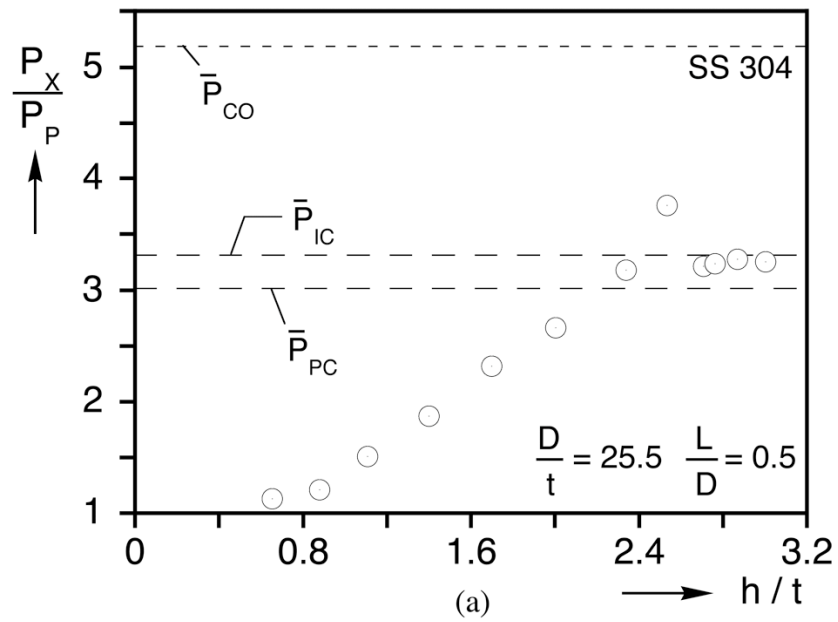


Fig. 3.2 Crossover pressures for tubes with nominal  $D/t = 25.5$ : (a)  $P_X$  as a function of arrestor thickness (b)  $P_X$  as a function of arrestor length



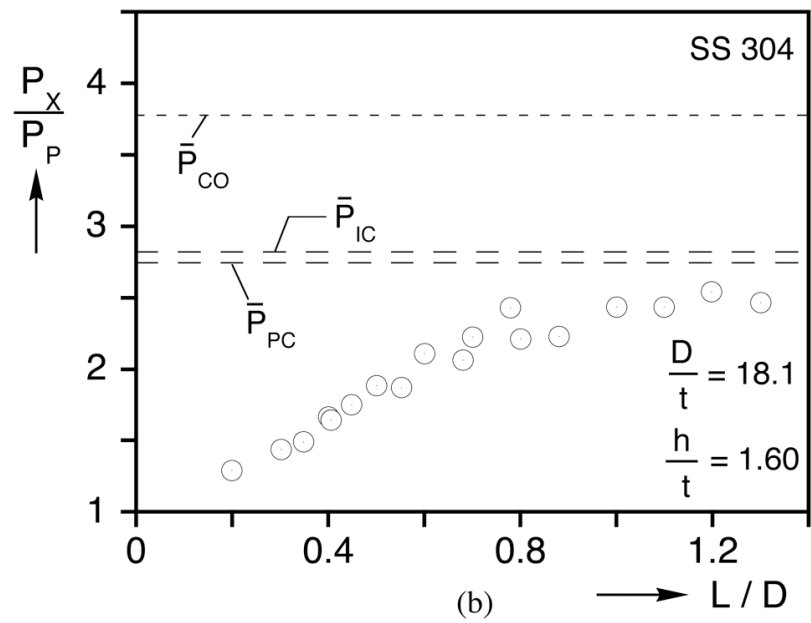
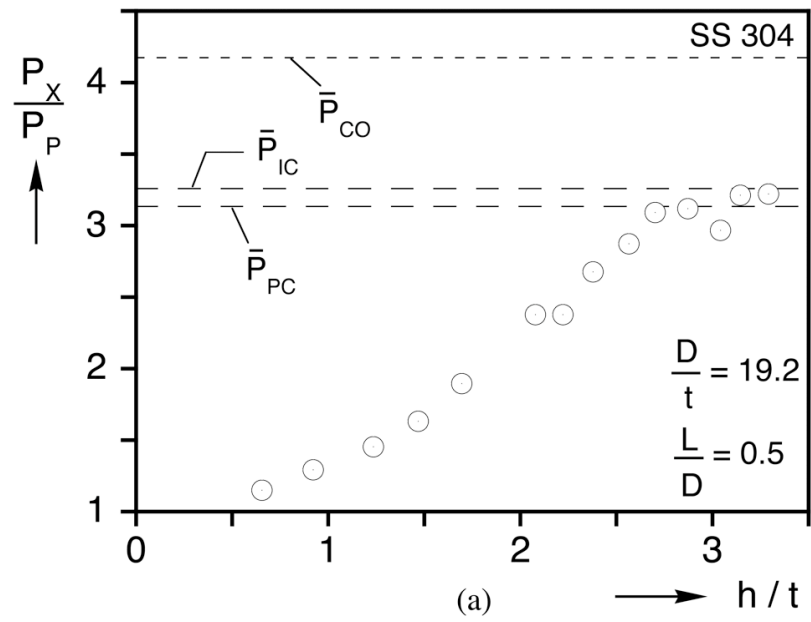


Fig. 3.3 Crossover pressures for tubes  $D/t = 19$ : (a)  $P_X$  as a function of arrestor thickness (b)  $P_X$  as a function of arrestor length

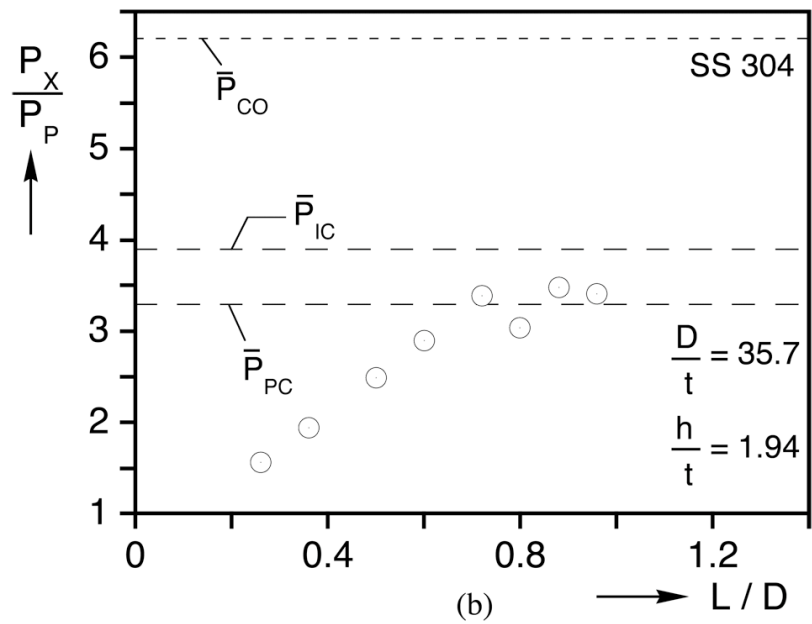
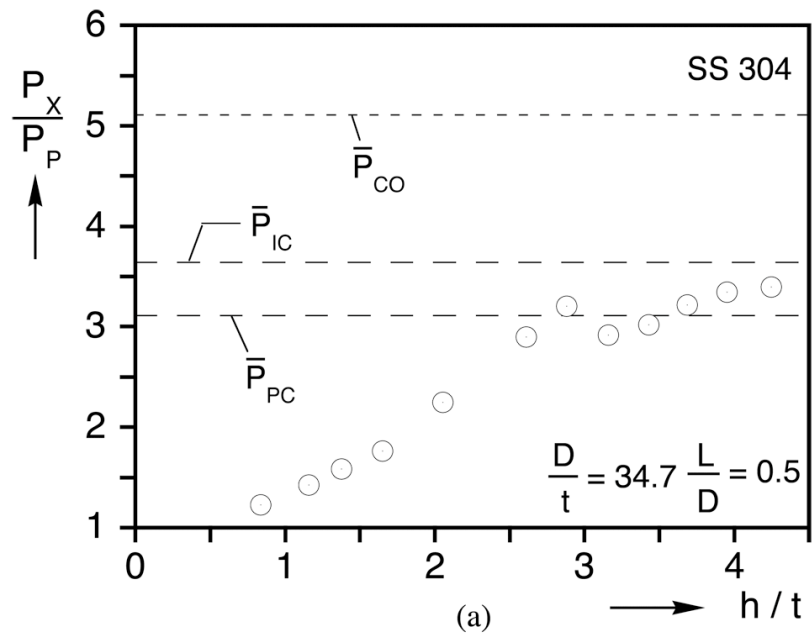


Fig. 3.4 Crossover pressures for tubes with nominal  $D/t = 35$ : (a)  $P_X$  as a function of arrestor thickness (b)  $P_X$  as a function of arrestor length

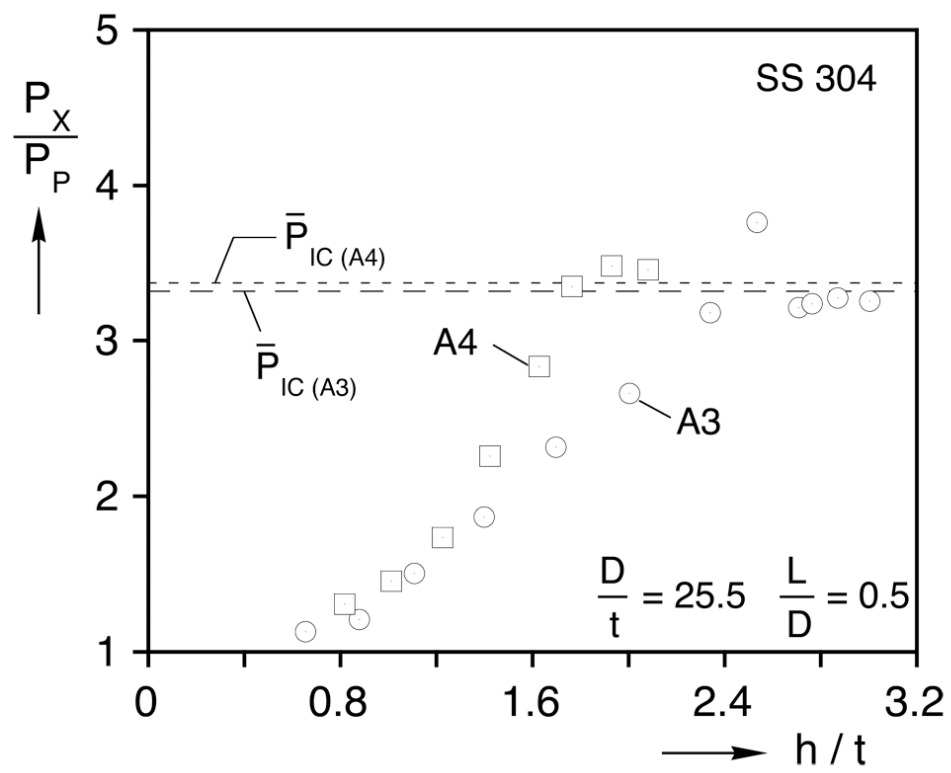


Fig. 3.5 Comparison of arrestor crossover pressure as function of arrestor thickness for two arrestor materials

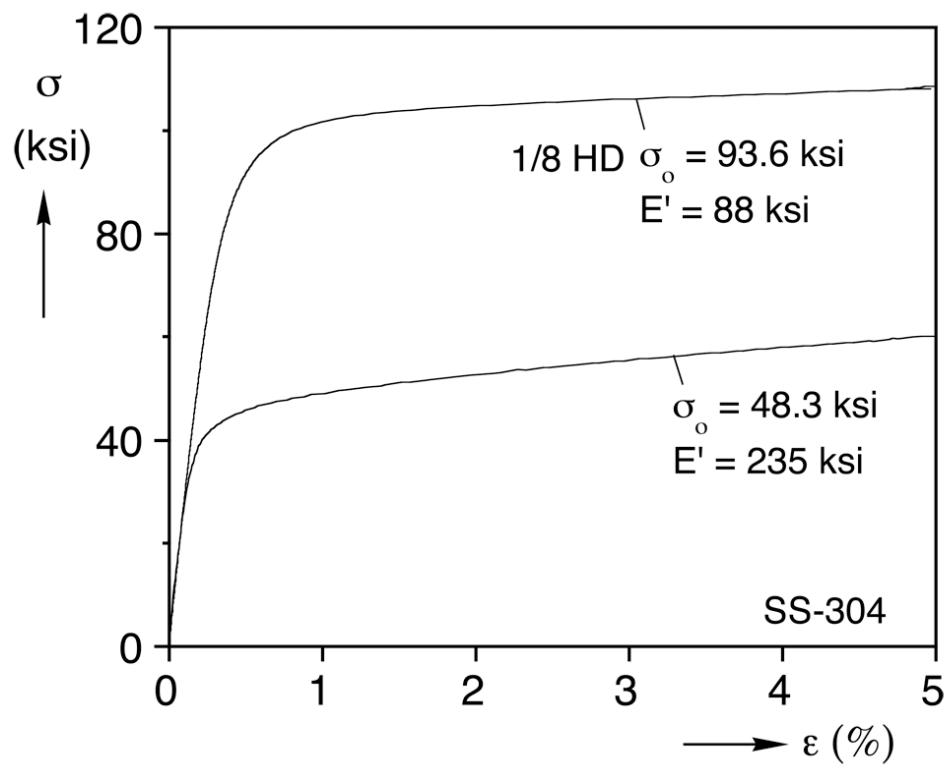


Fig. 3.6 Comparison of the typical stress-strain responses of two SS-304 materials

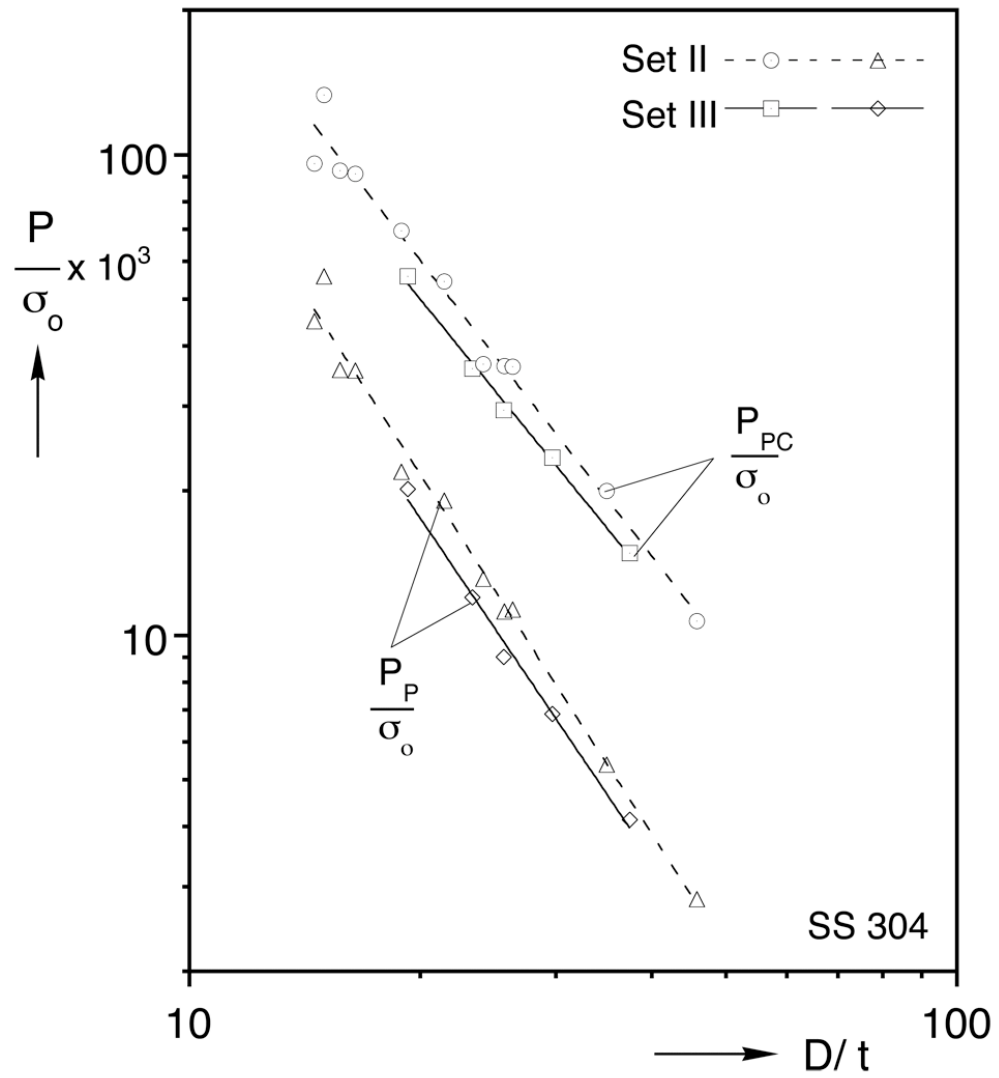


Fig. 3.7 Propagation and confined propagation pressure measured for two SS-304 alloys as a function of tube  $D/t$

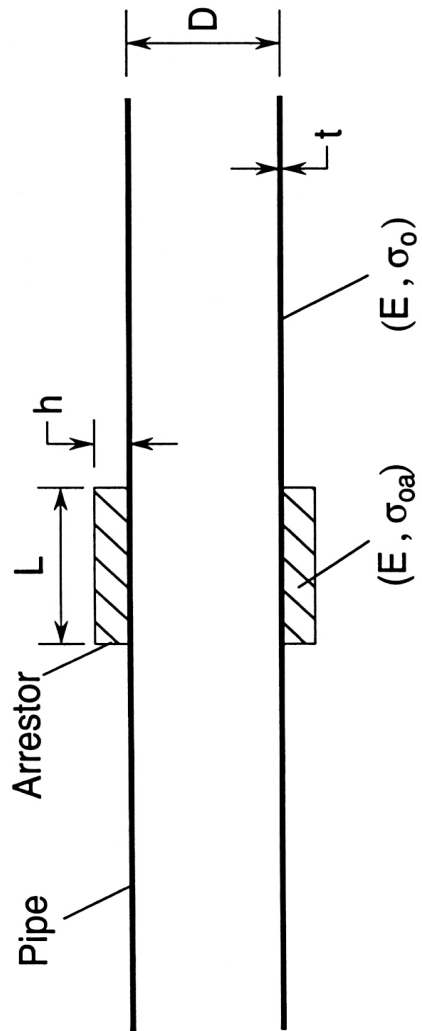


Fig. 4.1 Main pipe and slip-on buckle arrestor parameters

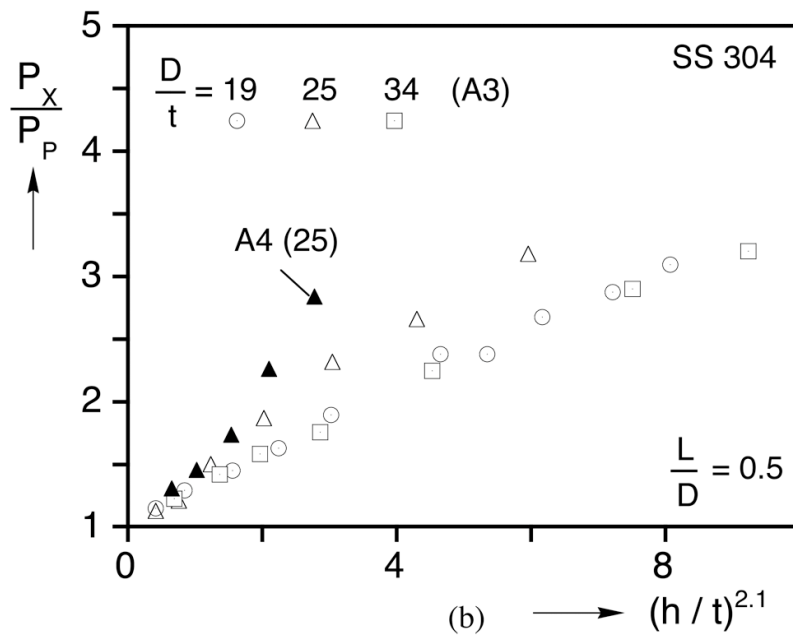
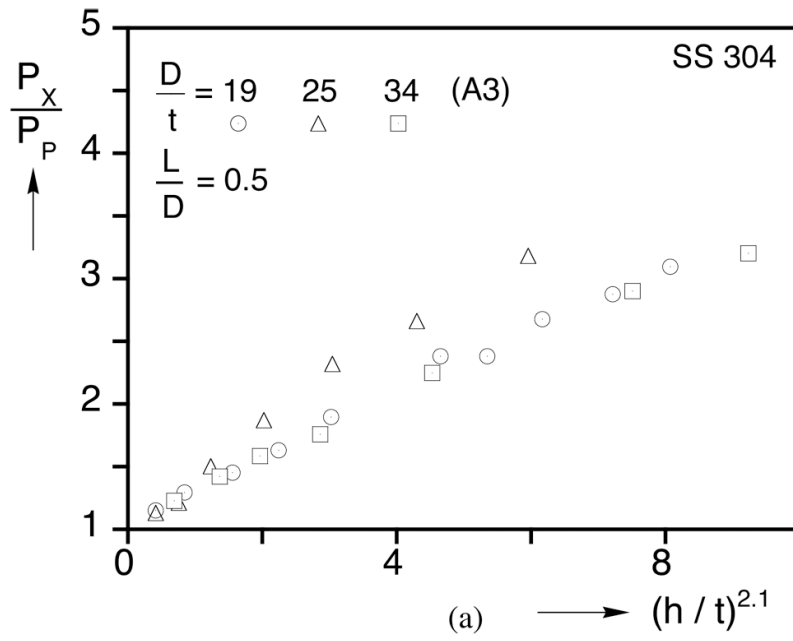


Fig. 4.2 Crossover pressure as a function of powerlaw parameter  $(h/t)^{2.1}$ :  
(a) for arrestor material A3 only and (b) A3 & A4

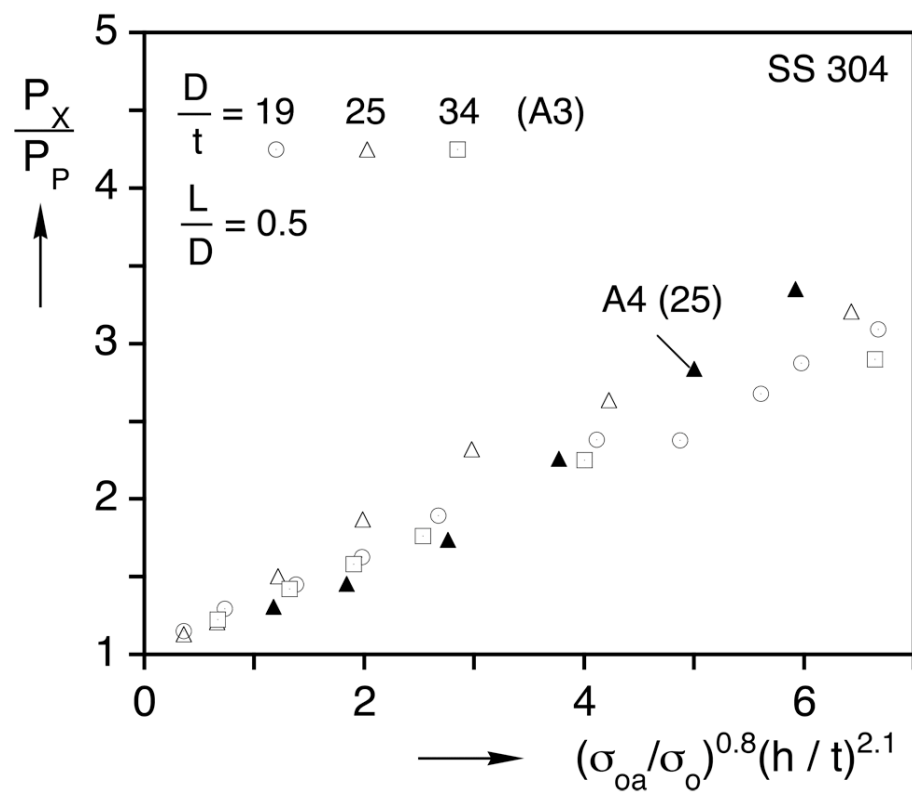


Fig. 4.3 Correlated data for arrestor materials A3 and A4



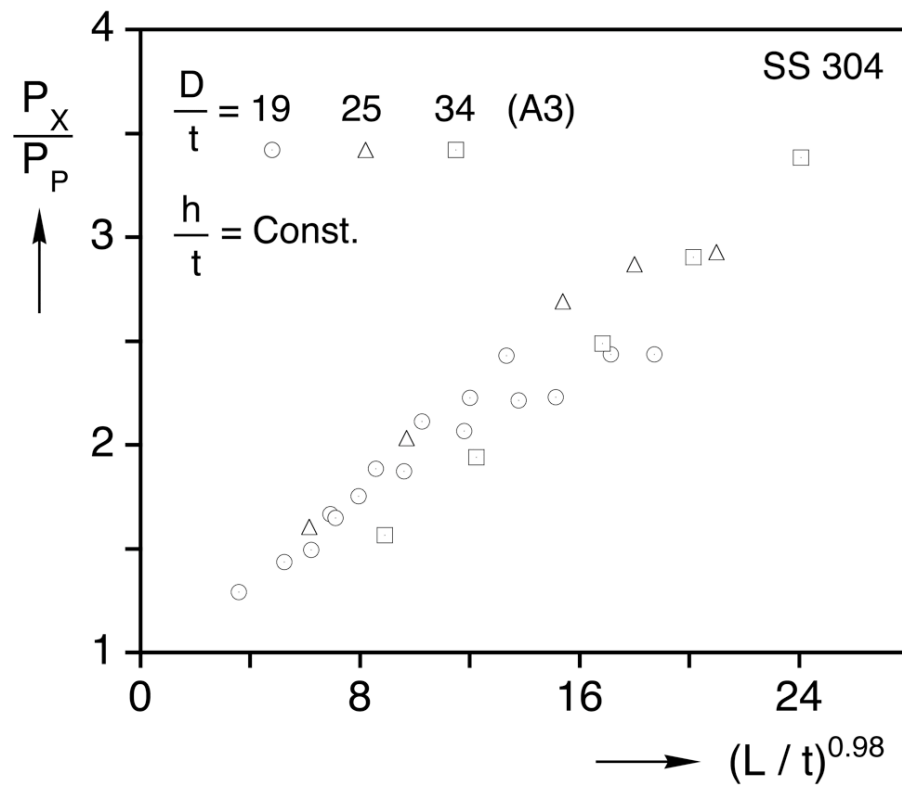


Fig. 4.4 Crossover pressure as a function of powerlaw parameter  $(L/t)^{0.98}$

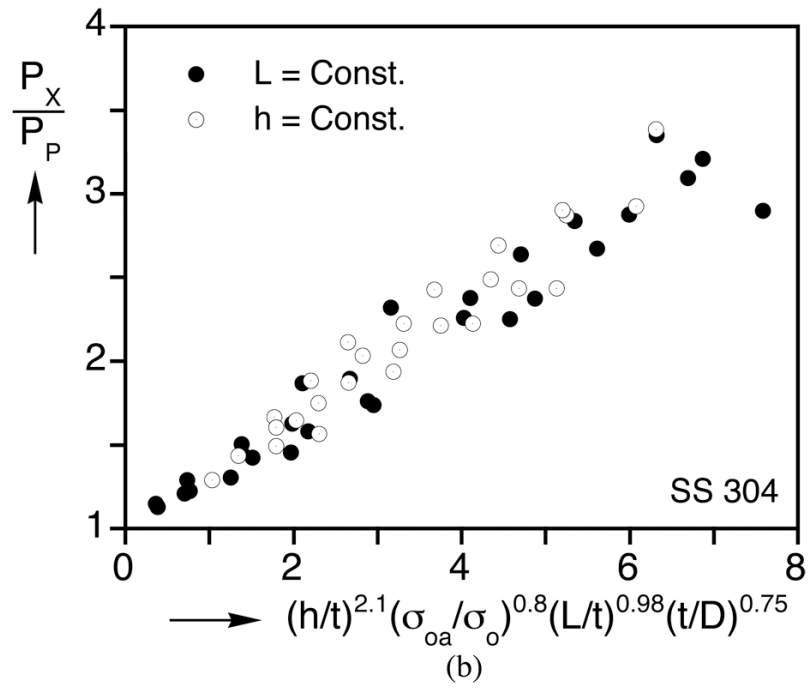
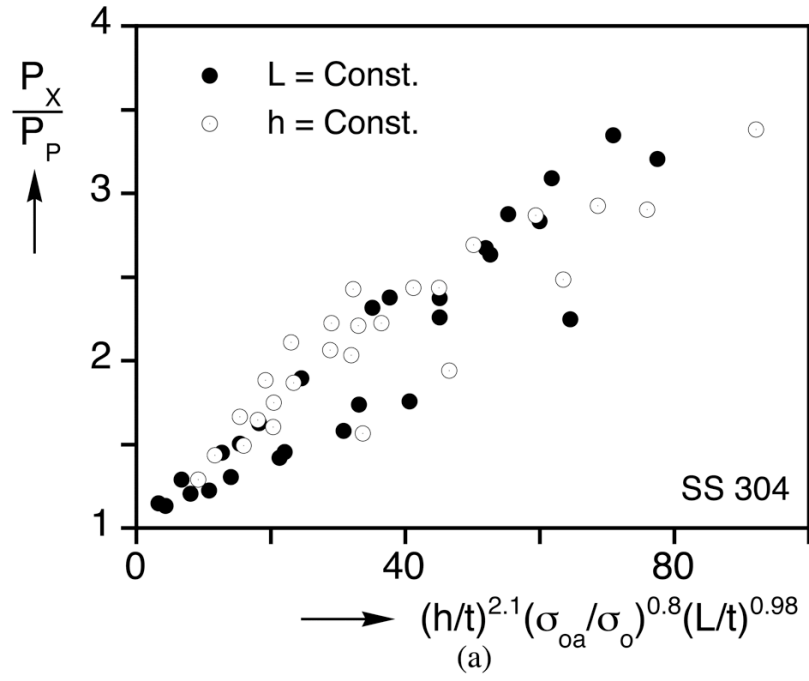


Fig. 4.5 Crossover pressure as a function of powerlaw parameters: (a) without and (b) with the effect of the parameter  $(D/t)^{\alpha_3}$

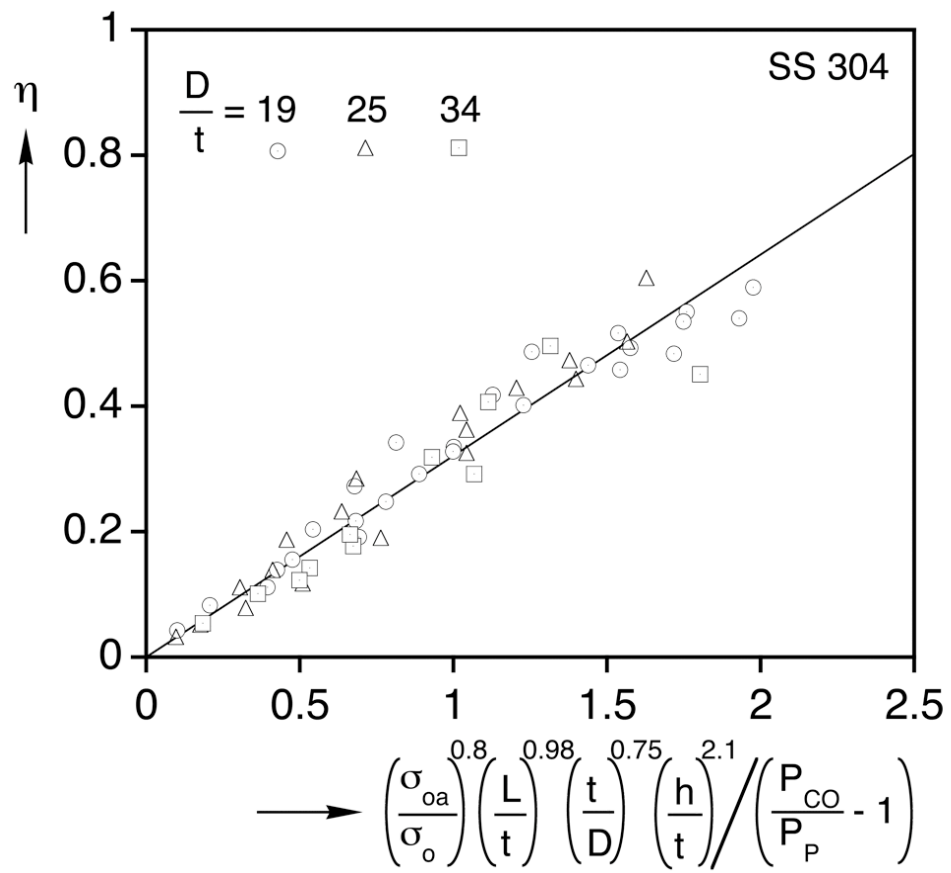


Fig. 4.6 Empirical expression for arresting efficiency of slip-on buckle arrestors

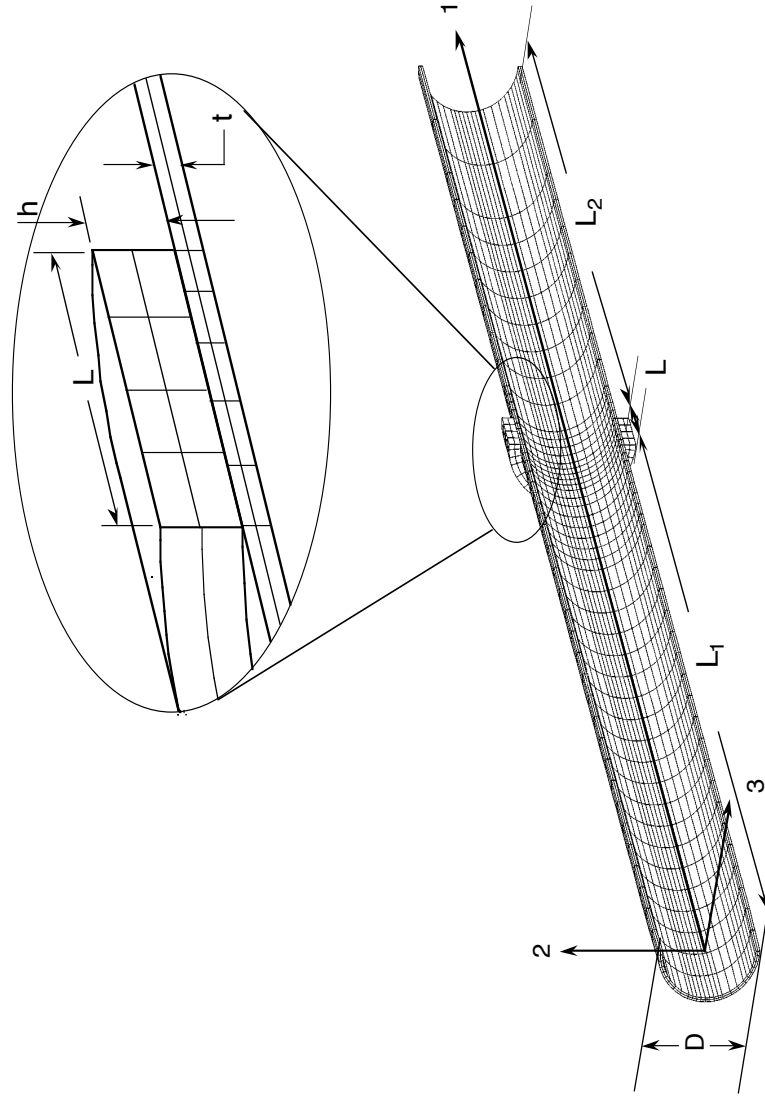


Fig. 5.1 Geometry and mesh of FE model of buckle initiation, propagation, arrest and crossover

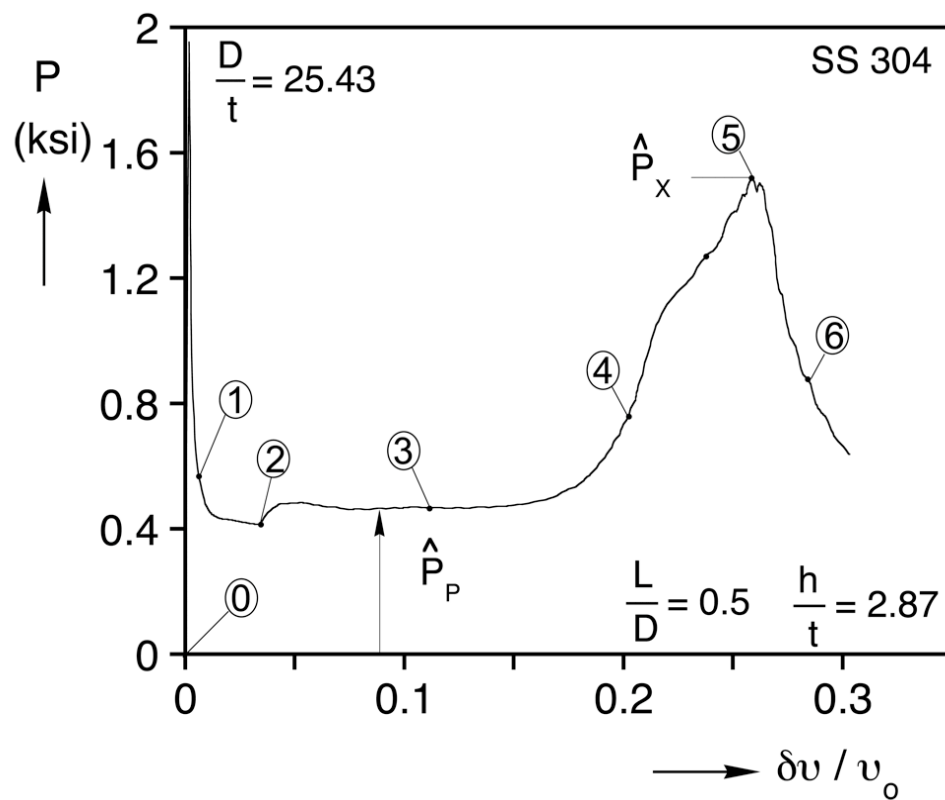


Fig. 5.2 Simulation of buckle initiation, propagation, arrest and crossover.  
 (a) Pressure-change in volume response

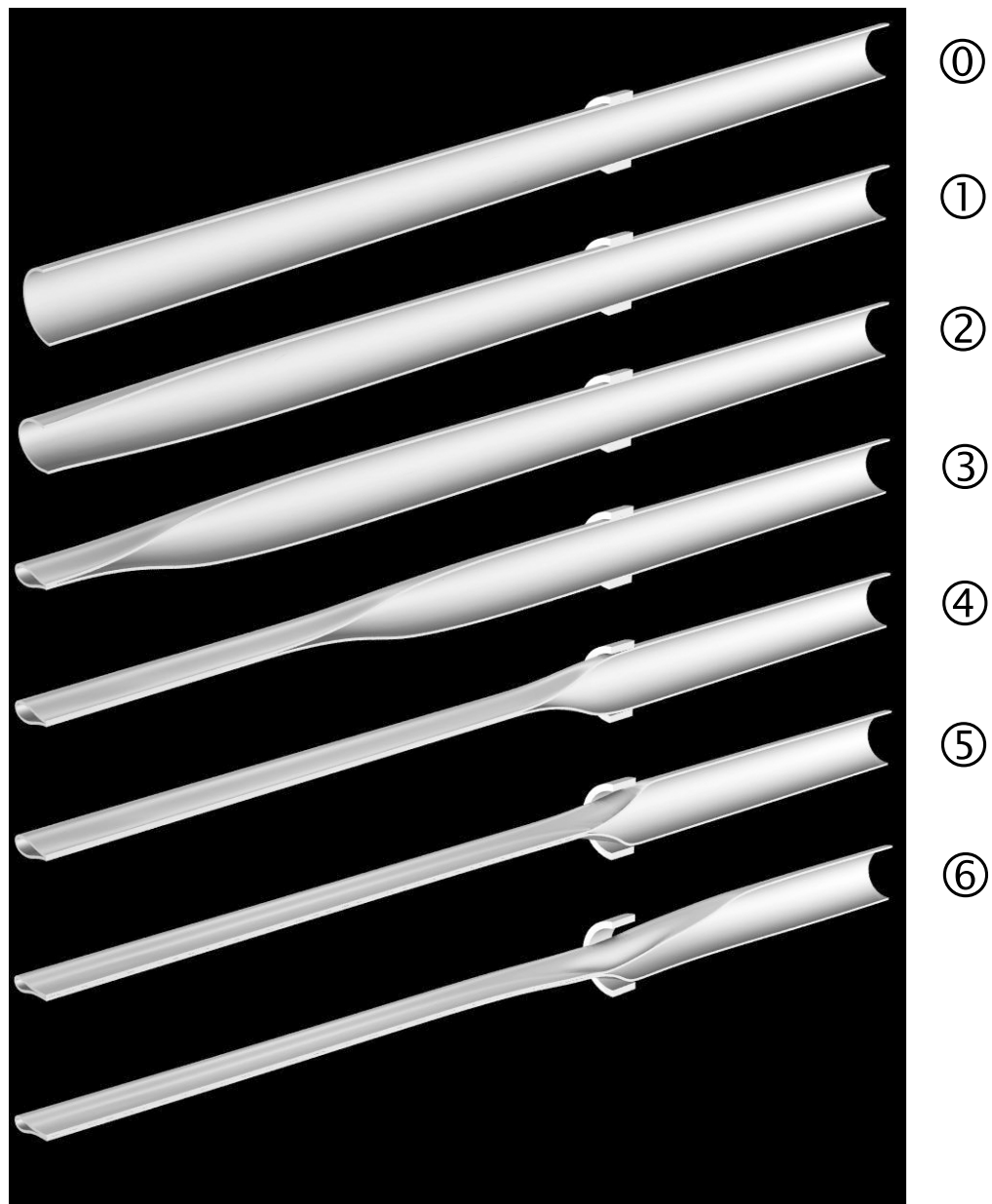


Fig. 5.2 (b) Sequence of corresponding deformed configurations

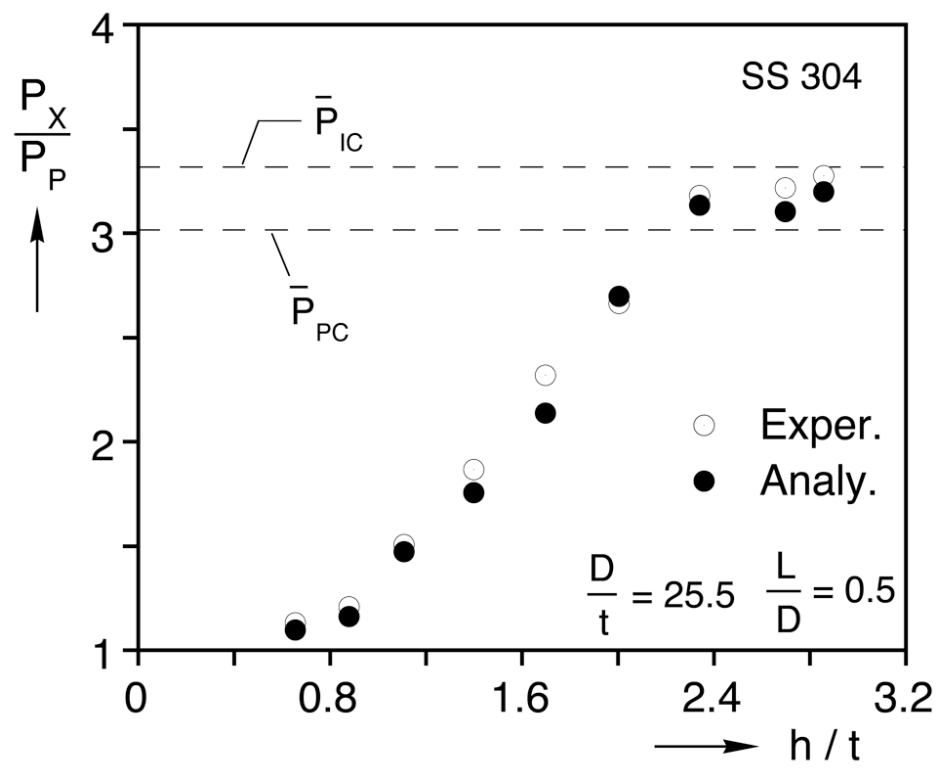


Fig. 5.3 Comparison of measured and predicted crossover pressures for tubes with nominal  $D/t = 25.5$

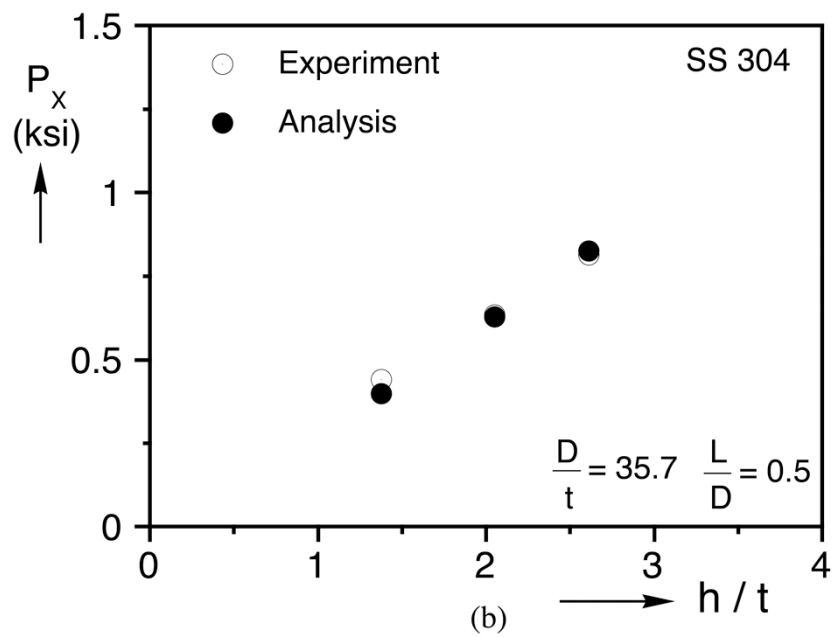
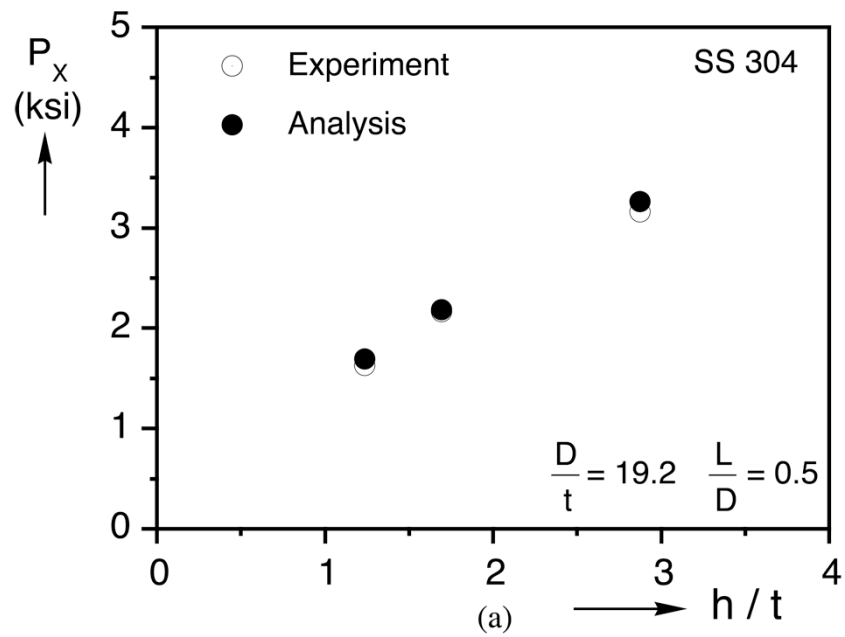


Fig. 5.4 Comparison of measured and predicted crossover pressures for tubes with (a) nominal  $D/t = 19.2$  (b) nominal  $D/t = 35.7$



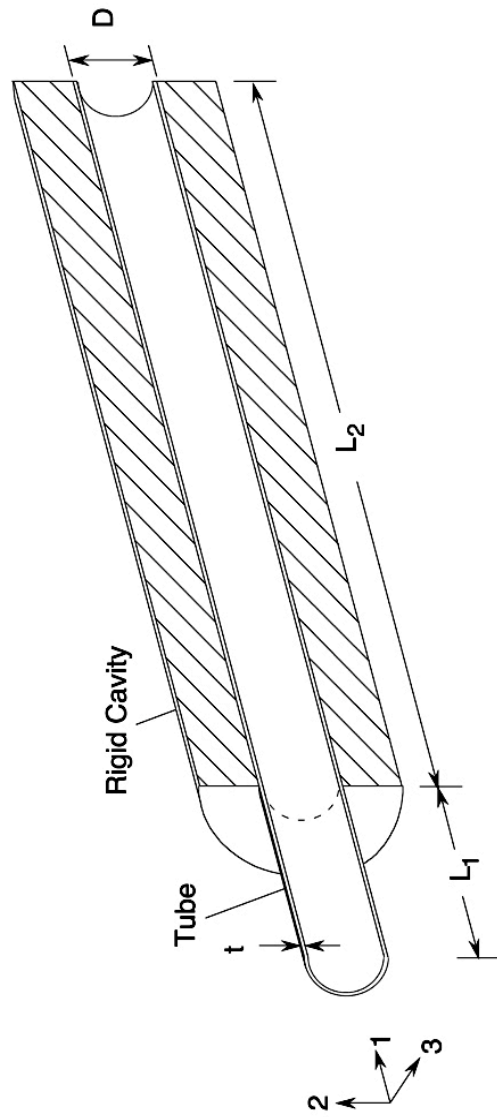


Fig. 5.5 Geometry of FE model of the confined buckle propagation

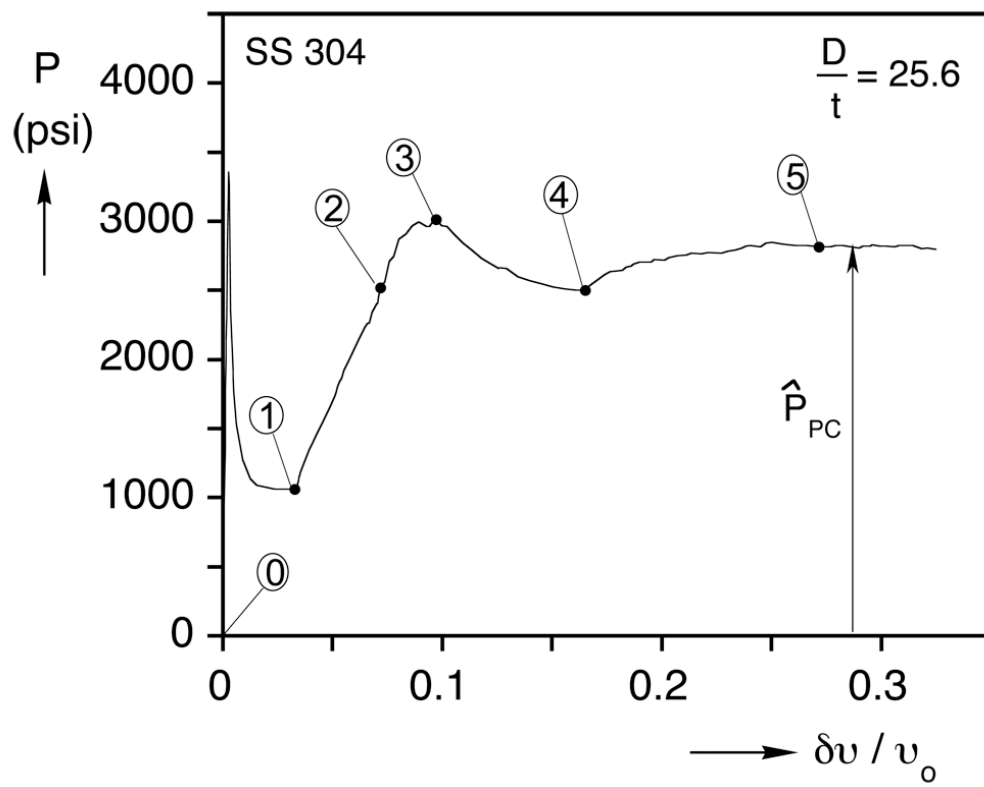


Fig. 5.6 (a) Pressure-change in volume response recorded in numerical simulation of a confined buckle propagation test

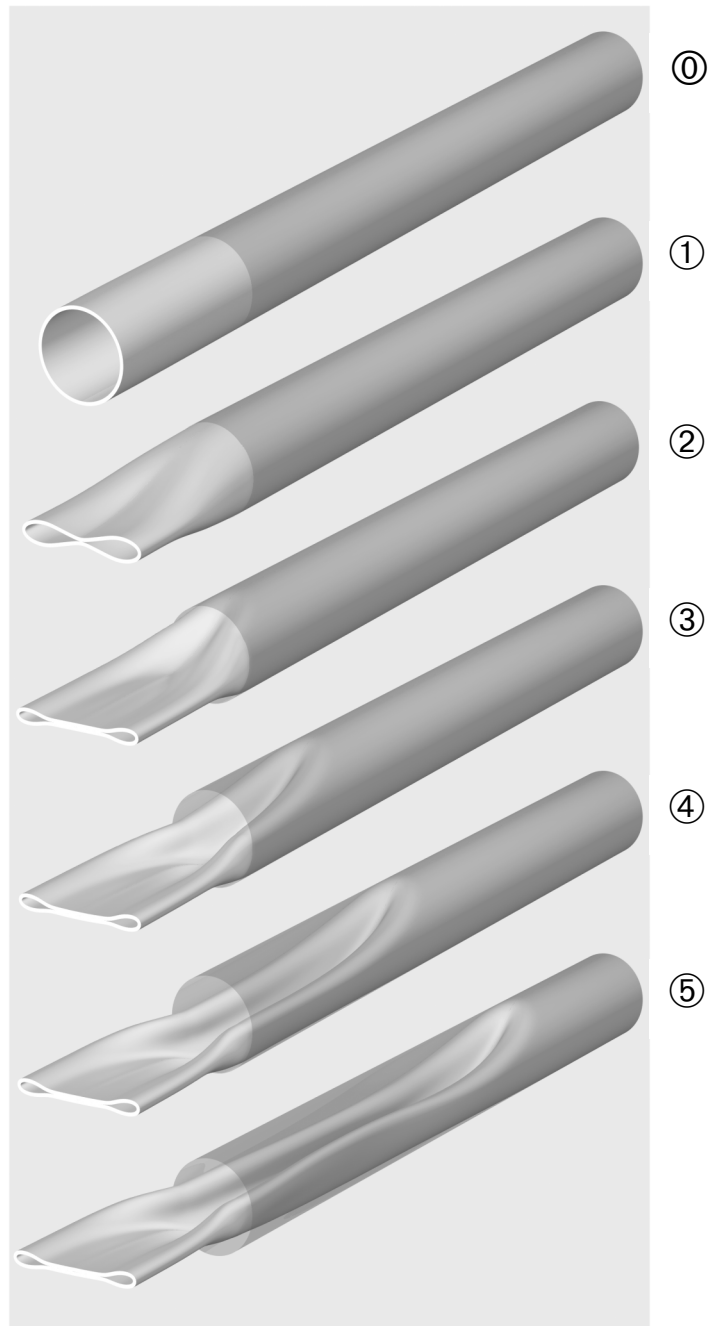


Fig. 5.6 (b) Sequence of deformed configurations of confined propagating collapse corresponding to response in Fig. 5.6(a)



Fig. 5.7 (a) Cross section of confined collapse showing the profile of the collapsing front ( $D/t = 25.6$ )

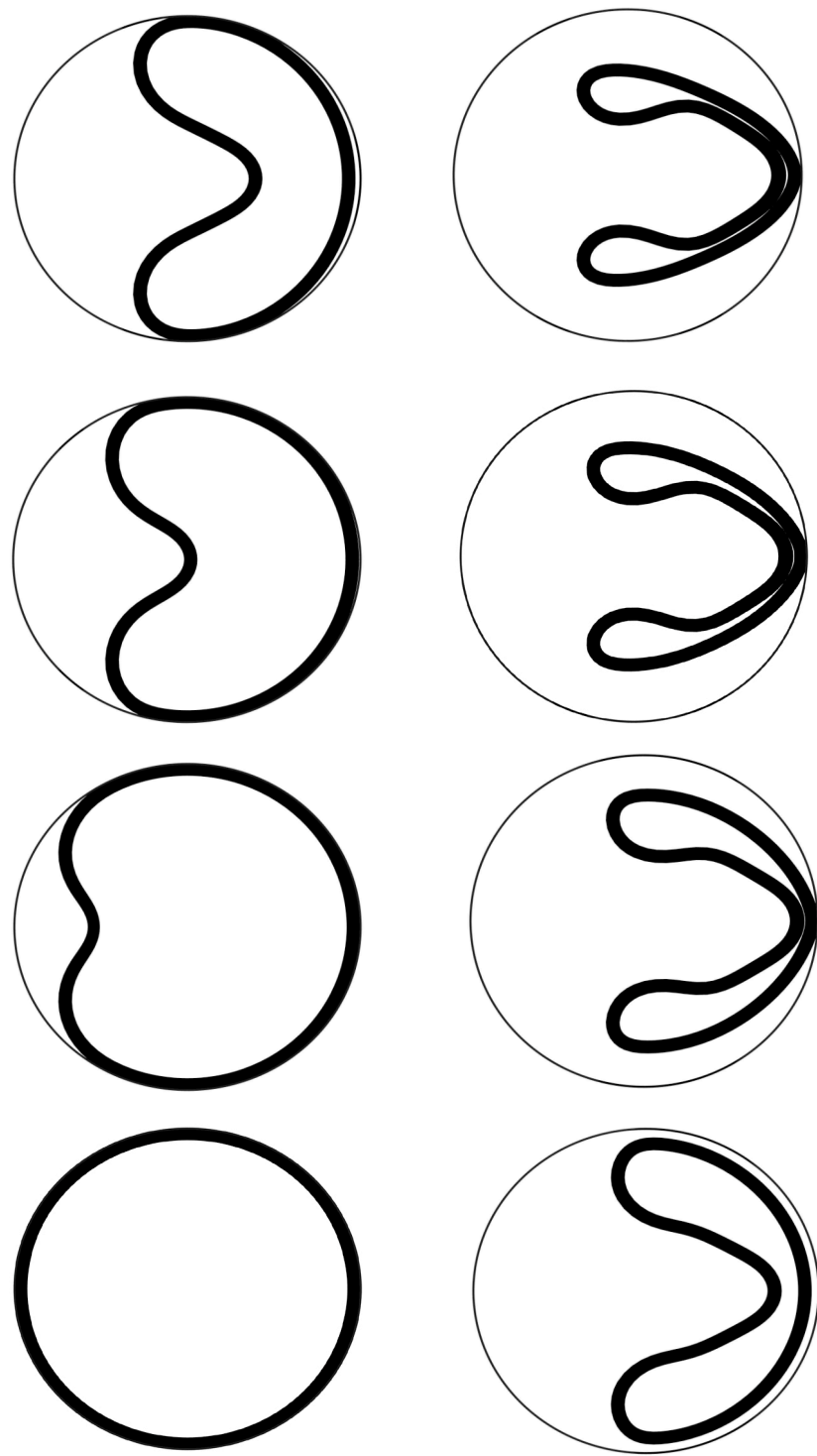


Fig. 5.7 (b) Calculated deformed tube cross sections taken along the length of confined buckle profile ( $D/t = 25.6$ )

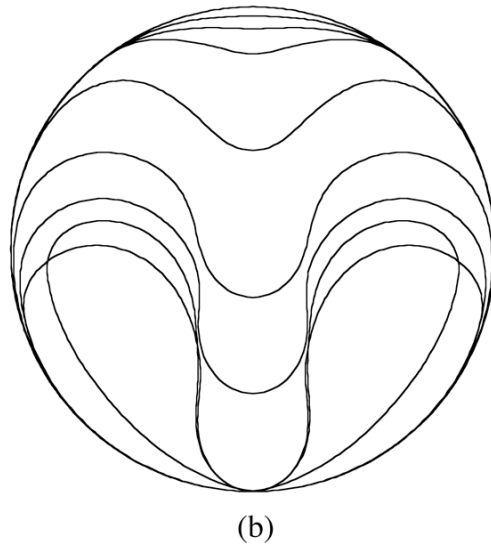
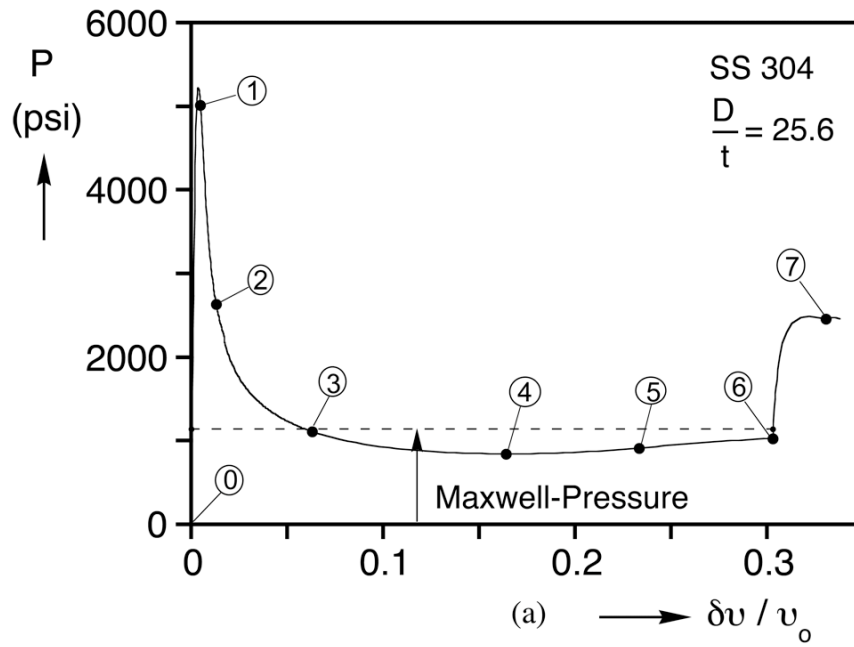


Fig. 5.8 (a) Calculated pressure-change in volume response for a confined tube collapsing uniformly and (b) sequence of deformed configurations corresponding to points marked on response in Fig. 5.8(a)

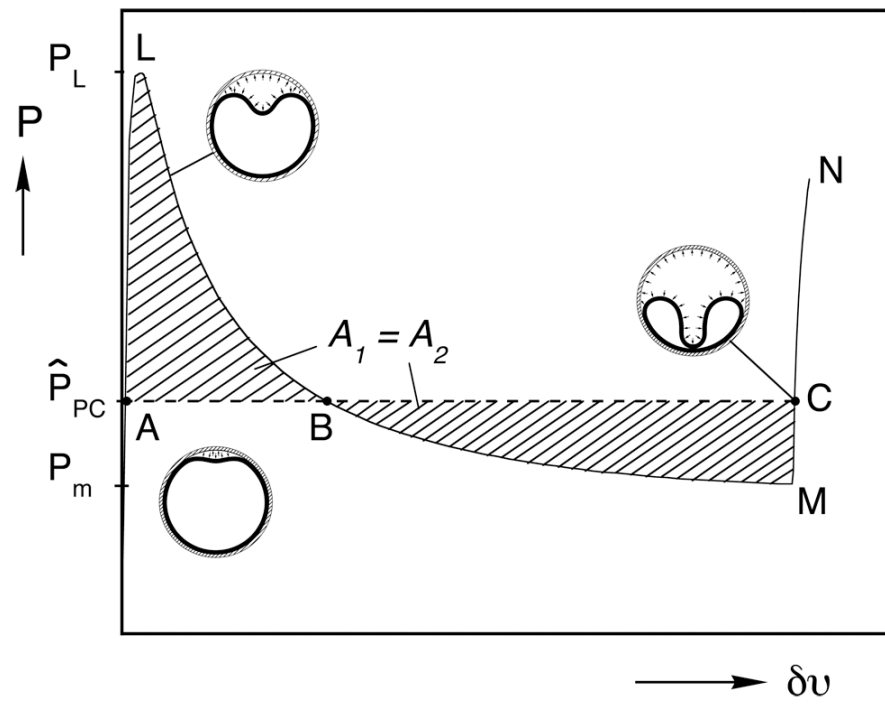


Fig. 5.9 Schematic of  $P$ - $\delta v$  uniform collapse response and the Maxwell construction

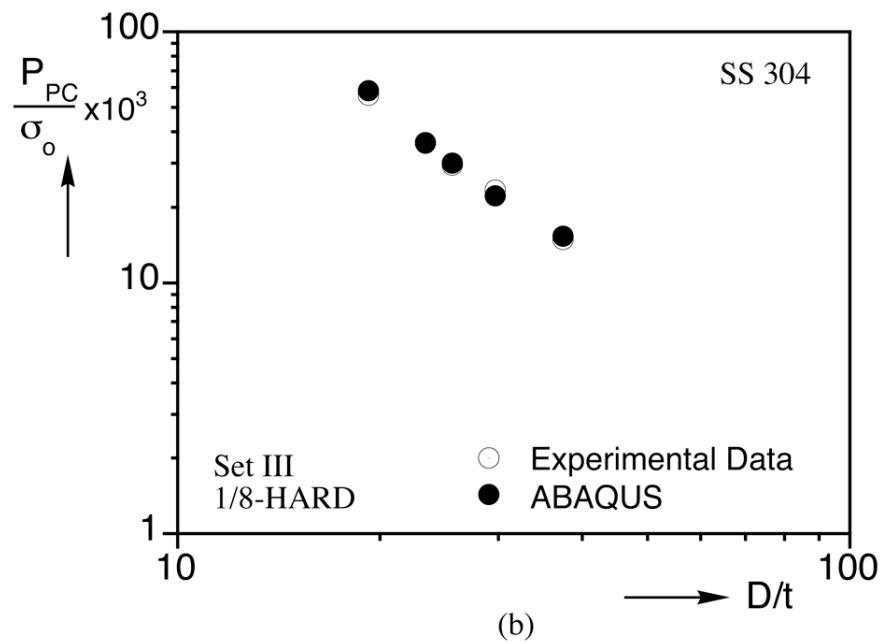
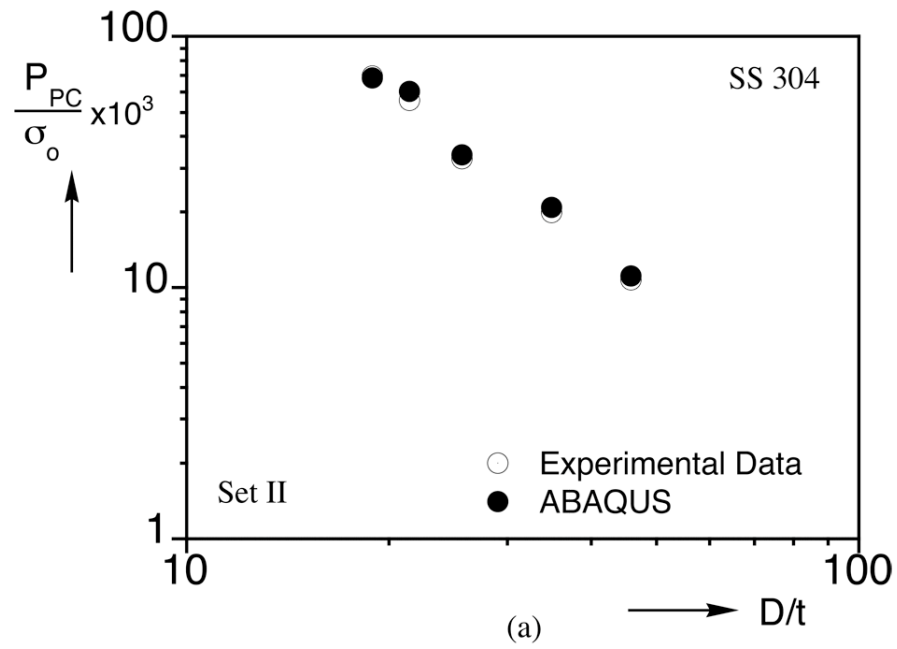


Fig. 5.10 Comparison of measured and predicted confined propagation pressures of two sets of SS-304 tubes tested: (a) Set II (b) Set III



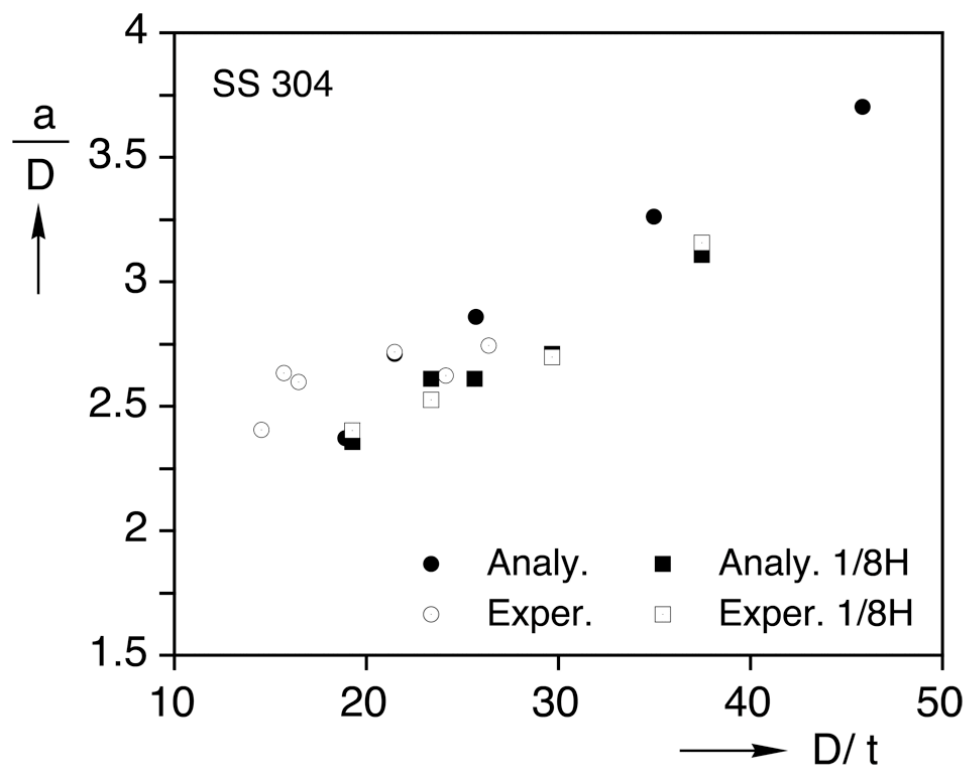


Fig. 5.11 Profile length vs. tube  $D/t$ : experiments and predictions

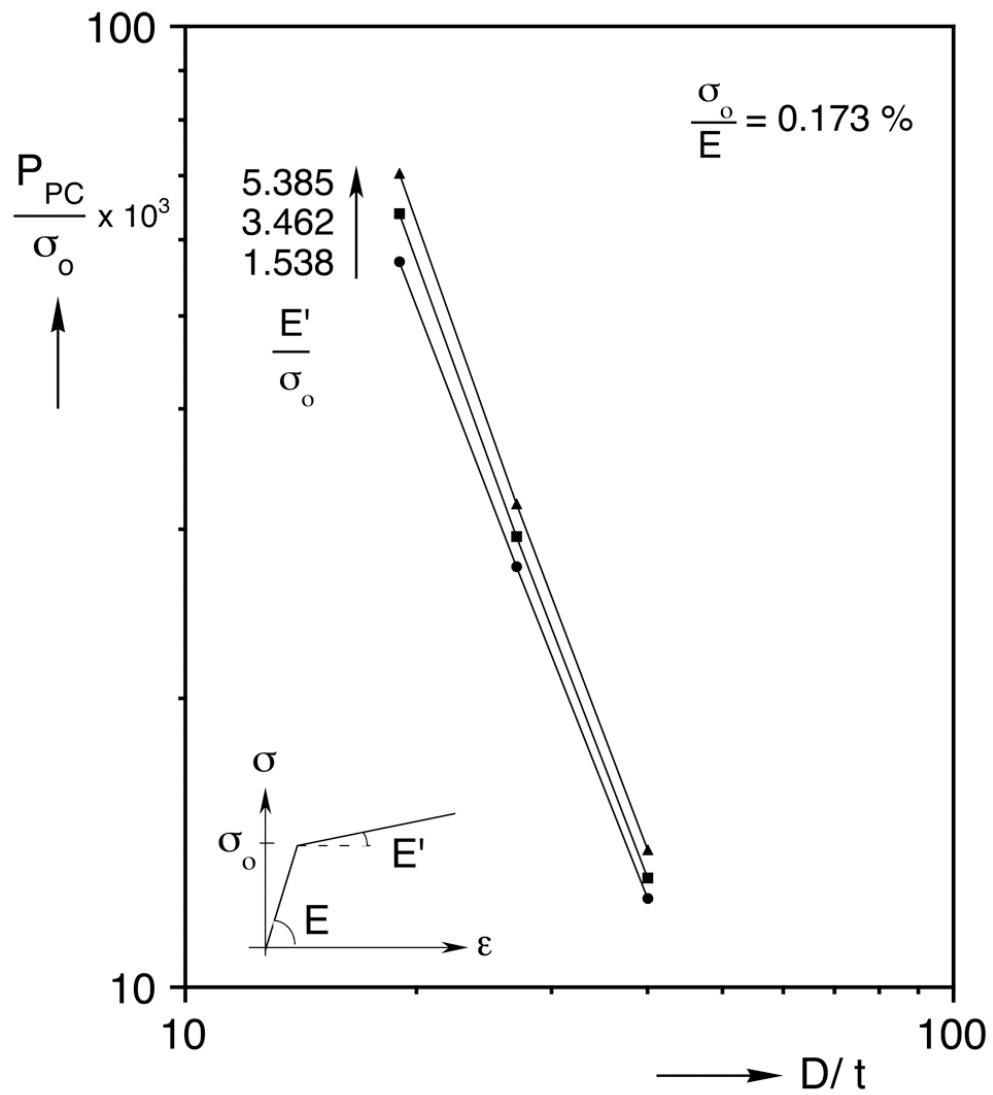


Fig. 5.12 Calculated confined propagation pressure vs. tube  $D/t$  for different material hardening parameters

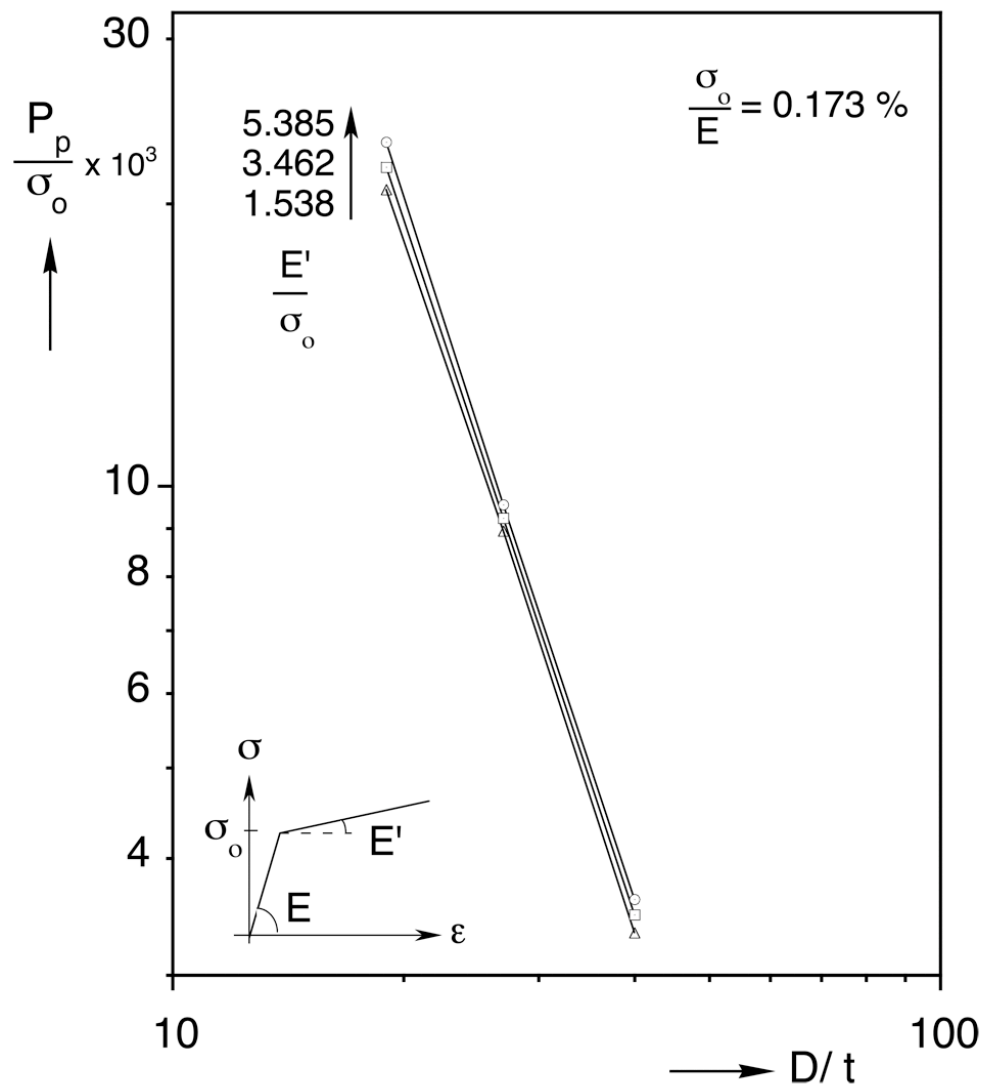


Fig. 5.13 Calculated propagation pressure vs. tube  $D/t$  for different material hardening parameters

## Appendix A: Design of Slip-On Buckle Arrestors: An Example

Pipe Parameters:

| $D$<br>in | $t$<br>in | $\frac{D}{t}$ | $\sigma_o$<br>(ksi) | $\Delta_o$<br>% |
|-----------|-----------|---------------|---------------------|-----------------|
| 10.625    | 0.4183    | 25.4          | 41.4                | 0.5             |

Arrestor Parameters:

| $D_i$<br>in | $\sigma_{oa}$<br>(ksi) | $L_a$<br>in | $h$<br>in |
|-------------|------------------------|-------------|-----------|
| 10.625      | 41.4                   | 53.125      | ---       |

Unknown parameter:

Arrestor thickness ( $h$ )

Pipe Critical Pressures:

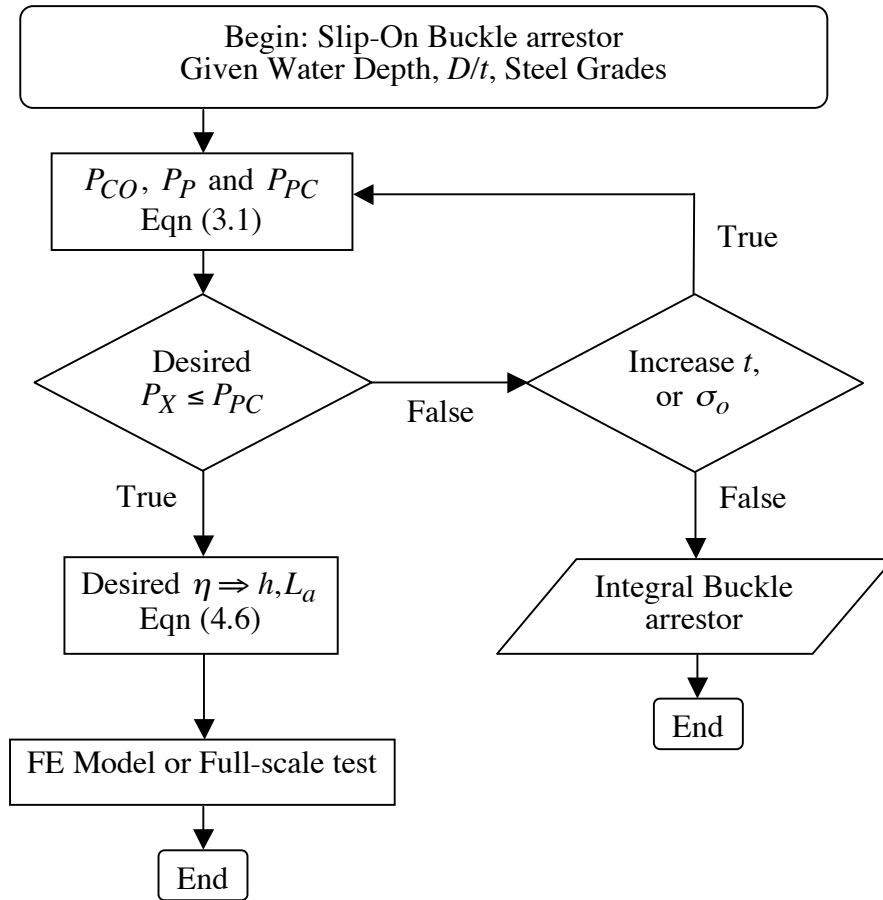
| $\hat{P}_{CO}$<br>psi | $\hat{P}_P$<br>psi | $\hat{P}_{PC}$<br>psi |
|-----------------------|--------------------|-----------------------|
| 2096                  | 500                | 1493                  |

The collapse pressure of the pipe with the initial imperfection  $\Delta_o = 0.005$  is calculated using BEPTICO. The propagation and confined propagation pressures, which determine the limits of arresting efficiency, are obtained from Eqs. (3.1).

The first step involves comparison of the pressure at the maximum operating depth of the pipeline with the confined propagation pressure (see flow chart in Fig. A.1). If the design pressure is lower than the confined propagation pressure then the empirical formula for the arrestor efficiency can be used

directly. In this example the arrestor length is chosen to be  $0.5D$  long. If we assume the design pressure is 1298 psi, which makes the arresting efficiency of 0.5. The corresponding arrestor thickness can be obtained from the arresting efficiency Eq. (4.6), which yields  $h = 0.205$  in. On the other hand, if the design pressure is higher than the propagation pressure, the pipe wall thickness or grad can be increased and the process is repeated. Alternatively the pipe dimensions can stay the same and the integral buckle arrestor option explored.

Fig. A.1 Design flowchart



## Appendix B: Error Analysis

In Chapter 4 a set of experimental results were used to derive the following expression for the arresting efficiency of slip-on buckle arrestors in terms of the major problem parameters:

$$\eta = \frac{A_1 \left( \frac{\sigma_{oa}}{\sigma_o} \right)^{0.8} \left( \frac{t}{D} \right)^{0.75} \left( \frac{L}{t} \right)^{0.98} \left( \frac{h}{t} \right)^{2.1}}{\left( \frac{P_{CO}}{P_P} - 1 \right)} \quad (B.1)$$

Each parameter ( $x$ ) was either measured or calculated with some small uncertainty ( $u_x$ ), which is usually known or can be estimated. The uncertainty of the arresting efficiency ( $u_\eta$ ) can then be estimated as follows:

$$\frac{u_\eta}{\eta} = \sqrt{\left( 0.75 \frac{u_D}{D} \right)^2 + \left( 2.33 \frac{u_t}{t} \right)^2 + \left( 0.98 \frac{u_L}{L} \right)^2 + \left( 2.1 \frac{u_h}{h} \right)^2 + \left( 0.8 \frac{u_{oa}}{\sigma_{oa}} \right)^2 + \left( 0.8 \frac{u_a}{\sigma_a} \right)^2 + \left( \frac{P_{CO}}{P_{CO} - P_P} \frac{u_{P_{CO}}}{P_{CO}} \right)^2 + \left( \frac{P_{CO}}{P_{CO} - P_P} \frac{u_{P_P}}{P_P} \right)^2} \quad (B.2)$$

The collapse pressure used in (B.1) was calculated using the custom computer program BEPTICO. Consequently the uncertainty had to be evaluated numerically by varying the key parameters one at a time within its range of uncertainty. If we accept that the collapse pressure is a function of the following major parameters

$$\hat{P}_{CO} = \hat{P}_{CO}(D, t, \sigma_o, E) \quad (B.3)$$

its uncertainty ( $u_{\hat{P}_{CO}}$ ) is given by:

$$u_{\hat{P}_{CO}} = \sqrt{\left(\frac{\partial \hat{P}_{CO}}{\partial D} u_D\right)^2 + \left(\frac{\partial \hat{P}_{CO}}{\partial t} u_t\right)^2 + \left(\frac{\partial \hat{P}_{CO}}{\partial \sigma_o} u_{\sigma_o}\right)^2 + \left(\frac{\partial \hat{P}_{CO}}{\partial E} u_E\right)^2} \quad (\text{B.4})$$

The measurement uncertainties of diameter and thickness are  $\pm 0.0005$ .

The uncertainty in the yield stress stresses is given by:

$$\frac{u_{\sigma}}{\sigma} = \sqrt{\left(\frac{u_F}{F}\right)^2 + \left(\frac{u_t}{t}\right)^2 + \left(\frac{u_w}{w}\right)^2} \quad (\text{B.5})$$

where  $F$  is the measured force and  $t$  and  $w$  are the specimens cross sectional dimensions.

The uncertainty of the strain measured in uniaxial tests is given by

$$\frac{u_{\varepsilon}}{\varepsilon} = \sqrt{\left(\frac{u_{\Delta R}}{\Delta R}\right)^2 + \left(\frac{u_R}{R}\right)^2 + \left(\frac{u_G}{G}\right)^2} \quad (\text{B.6})$$

The specification gives 3% uncertainty in resistance ( $R$ ), and 0.5% uncertainty in Gage Factor ( $G$ ).

The uncertainty in the elastic modulus  $E$  in modulus is estimated using (B.5) and (B.6) as follows:

$$\frac{u_E}{E} = \sqrt{\left(\frac{u_{\sigma}}{\sigma}\right)^2 + \left(\frac{u_{\varepsilon}}{\varepsilon}\right)^2} \quad (\text{B.7})$$

Three representative examples in which this procedure was used to estimate the uncertain first of the collapse pressure and second of the arresting efficiency are listed in Table B.1. The same procedure can be used to estimate the uncertainty of any efficiency calculation.

Table B.1 Parameters and uncertainties for three examples  
( $L/D = 0.5$ , and  $h/t = 1.94$ )

| $D$<br>In | $t$<br>in | $\sigma_o$<br>ksi | $\hat{P}_{CO}$<br>psi | $\hat{P}_P$<br>psi | $\frac{u_{\hat{P}_{CO}}}{\hat{P}_{CO}} \%$ | $\frac{u_{\eta}}{\eta} \%$ |
|-----------|-----------|-------------------|-----------------------|--------------------|--|----------------------------|
| 1.2500    | 0.0366    | 47.75             | 1434                  | 281                | 4.49                                       | 8.78                       |
| 1.2515    | 0.0495    | 41.36             | 2597                  | 501                | 2.29                                       | 4.92                       |
| 1.2511    | 0.0649    | 49.56             | 4693                  | 1075               | 1.46                                       | 3.45                       |



## References

- Bastard, A. H., and Bell, M. (2001). Evaluation of buckle arrestor concepts for reeled pipe. Proceedings of the 20<sup>th</sup> international conference offshore mechanics and arctic engineering, Rio de Janeiro, Brazil, June.
- Dyau, J.-Y., and Kyriakides, S. (1993). On the propagation pressure of long cylindrical shells under external pressure. *Int. J. Mech. Sci.*, 35, 675-713.
- Johns, T. G., Mesloh, R. E., and Sorenson, J. E. (1978). Propagating buckle arrestors for offshore pipelines. *ASME J. Pressure Vessel Technol.*, 100, 206-214.
- Kyriakides, S., and Babcock, C. D. (1979). On the dynamics and the arrest of propagating buckle in offshore pipelines. *Proceedings of the offshore technology conference*, OTC 3479, p. 1035-1045.
- Kyriakides, S., and Babcock, C. D. (1980). On the 'slip-on' buckle arrestor for offshore pipelines. *ASME J. Pressure Vessel Technol.*, 102, 188-193.
- Kyriakides, S., and Babcock, C. D. (1981). Experimental determination of the propagation pressure of circular pipes. *ASME J. Pressure Vessel Technol.*, 103, 328-336.
- Kyriakides, S., and Babcock, C. D. (1982). The spiral-arrestor: a new arrestor design for offshore pipelines. *ASME J. Energy Resour.*, 104, 73-77.
- Kyriakides, S. (1986). Propagating buckles in long confined cylindrical shells. *Int. J. Solids Struct.*, 22, 1579-1597.
- Kyriakides, S. (1993). Propagating instability in structures. *Advances in Applied Mechanics*, vol. 30, Hutchinson, J. W., and Wu, T. Y., eds., Academic, Boston, 67-189.
- Kyriakides, S., Corona, E., and Dyau, J.-Y. (1994) Pipe collapse under bending, tension, and external pressure (BEPTICO), Computer program manual, EMRL Report No. 94/4.

- Kyriakides, S., Park, T.-D., and Netto T. A. (1998). On the design of integral buckle arrestors for offshore pipelines. *Applied Ocean Research*, 20, 95-114.
- Kyriakides, S. (2000). On the design of clamped buckle arrestors for offshore pipelines. *MSS&M Rep. No. 00/4*, Univ. of Texas at Austin, Austin, TX.
- Kyriakides, S. (2002). Efficiency limits of slip-on type buckle arrestors for offshore pipelines. *ASCE Journal of Engineering Mechanics*, 128, 102-111.
- Kyriakides, S., and Lee, L.-H. (2005). Buckle propagation in confined steel tubes. *International Journal of Mechanical Sciences*, 47, 603-620.
- Langner, C.G. (1999). Buckle arrestors for deepwater pipelines. *Proceeding of the offshore technology conference, OTC 10711*, vol. 3., p. 17-28.
- Murphey, C.E., and Langner, C. G. (1985). Ultimate pipe strength under bending, collapse and fatigue. *Proceedings of the fourth international conference offshore mechanics and arctic engineering*, vol. 1, p. 467-477.
- Park, T.-D., and Kyriakides, S. (1997). On the performance of integral buckle arrestors for offshore pipelines. *ASME International Journal of Mechanical Sciences*, 39, 643-669.
- Olso, E., and Kyriakides, S. (2003). Internal ring buckle arrestors for pipe-in-pipe systems. *International Journal of Nonlinear Mechanics*, 38, 267-284.
- Yeh, M.-K., and Kyriakides, S. (1986). On the collapse of inelastic thick-walled tubes under external pressure. *ASME Journal of Energy Resources Technology*, 108, 35-47.
- Yeh, M.-K., and Kyriakides, S. (1988). Collapse of deep water pipelines. *ASME Journal of Energy Resources Technology*, 110, 1-11. (also OTC 5215, 1986).

## **Vita**

Liang-Hai Lee was born in Taipei, Taiwan on May 25, 1973, the son of Tai-Hsiung Lee, and Chun-Chin Zeng. After completing his high school education at National Overseas Chinese Experimental Senior High School in 1991, he entered The Chung Hua University, and received the degree of Bachelor of Science in Civil Engineering in July, 1995. In July 1997, he received a Master of Science degree in Structural Engineering at the same University. From 1997 to 1999 he worked as a research assistant at The National Chiao Tung University. In August, 1999, he pursued his Ph.D. at The University of Texas at Austin. He has co-authored the following papers:

Corona, E., Lee, L.-H., and Kyriakides, S. (2006). Yield anisotropy effects on buckling of circular tubes under bending. *International Journal of Solids & Structures*, 43, 7099-7118.

Kyriakides, S., and Lee, L.-H. (2005). Buckle propagation in confined steel tubes. *International Journal of Mechanical Sciences*, 47, 603-620.

Lee, L.-H., and Kyriakides, S. (2004). On the arresting efficiency of slip-on buckle arrestors for offshore pipelines. *International Journal of Mechanical Sciences*, 46, 1035-1055.

Permanent address: 4F, No.5, Ln.201, Chengkung Rd., Luchou, Taipei, 247,  
Taiwan.

This dissertation was typed by the author.